

**A STUDY  
ON THE INFLUENCE OF WELD PARAMETERS ON PERFORMANCE  
OF CENTRIFUGAL EXTRACTOR USED IN FAST REACTOR FUEL  
REPROCESSING**

*by*

**A. RAVISANKAR  
(ENGG02200704013)**

INDIRA GANDHI CENTER FOR ATOMIC RESEARCH  
KALPAKKAM

*A thesis submitted to the  
Board of Studies in Engineering Sciences  
in partial fulfillment of requirements  
for the award of the degree*

*of*

**DOCTOR OF PHILOSOPHY**

*of*

**HOMI BHABHA NATIONAL INSTITUTE**

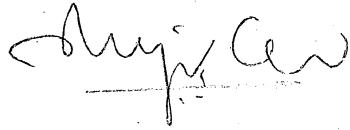


**NOV, 2013**

# Homi Bhabha National Institute

## Recommendations of the Viva Voce Board

As members of the Viva Voce Board, we certify that we have read the dissertation prepared by A.Ravisankar entitled "A Study on the influence of weld parameters on performance of centrifugal extractor used in fast reactor fuel reprocessing" and recommend that it may be accepted as fulfilling the dissertation requirement for the Degree of Doctor of Philosophy.



Date: 09 April 2015

Chairman - Dr. T. Jayakumar



Date: 9/4/2015

Guide / Convener - Dr. S. Venugopal



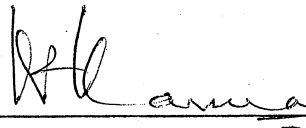
Date: 09/4/2015

Member 1 - Dr. A. K. Bhaduri



Date: 9/4/2015

Member 2 - Dr. K. Velusamy



Date: 9.4.2015

External Examiner - Prof. K. P. Karunakaran

Final approval and acceptance of this dissertation is contingent upon the candidate's submission of the final copies of the dissertation to HBNI

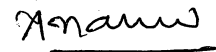
## STATEMENT BY AUTHOR

This dissertation has been submitted in partial fulfillment of requirements for an advanced degree at Homi Bhabha National Institute (HBNI) and is deposited in the Library to be made available to borrowers under rules of the HBNI.

Brief quotations from this dissertation are allowable without special permission, provided that accurate acknowledgement of source is made. Requests for permission for extended quotation from or reproduction of this manuscript in whole or in part may be granted by the Competent Authority of HBNI when in his or her judgment the proposed use of the material is in the interests of scholarship. In all other instances, however, permission must be obtained from the author.

*Kalpakkam,*

*Date:*

  
A. Ravisankar

## THESIS CERTIFICATE

This is to certify that the thesis entitled "A STUDY ON THE INFLUENCE OF WELD PARAMETERS ON PERFORMANCE OF CENTRIFUGAL EXTRACTOR USED IN FAST REACTOR FUEL REPROCESSING" submitted by A. Ravisankar to Homi Bhabha National Institute, Mumbai for the award of the degree of Doctor of Philosophy is a bona fide record of research work carried out by him under my supervision. The work is original and has not been submitted earlier as a whole or in part for a degree / diploma at this or any other Institution / University.

Kalpakkam,

Date: 9/4/2015



Dr. S. Venugopal

(Guide)

डॉ. एस. वेणुगोपाल स्वामी  
Dr S Venugopal, OS  
सह निदेशक / Associate Director  
सुदूर प्रहरतन, रोबोटिक्स, किरणन  
परीक्षण एवं पीआईई (जी आर आई पी) वर्ग  
Group for Remote Handling Robotics,  
Irradiation Experiments & PIE (GRIP)  
परमाणु ऊर्जा विभाग / Department of Atomic Energy  
भारत सरकार / Government of India  
इंगामअके, कल्पक्कम / IGCAR, KALPAKKAM - 603 102

## **Acknowledgements**

I thank my guide Dr. S. Venugopal, AD, GRIP, IGCAR, Kalpakkam for his able guidance and encouragements during the course of this thesis work. I am also grateful to him for his thoughtful advice, support availability and keenness.

The kind support, suggestions, constructive criticisms and encouragement given by the members of my doctoral committee are thankfully acknowledged.

I am deeply indebted to my guru Shri. G.R. Balasubramanian, Former Technical adviser to Chairman AEC for his kind support, guidance and parting technical freedom during initial development phase of Hot cell equipments and Remote handling systems.

I wish to thank Dr. Baldev Raj, former Director, IGCAR for having motivated me to take up the doctoral research and for his continuous support and encouragement. I wish to acknowledge and thank Shri. S. C. Chetal, former Director, IGCAR for his support and help.

I would also like to acknowledge and express my sincere thanks Dr. P.R. Vasudevarao, Director, IGCAR for his continuous support and encouragements. I am also grateful to Dr. R. Natarajan, Former PD, FRFCF & Director, RpG for his support and kind co-operation.

The personal support and interest shown by all of them has created an enabling environment.

I would like to thank Dr. Sudhir Babu Koganti, Former Head, RRDD and Dr. P V. Sivaprasad who were responsible for laying the initial foundations of the present work.

I am also thankful to Mr. V. Satish Kumar, Mr. S. Venkata Satyam, Mr. Palanivel and Mr. Gaurav Rajput for their support and co-operation during my research work.

My special thanks are also due to, Mr. Kempulraj, Head, CWD and his team and Mr. Mahadevan and his team for their support and help rendered in manufacturing of the bowls and data acquisition, respectively.

The technical discussions I had with, Dr. G. Amarendra, Head, MPD, Dr. C. Phaniraj, MMG, Dr. B. Venkatraman, AD, RSEG and Dr. B.P.C. Rao, Head, NDED would not be forgotten.

I acknowledge with gratitude, the help and support given by all my colleagues from Reprocessing Group. I also wish to thank all my office staff for their kind co-operation and help in documentation and fulfilling administrative procedures.

Finally, and most importantly, I would like to express my warmest appreciation to my family and friends for their whole-hearted support and love in the course of my research work.

## **ABSTRACT**

Thin cylindrical cross-sectional components constitute an important class of axisymmetric structures and are being used in static as well as in dynamic conditions in many engineering applications. Centrifugal extractor (CE), which is being used in nuclear spent fuel reprocessing, can be classified under thin walled equipment. The reliability and high performance of CE is of paramount importance in nuclear industry. Generally, the individual parts are welded for integration of the CE assembly. The objective of the present thesis is to estimate the temperature as well as distortion and residual stress distribution and thereby optimizing the welding parameters based on numerical simulation during welding of AISI type 304 stainless steel of thin walled centrifugal extractors by gas tungsten arc welding (GTAW) for achieving better performance of CE.

The presence of tensile residual stresses increases the susceptibility of a weld to fatigue damage, stress corrosion cracking (SCC) in certain combination of metal and environment and fracture. During the manufacture of thin walled components, these residual stresses, result in distortions that make it difficult to control the dimensions of the components. In the case of CE, the distortions would result in unbalanced mass and eccentricity, which in turn affects the dynamic stability of centrifugal extractor (CE) such as high amplitude of vibrations and bearing stiffness etc. Thus, the control of residual stresses and distortion is important to avoid service failures and to control the dimensional variations of the components during welding thin walled sections. The measurement of temperature distribution and residual stresses in the regions adjacent to weld during and after the welding process are of prime importance for understanding the distribution of both distortion and residual stresses and the influence of process parameters on the same.

In order to evaluate the temperature and the residual stress distribution of a GTAW circumferential butt joint of AISI 304 stainless steel pipe, the influence of heat source parameters has been studied through numerical simulation. Heat source fitting is carried out against heat inputs ranging from 200-500 J/mm to arrive at optimal heat input for obtaining adequate weld penetration and minimum heat affected zone (HAZ). The heat source analysis revealed that the choice of heat input is 300 J/mm. For this heat input, the influence of different weld speeds and powers on the temperature distribution and the residual stresses is studied at different welding speeds from 0.5 mm/s to 3 mm/s and at different power levels ranging from 150 W to 900 W. The longitudinal and circumferential residual stresses induced on the inner and outer surfaces as well as along the radial direction are found to be increased significantly with the increase in the weld speed and power.

At a location 3mm away from the WC, the increase in tensile stress was found to be 150 MPa on the inner surface, whereas the increase in compressive stress was 100 MPa on the outer surface. The transition from tensile to compressive and vice-versa was found to occur at a 1.25 mm depth i.e. at the mid section, through wall thickness from the outer surface. Similarly, the circumferential residual stress distribution also exhibited the same trend with the magnitude of increase in tensile stresses as 120 MPa on the inner surface, while it was 100 MPa for compressive stresses on the outer surface. The transition from tensile to compressive and vice-versa occurred at the radial distance from the outer surface which was found to be between 0.5 and 1.0 mm. Whereas the radial residual stresses are found to be negligible and are not influenced by the variation in the weld speed and power. The results obtained from the numerical simulation are validated with full scale shop floor welding experiments which are found to be in reasonable agreement with each other.

As the welding input parameters play a significant role in the final distortions, an attempt has also been made to investigate the influence of various weld parameters on distortion. There by the dynamic behavior of actual CE rotating bowl geometry studied by optimizing the weld process parameters for improving the performance of those bowls. In this regard, a synergistic approach is followed in which the experiments were conducted for the important cases obtained from the numerical analysis for different conditions such as welding speed, clamping conditions, number of passes and weld sequence. For a particular location at 68mm from the bottom of CE bowl the longitudinal distortions along its length of the bowl at angle  $60^\circ$  from the weld start position after welding is found to be maximum which is 66 microns and the numerical analysis predicted it as 50 microns. The distortions checked for different weld speeds ranging from 0.5mm/sec to 2mm/sec shows a maximum value of 200 microns at 2mm/sec and 75 microns at 0.5mm/sec. Similarly in continuous welding it is observed a maximum distortion of 210 microns. The dynamic behavior is studied comprehensively through numerical analysis by introducing the obtained distortions on the surface of the bowl after welding. The critical speeds are clearly identifiable from the rotor frequency response which indicates that the second mode (as operating at 3000 rpm) is important as it falls within the operating speed.

This thesis would contribute for the significant modifications in heat input parameters and clamping conditions towards the improvement of dynamic performance that concerned to the welding in the field of thin walled centrifugal extractor rotors.

# TABLE OF CONTENTS

	<b>Page No.</b>
ACKNOWLEDGEMENTS.....	v
ABSTRACT.....	vii
LIST OF FIGURES.....	xii
LIST OF TABLES.....	xvi
LIST OF PUBLICATIONS.....	xvii
NOMENCLATURE.....	xviii
<b>CHAPTER 1 Introduction</b>	
1.1 Nuclear fuel reprocessing.....	4
1.2 Process and Equipments Development of FRP.....	7
1.3 Centrifugal extractors.....	8
1.4 Welding of thin walled centrifugal extractor rotating bowl.....	10
1.5 Motivation of this study.....	14
1.6 Objectives and scope of the research.....	16
1.7 Thesis outline.....	17
<b>CHAPTER 2 An overview of literature on issues related to welding of thin sections</b>	
2.1 Introduction.....	20
2.2 Distortions.....	27
2.3 Residual stresses.....	28
<b>CHAPTER 3 Numerical modeling of welding of thin walled cylindrical components</b>	
3.1 Thermal analysis.....	36
3.1.1 Thermal Model: Temperature distribution.....	37
3.1.2 Thermo elastic-plastic mechanical Model: Distortions and Residual stresses.....	39
3.2 Finite element formulation .....	41
3.3 Material properties.....	45

3.4	Welding of thin walled pipe.....	47
3.5	Rotating bowl assembly.....	48
3.5.1	Welding fixtures.....	50
<b>CHAPTER 4</b>	<b>Results &amp; Discussions</b>	
4.1	Heat source fitting.....	54
4.2	Welding temperature characteristics (Thermal analysis).....	59
4.2.1	Influence of weld speed and power on temperature distribution.....	63
4.3	Distortions.....	64
4.3.1	Radial distortions along longitudinal direction (Z-coordinate).....	66
4.3.2	Longitudinal distortions along longitudinal direction (Z-coordinate).....	67
4.4	Distortion on 3-plane circumferential butt joint.....	68
4.5	Micro structure.....	79
4.6	Dynamic Analysis.....	80
4.7	Welding residual stress (Mechanical analysis).....	83
4.7.1	Longitudinal stress.....	85
4.7.1.1	Influence of weld speed and power.....	87
4.7.2	Circumferential stress.....	88
4.7.2.1	Influence of weld speed and power.....	90
4.7.3	Radial Stress.....	90
4.8	Experimental validation.....	92
<b>CHAPTER 5</b>	<b>Conclusions &amp; Future Scope</b>	99
	<b>REFERENCES</b>	104

## LIST OF FIGURES

<b>S. No.</b>	<b>Title of the Figure</b>	<b>Page No.</b>
1.1	Process flow sheet of Fast Reactor Fuel Reprocessing.....	5
1.2	A typical View of 16-stage Centrifugal extractor bank.....	9
1.3	(a) Schematic of the CE and (b) Dimensions of the rotating bowl.....	11
2.1	Weld distortion in a circumferential pipe joint.....	28
2.2	Residual Stresses developed during welding of a butt joint.....	31
2.3	Axial stress distribution inside and outside surfaces of circumferential pipe joint considered by (Deng <i>et al.</i> [66]).....	32
2.4	Hoop stress distribution inside and outside surfaces of circumferential pipe joint considered by (Deng <i>et al.</i> [66]).....	32
3.1	Goldak Double Ellipsoid Heat Source Model [75].....	37
3.2	Finite element model (a) 2-D mesh and (b) 3-D mesh with boundary conditions.....	39
3.3(a)	Temperature dependent thermo-physical properties.....	45
3.3(b)	Temperature dependent thermo-mechanical properties.....	45
3.4	2-D line diagram of the model with boundary conditions.....	47
3.5	2D Finite element mesh of rotating bowl.....	48
3.6(a)	Variation of thermal properties against temperature of SS 304L.....	49
3.6(b)	Variation of mechanical properties against temperature of SS304L.....	49
3.6(c)	True Stress vs strain curve for SS 304L.....	50
3.7	Fixture for tack welding.....	51
3.8	Special fixture for welding.....	51
4.1	Schematic 2-D line diagram of cylindrical work piece with boundary condition.....	55

4.2	Temperature distribution for different cases of heat source fitting.....	56
4.3	The weld pool shapes obtained by experiments and FE simulation.....	57
4.4	3-D Temperature profile on the outer surface.....	58
4.5	3-D Temperature profile on the outer surface.....	59
4.6(a)	Simulated transient thermal cycles at the weld centre.....	61
4.6(b)	Comparison between simulated transient thermal cycles for four different cases at different locations longitudinally 10 mm away from weld centre.	61
4.6(c)	Comparison between simulated transient thermal cycles for four different cases at different locations longitudinally 20mm away from weld centre..	62
4.6(d)	Comparison between simulated transient thermal cycles for four different cases at different locations longitudinally 30mm away from weld centre..	62
4.6(e)	Comparison between simulated transient thermal cycles for four different cases at different locations longitudinally 40mm away from weld centre..	63
4.7(a)	Radial distortions along the longitudinal direction (Z coordinate) on the inner surface.....	64
4.7(b)	Radial distortions along the longitudinal direction (Z coordinate) on the outer surface.....	65
4.8(a)	Longitudinal distortions along the longitudinal direction (Z coordinate) on the inner surface.....	65
4.8(b)	Longitudinal distortions along the longitudinal direction (Z coordinate) on the outer surfaces.....	66
4.9(a)	Variation of wall thickness along the radial direction.....	67
4.9(b)	Variation of component length along the longitudinal direction (Z coordinate).....	68
4.10	Experimental set up used for welding of 3-plane circumferential butt joint.....	69
4.11	Measurement locations of thermocouples on the rotating bowl assembly surface.....	70
4.12	Direction of Welding along its circumference.....	71

4.13	Segments of Welding used in sequential welding.....	72
4.14	Longitudinal and transverse distortion measurement locations on the surface of rotating bowl assembly.....	73
4.15	Typical temperature Contour on the outer surface of rotating bowl at 100sec.....	74
4.16(a)	Temperature distribution along its length of the weld for the First sector..	74
4.16(b)	Temperature distribution along its length of the weld for the second sector.....	75
4.17	Longitudinal distortions along its length of the bowl at angle 60° from the weld start position before and after welding.....	75
4.18	Contour of Longitudinal distortions of the bowl at room temperature after welding.....	76
4.19	Longitudinal distortions along its length of the bowl at angle 120° from the weld start position for different weld speeds.....	77
4.20	Longitudinal distortions along its length of the bowl at angle 120° from the weld start position for different sequences of welding.....	77
4.21	Longitudinal distortions along its length of the bowl at angle 120° from the weld start position for different clamping conditions.....	78
4.22	Longitudinal distortions along its length of the bowl at angle 120° from the weld start position against number of passes.....	78
4.23	Microstructure of Weld zone and HAZ of TIG welded component.....	79
4.24	Microstructure of TIG welded component of 2mm thick.....	80
4.25	2D model of Rotating bowl assembly.....	80
4.26	Motor critical speed map against bearing stiffness.....	82
4.27(a)	Variation of critical speeds against bearing stiffness for different weld speeds.....	82
4.27(b)	Variation of critical speeds against bearing stiffness.....	83
4.28(a)	Comparison between longitudinal residual stresses for different cases at 180° section from the weld start position on the inner surface.....	84

4.28(b)	Comparison between longitudinal residual stresses for different cases at 180° section from the weld start position on the outer surface.....	84
4.28(c)	Comparison between longitudinal residual stresses for different cases at 180° section from the weld start position along the radial direction from outer surface at 3 mm away from WC.....	86
4.28(d)	Comparison between longitudinal residual stresses for different cases at 180° section from the weld start position along the radial direction from outer surface at 14 mm away from WC.....	86
4.29(a)	Comparison between circumferential residual stresses for different cases at 180° section from the weld start position on the inner surface.....	88
4.29(b)	Comparison between circumferential residual stresses for different cases at 180° section from the weld start position on the outer surface.....	89
4.29(c)	Comparison between circumferential residual stresses for different cases at 180° section from the weld start position along the radial direction from outer surface at 4mm away from the WC.....	89
4.30(a)	Comparison between radial residual stresses for different cases at 180° section from the weld start position on the inner surface.....	91
4.30(b)	Comparison between radial residual stresses for different cases at 180° section from the weld start position on the outer surface.....	91
4.31	Experimental setup used (a) schematic diagram and (b) welding setup with clamping fixture and data logging system.....	93
4.32	Location of thermocouples and weld direction.....	93
4.33(a)	Comparison of experimentally obtained temperature profiles with FE simulation for different locations.....	95
4.33(b)	Comparison of experimentally obtained Residual stresses with FE simulation for different locations.....	96
4.34	Experimental setup used (a) Component welding process (b) Dial gauge measurements for distortions.....	97
4.35	Comparison of distortion obtained experimentally with those from FE simulation.....	98

## LIST OF TABLES

<b>S No.</b>	<b>Title of the table</b>	<b>Page No.</b>
1.1	Typical comparison of TRFR and FRFR.....	7
3.1	Chemical composition (in Wt %) of AISI 304 stainless steel.....	46
3.2	Material properties used for FE simulation.....	46
3.3	Welding process parameters used for heat source fitting.....	46
4.1	Heat source characteristic parameters.....	57
4.2	Summary of different combinations of weld speed and power.....	59
4.3	Measurement locations of thermocouples on the rotating bowl assembly surface.....	70
4.4	Longitudinal and transverse distortion measurement locations on the surface of rotating bowl assembly.....	72
4.5	Weld input parameters and weld bead geometry details.....	73

## LIST OF PUBLICATIONS

### Journal Publications:

1. A. Ravisankar, Satish K. Velaga, Gaurav Rajput, S. Venugopal., *“Influence of welding speed and power on residual stress during Gas Tungsten Arc Welding (GTAW) of thin sections with constant heat input: a study using numerical simulation and experimental validation”* *Journal of Manufacturing Processes*, 2014, Vol. 16, pp. 200-211.  
<http://dx.doi.org/10.1016/j.jmapro.2013.11.002>.
2. A. Ravisankar, S.Venkata Satyam, S. Venugopal (2013), *“Effect of weld parameters on the dynamic performance of thin walled centrifugal extractor rotating bowl”*. *Journal of Mechanical Engineering Science*, 2014. doi:10.1177/0954406214544726

### Publications in Conference Proceedings:

1. A. Ravisankar, V. Satish Kumar, Gaurav Rajput, S. Murugan, S. Venugopal, Numerical simulation of welding distortion: A comparative study of variable weld speeds and powers with constant heat input, Int. conference on advances in manufacturing technology – ICAMT -2012, Chennai, India, June 15-17, 2012.

## NOMENCLATURE

$\sigma$	Stress (MPa)
$\sigma_y$	Yield stress
$\varepsilon$	Total strain
$\varepsilon_{el}$	Elastic strain
$\varepsilon_{th}$	Thermal strain
$K$	Stiffness of the material
$\bar{\varepsilon}_p$	Plastic strain
$\dot{\varepsilon}$	Strain rate
$\rho$	Density of the material ( $\text{Kgm}^{-3}$ )
$C_p$	Specific heat at constant pressure
$A$	Cross Sectional Area
$a_f$	Length of front ellipsoidal of heat source (mm)
$a_r$	Length of front rear of heat source (mm)
$R_o$	Outer radius of cylinder (mm)
$b$	Half width of heat source (mm)
$c$	Penetration depth of heat source (mm)
$E$	Young's Modulus of Column
$f_f$	Fraction of heat in front ellipsoidal of heat source
$f_r$	Fraction of heat in rear ellipsoidal of heat source

$T$	Current temperature at cylinder surface
$\Delta T$	Difference between the reference temperature and actual temperature
$\eta$	Arc efficiency (%)
$h_{total}$	Combined convection and radiation heat transfer coefficient ( $\text{Wm}^{-2}\text{K}$ )
$\sigma_b$	Stefan-Boltzman constant ( $5.6703 \times 10^{-8} \text{ Wm}^{-2}\text{K}^{-4}$ )
$\alpha$	Co-efficient of thermal expansion (per degree)
$\sigma_t$	Tensile stress (MPa)
$\sigma_c$	Compressive stress (MPa)
$\sigma_h$	Transverse or hoop stress
$\sigma_l$	longitudinal stress
$r_i$	Cylinder inner radius (mm)
$r_o$	Cylinder outer radius (mm)
$r$	Cylinder mean radius
$D$	Outer Diameter of Cylinder
$t$	Cylinder Wall Thickness
$q(r)$	Surface flux at radius $r$ ( $\text{Wm}^{-2}$ )
$q(0)$	Maximum flux at the center of the heat source ( $\text{Wm}^{-2}$ )
$q_{loss}$	Total heat loss
$U$	Voltage (Volts)
$I$	Current (Amperes)
$V,S$	Weld speed ( $\text{mms}^{-1}$ )

ASTM	American Society for Testing and Materials
BWR	Boiling Water Reactor
CORAL	Compact Reprocessing of Advanced Fuels in Lead Cell
PHWR	Pressurized Heavy Water Reactor
FBTR	Fast Breeder Test Reactor
PFBR	Prototype Fast Breeder Reactor
FE	Finite Element
FEM	Finite Element Methods or Finite Element Modeling
FV	Finite Volume
FZ	Fusion Zone
TIG	Tungsten Inert Gas
GMAW	Gas Metal Arc Welding
GTAW	Gas Tungsten Arc Welding
HAZ	Heat Affected Zone
WZ	Weld zone
IGSCC	Inter-granular Stress Corrosion Cracking
RO	Root Opening
WL	Weld Line
WP	Weld Pool

## **Chapter 01**

### **INTRODUCTION**

Gas tungsten arc welding (GTAW) technique [1-2] is widely used to weld thin sections made of stainless steel and non-ferrous metals such as aluminum, magnesium and copper alloys as well. The circumferential butt joint [3-5] is a common type of pipe joint in a variety of engineering applications such as oil and gas industries, nuclear, thermal power plants and chemical plants. The thermal cycles due to welding process produce nonlinear plastic deformation and in turn results in residual stress formation in the weld metal. The presence of tensile residual stresses increases the susceptibility of a weld to fatigue damage [6], stress corrosion cracking (SCC) [7] under certain combination of materials and environment and fracture [8]. While manufacturing thin walled components, these residual stresses may cause distortion of the component and make it difficult to control the dimensions of the components. Therefore, control of these distortions, residual stresses and their distribution is an important aspect to avoid service failures and to

control the dimensional tolerances of the components in particular, during welding of thin walled sections. In this regard, a thorough understanding on the distortion, residual stresses and the influence of various welding parameters on the distribution of the residual stress is required. The measurement of temperature distribution, distortion pattern and residual stresses in the regions adjacent to the weld line during and after the welding process is of prime importance for understanding the nature and behavior of the distortion, residual stresses and the influence of process parameters on the performance of weld component.

There have been numerous investigations [9-15] that pertain to the numerical analysis with experimental validation to understand the temperature distribution, distortions and the residual stresses. Generally, the welding is carried out at high speed by giving more power for achieving high productivity. The regions near the weld center undergo severe thermal cycles because of high concentrated heat source, which in turn generates the residual stresses in the weld metal in longitudinal as well as in circumferential directions. There are a few studies [16-20] that deal with the measurement of thermal cycles and residual stresses in thin walled cylinders particularly for different weld speeds and powers keeping the heat input as constant. Further, a limited literature [21-23] is available on the variation in longitudinal and circumferential residual stresses along the radial distance from the outer surface for different weld speeds and powers with constant heat input. Malik et al., [24] have evaluated the longitudinal residual stresses on the inner and outer surfaces of cylinder for varying welding speeds with different heat input per unit volume. Their investigations reveal that the weld speed and power have strong influence on the residual stress and their distributions. The relationship between the weld speed and power versus residual stress and their distributions can be established at constant heat input, through

Finite element modeling (FEM) and these FEMs can be used for optimizing weld parameters for obtaining sound welds.

In contrast, with the welding-induced residual stress that is mostly localized in the neighborhood of the weldment, welding-induced distortion can spread over the entire welded structure. Therefore, in assembling welded components into another structure, tremendous fit-up problems could be present, because of the dimensional change of the substructures due to welding. However, even when the code requirements are met, welding-induced distortion could affect the performance of the welded structure in service as well. In pipe welding, diameter change is the most usual deformation type. After welding, the pipe diameter is changed from the original diameter because of welding shrinkage. The weld distortions depend on several factors such as geometrical size, welding parameters, weld sequence and applied boundary conditions. Finally, these distortions which in turn cause the unbalanced mass and eccentricity will affect the dynamic stability of thin walled rotating bowls.

Finite element (FE) is a proven tool [25-26] for accurate assessment of thermo-mechanical behavior in circumferentially joined thin-walled structures and it is being used in the evaluation of thermal cycles, welding residual stresses and distortions. However, the present computational efforts combined rapid developments in numerical methods and modeling techniques, have enabled computational weld mechanics to solve wide variety of problems that interested in many industrial applications. Especially welding is a great concern in power plants, refineries and pressure vessels, nuclear reactors, building and bridges, automotive, trucks and trains, ships, offshore structures, aerospace structures, micro electronics and many others engineering fields as well. Similarly, due to the manufacturing difficulties associated with the nuclear spent fuel

reprocessing plants of fast breeder reactor, design of equipments with stringent dimensional tolerances, which is a major concern, can be maintained by adopting proper welding techniques.

### **1.1 Nuclear fuel reprocessing**

The commercial success of fast reactor nuclear fuel reprocessing and recycling increases the available energy from the nuclear fuels to reasonable extent. With reprocessing and recycling the fuel supplies can be guaranteed for many centuries, as compared to once through option of direct disposal of irradiated fuel. This is particularly important for India, where the available resources of fissile uranium are limited but the resources of fertile thorium are abundant. This can be made use of only after irradiation within reactor and the resultant  $U^{233}$  can be used as fuel only after reprocessing. Based on the available resources in India, a three stage nuclear power program wherein initially natural uranium fueled reactors will produce electricity and plutonium [27] is planned. This in turn can be used as driver fuel in fast reactors in the second stage. For reasons of economy, the irradiated fuel from fast reactors has to be reprocessed with short cooling times. However, fast reactor fuel reprocessing (FRFR) faces many challenges like designing equipments with remotization and automation in highly radioactive environment like Head end, Extraction and Reconversion operations. Therefore, recycling of irradiated fuel to make use of plutonium present in it by reprocessing is vital. The irradiated fuels discharged from fast reactors have to be reprocessed with least delay, commensurate with current technological levels to enable faster growth. Fast reactor fuels are generally reprocessed by the conventional Plutonium (Pu) - Uranium (U) reduction extraction (PUREX) process [28] (based on solvent extraction for separating Pu and U). However, the high levels of Pu and high burn-up of fast reactor fuels introduce number of challenges in reprocessing.

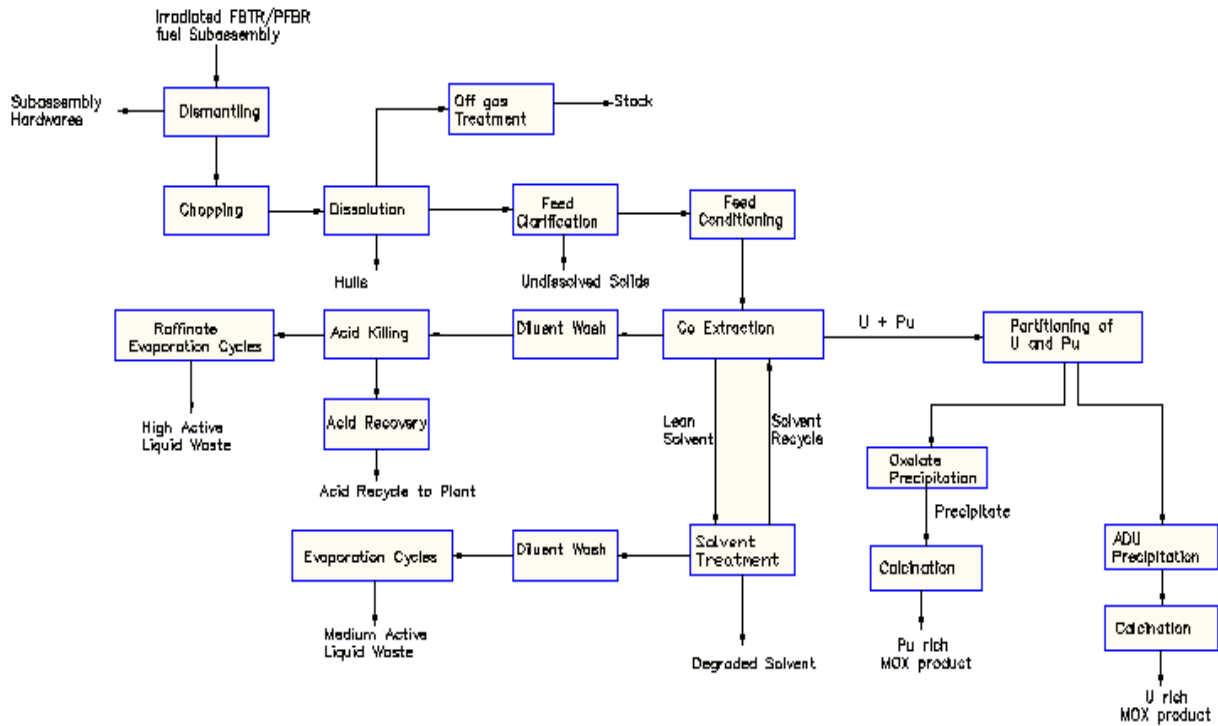


**Fig.1.1: Process flow sheet of Fast Reactor Fuel Reprocessing**

A pilot plant, compact reprocessing of advanced fuels in lead mini cell (CORAL), has been setup to reprocess the few subassemblies of fast breeder test reactor (FBTR). All the components of CORAL have been totally developed for remote operation and built in-house. Basically, the process involves chopping, dissolution, feed clarification, solvent extraction and partitioning. The process flow sheet of fuel reprocessing is shown in Fig.1.1. Single pin chopping process has been developed for cutting the fuel into small pieces to increase the rate of dissolution. A novel dissolution method, called electro oxidative dissolution technique, has been developed. To remove the fines which may be generated during dissolution, a high-speed centrifuge that can be remotely operated and maintained has been developed. The high radiation levels in the solution demand the development of short residence time contactors such as centrifugal extractors to minimize the solvent damage. Such contactors have been developed for a wide range of flow

rates. Electrolytic in-situ partitioning methods have also been developed to obtain plutonium and uranium in pure form separately.

For the remote operation and maintenance of these equipments, articulated master slave manipulators, remote samplers etc., have been incorporated in the plant. The operation of CORAL serves to understand process problems, gain operational experience and also provide solutions to the prototype plant, FRFR Plant, under construction.

It is well-recognized that the success of the fast breeder reactor (FBR) power program lies in reducing the fissile inventory in the fuel cycle. To this end, irradiated fuels have to be processed and fabricated within short cooling times. Towards achieving this goal, the equipment are being developed with the main emphasis of reducing high level waste generation, recovery of minor actinides and development of matrices for safe, long-term disposal of nuclear waste. Increasing plant life and reliability of equipment are areas which have significant role on the fuel cycle economy. To achieve this, a comprehensive program is being implemented in the following areas.

- Specification of stainless steel with tight control over trace elements.
- Choice of alternate materials like titanium-tantalum-niobium alloys for selected equipment.
- Implementation of quality control procedures during fabrication and installation.
- Development of in-service inspection for critical equipment like dissolver, evaporators and high level liquid waste storage tanks.

## 1.2 Process and equipment development for FRFR plant

The development of process and equipment for FRFR plant has been carried out and the initial testing of all these equipment was done successfully at the laboratory scale prior to their deployment in the realistic hot conditions. Some of the equipments developed were being used in the reprocessing campaigns of thorium fuel rods to recover  $U^{233}$  used in the fabrication of FBR MOX fuel for the irradiation experiments in FBTR. In the fast reactor fuel reprocessing, the fuel pins being very slender with more Pu content (hence more safety with respect to criticality), harder cladding material and high heat generating nature compared to thermal reprocessing, the single pin chopper (SPC) is adopted for a safe and smooth chopping operation.

**Table. 1.1 Typical comparison of TRFR and FRFR**

S. No.	Property	TRFR	FRFR
1	Pu/(U+Pu)	0.004	0.15 to 0.7
2	Specific activity	200 Ci/l	1000 Ci/l

In comparison with thermal reactor fuel reprocessing (TRFR), FRFR possesses challenges in manifolds in accordance with the associated decay heat and Pu content. Table 1.1 provides a comparison between TRFR and FRFR. The higher decay heat of the fast reactor SF offers great restriction in the time of contact between the fuel and solvent, breaching which the tri-butyl phosphate (TBP) get heavily degraded giving rise to its degraded products. The development of several variants of centrifugal extractors took care of this problem thereby improving the solvent extraction performance. Centrifugal extractor (CE) [28-29] that can be classified under thin

walled equipment, which is a critical equipment used in the nuclear spent fuel reprocessing plants of FBR to recover U and Pu leaving highly radioactive fission products, whose dimensions are also critical and sensitive against welding process parameters is considered in the present study.

### **1.3 Centrifugal extractor**

CE banks are used in the nuclear fuel reprocessing plants of FBR spent fuel (SF), by PUREX process in the solvent extraction step, to recover valuable U and Pu leaving highly radioactive fission products. Solvent (30% TBP in n-dodecane) used has greater affinity to fissile materials (U, Pu) leading to ease of separation from highly radioactive fission products. The CE has the advantages of fine dispersion through shearing of liquid layers between the stationary bowl and rotating bowl and fast phase separation due to high centrifugal force (200 – 1000g) leading to reduced contact time and less radiation damage to solvent. Consequently, CE occupies less volume inside the cell with less criticality problems. Steady state is achieved faster and stage equilibrium will not be disturbed due to stoppage of unit unlike differential units like pulse column. The special features are separation of individual phases in the high speed-rotating bowl by Centrifugal force. Pumping to adjacent stage is achieved through gravity due to static head difference between collection chambers and the mixer.

Ideally the CE, being a single integral unit comprising of the stationary bowl, bank plates, interconnecting pipes, feed, discharge and sweep air pipe lines, has to be machined as a single piece by special machining techniques. Since the above machining techniques are not available indigenously it has been fabricated in six individual components, namely, bottom plate with baffles, mixing chamber, organic chamber, aqueous chamber, holding plate, organic and aqueous

chamber interconnecting pipes. Later these components are welded together. Similarly rotating bowl has been made in six individual components such as barrel, baffle plates & holder, organic & aqueous chambers and top plate. They are then fitted, aligned and welded together.



**Fig. 1.2: A typical View of 16-stage Centrifugal extractor bank**

The CE bank is compact in design and a typical view of 16 stage CE bank is shown in Fig.1.2. The fabrication objective is to get linear run out less than 20 microns. Owing to the stringent interchangeable tolerances and precision requirements, all the machining has to be carried out in CNC machines such that the error in individual component is kept as minimum as possible. Overall dimensions are critical because the corresponding organic and aqueous weirs of rotating bowl and stationary bowl should match to improve the performance of the bank. So both organic weir and aqueous weir diameter of rotating bowl must be maintained critical for the working of the extractor bank, where in a special care should be taken while machining.

Normally, this type of thin section high speed rotating bowls are fabricated using electron beam welding where as conventionally readily available pulse Tungsten inert gas (TIG) welding technique using special welding fixture was adopted in order to control distortion. Bending of interconnecting pipe is also difficult since it has to be bent to short radius with different angles at inlet and outlet ports posing lot of challenges in designing and fabrication of bending fixtures. The CE being critical in dimensional tolerances requires rigorous and standardized mock up trials for machining, fit up, welding, and balancing prior to the actual fabrication.

#### **1.4 Welding of thin walled centrifugal extractor rotating bowl**

Thin cylindrical cross sectional components constitute an important class of axi-symmetric structures and are being used in both static as well as in dynamic conditions in most of the engineering applications. The reliability and high performance of such materials and structures in the form of thin-walled cylindrical components are of paramount importance in aerospace, marine, aeronautical structures, pressure vessels and nuclear applications. CE [29, 30] which can be classified under thin walled equipment is used in the nuclear spent fuel reprocessing plants of FBR to recover U and Pu leaving highly radioactive fission products. The separation takes place due to fine dispersion through shearing of liquid layers between the stationary and rotating bowls which results in fast individual phase separation due to high centrifugal field (200–1000g) in turn leads to reduction in contact time and less radiation damage to the liquid solvent.

The design of this particular equipment is such that the level of precision on its dimensions required for the bowl itself is extremely critical. The schematics of CE components are shown in Fig. 1.3(a). During the course of manufacturing of the rotating bowl, the individual parts are being finish-machined and are subsequently welded for integration of the bowl. During the

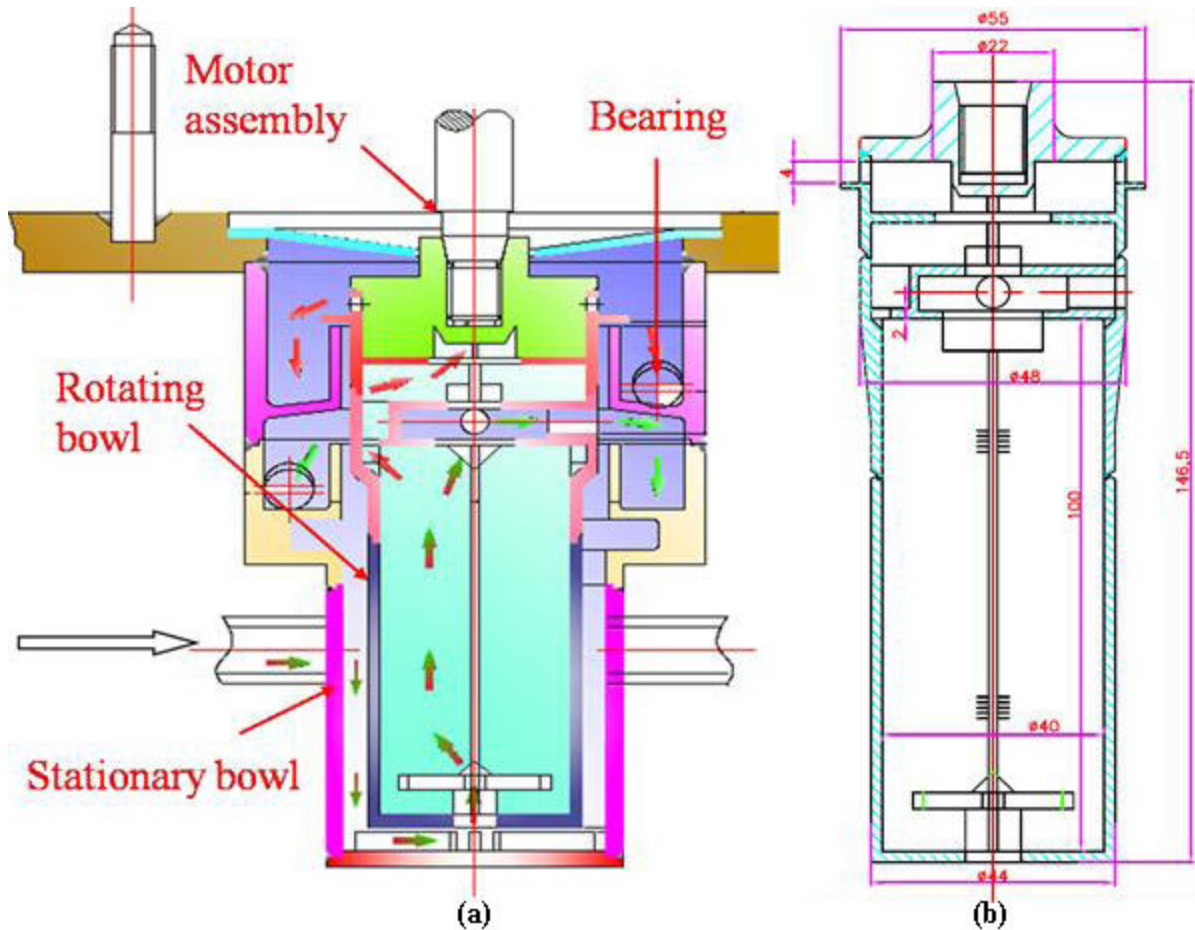


**Fig.1.3: (a) Schematic of the CE and (b) Dimensions of the rotating bowl**

of manufacturing there could be a possibility for the alteration of dimensions of the bowl as the result of distortion introduced while welding. The distortion can be corrected by re-machining of the bowl. The re-machining is seldom practiced because the distortion can be controlled by adopting good engineering practice during welding. Fig.1.3(b) gives the construction of rotating bowl. There are three circumferential welds in the bowl. These joints are to be welded from outside. Tolerances requirements of the finished welded bowl are quite critical such that the plane of upper weld and lower weld must be parallel with in  $\pm 0.015$  mm and the allowable diametrical tolerance of  $\pm 0.010$  mm and overall length tolerance  $\pm 0.015$  mm. The requirement

dictates that overall allowable tolerance of the finished unit shall not exceed the value of  $\pm 0.020$  mm for achieving a smooth and stable operation.

Based on previous experience, the value of the allowable specific unbalance is taken as 1gm-mm/Kg in the design of the CE rotating bowl of 40 mm diameter and with 2mm wall thickness operating at a max speed of 4000 rpm. Dimensional deviations may result in eccentricity and unbalanced residual mass which in turn leads to dynamic instability. When the operating speeds are approaching critical speeds, the amplitudes of vibrations due to the unbalanced mass will drastically increase causing an unwanted noise and turbulent fluid flow. The turbulent fluid flow results in chocking of the fluid. For a CE bowl with the length/diameter ( $L/D$ ) ratio above 3, the critical speed will often be the main factor controlling the maximum obtainable speed and it can therefore be desirable to increase the critical speed in order to obtain a high  $L/D$  ratio without sacrificing the maximum operating speed. The vibrations in this case are usually harmless, but as very large forces could be acting on the support, where the designer must take in to account the magnitude of these forces, and the foundation must be designed to withstand these forces.

Generally, for the best performance, the axis of symmetry and axis of rotation shall be coincided. But, in practice there is an eccentricity between these axes because of imbalance in masses. Even for the statically balanced bowl, it is possible that one end may have an eccentric center of gravity if correction has been applied to the opposite end for accurate balancing of masses. This can be noticeable when the bowl is under operation. Because of the eccentricity between these axes the annular gap between the rotating bowl and outer bowl varies during the operation. The rotation of the bowl results in a periodic variation in the annular gap at any point. The periodic variation in the gap can be termed as oscillation of the rotation bowl. The oscillation of the rotating bowl results in dynamic instability which can be corrected by couple or moment

balance. An induced distortion during welding of this straight bowl causes varying wall thickness along the face of the bowl as well as around the circumference. When these bowls are operated at higher speeds, the tiny local unbalanced areas (masses) along the face will result in unbalanced heavy load at higher speeds. During rotation at higher speeds, the unbalanced heavy load will push the rotating bowl radially outward and increases the eccentricity between the axes. Further, the irregularities, may lead to deformation of the shell of the bowl and results in shape-change of the bowl. This condition is called as whip or kinetic unbalance. This whip can be corrected by individual correction in every plane wherein imbalance exists, with great care during each and every step in manufacturing.

While fabrication of the bowl, the welding of thin sections is a crucial operation in deciding the dimensions of the final bowl. Tremendous efforts have been put in the past few decades by numerous researchers showing a remarkable development in new welding techniques for better quality products capable of excellent in-service against thermal and structural load bearing features. Masubuchi *et al.* [1] discusses various types of welding induced distortion, residual stresses in thin walled structure and the respective control and mitigation techniques. Distortions are considered as the most common defects occur during welding which can adversely affect the dimensional accuracy and thus lead to expensive corrective work. Hence, it is very essential to forecast the distortions in advance in order to minimize the negative effects, so that it helps in improving the quality of welded parts and finally to reduce the manufacturing costs as well. In general, residual stresses that would exist in a body if all external loads and restraints were removed, may introduce in the component during different phases of their life cycle. In engineering structures most of the residual stresses are induced during their manufacturing phase including casting and forging, sheet metal forming, shaping (shearing, bending, grinding,

machining etc.) and welding. Welding residual stresses are produced in a component as a consequence of local plastic deformations introduced by local temperature history consisting of a rapid heating and subsequent cooling phase. A number of catastrophic failures of high pressure vessels of thin-cylindrical shell structures due to longitudinal and circumferential welds are reported in the literature. Both weld residual stresses and distortions can significantly affect the performance and reliability of the welded components.

### **1.5 Motivation of this study**

There are a few studies [14-20] that deal with the measurement of thermal cycles and residual stresses in thin walled cylinders particularly for different weld speeds and powers keeping the heat input as constant. Further, a limited literature [21-23] is available on the variation in longitudinal and circumferential residual stresses along the radial distance from the outer surface for different weld speeds and powers with constant heat input. Distortions are considered as the most common defects occur during welding which can adversely affect the dimensional accuracy and thus lead to expensive corrective work. Hence, it is very essential to forecast the distortions in advance in order to minimize the negative effects, so that it helps in improving the quality of welded parts and finally to reduce the manufacturing costs as well.

The relationship between weld speed and power *versus* residual stress and their distributions can be established at constant heat input, through FE modeling. These FE models can be used for optimizing weld parameters for obtaining sound welds. However, the specific studies such as different conditions of weld speeds and powers with constant heat input on the variation in welding distortions along the longitudinal and radial directions are scarcely reported in the literature. Hence, different cases of weld speeds and power with constant heat input are

considered to study the variation in welding distortions. In this regard, a synergistic approach is followed involving both FEM using a coupled thermo-mechanical analysis and experimental work for estimating the induced distortion during welding. The dynamic behavior is studied comprehensively through numerical analysis by introducing the obtained distortions on the surface of the bowl after welding for different conditions such as welding speed, clamping conditions and weld sequence etc.

Thus, the complex phenomenon in these types of structural components demands the attention and focus of the researchers to ensure the structural integrity for improved performance and reliability. It is envisaged that the optimized design due to the optimized weld parameters, reduced failure rates, improved product life and most importantly leads to the better performance. The main purpose of this study is aimed at

- Ensuring a stringent dimensional tolerances on critical CE rotating bowl assembly by properly controlling the critical process parameters
- To minimize the welding induced distortions and residual stresses thereby improving quality and performance of the CE
- Avoiding the dynamic instability due to unbalanced residual mass
- Minimizing the wastage and mock-up trails
- Providing a robust technology to industries for manufacturing critical CE

## 1.6. Objectives and Scope of the research

The scope of the present work is limited to circumferential welding of thin walled cylindrical cross sectional components, primarily focusing the welding induced residual stresses and deformations. The present investigation is based on the combination of numerical simulations and experimental investigations for the analysis of complex welding phenomenon. The major affecting parameters are considered to analyze various contributing factors like temperature gradients, deformations and residual stresses and validated against experiments.

This work mainly comprised of the investigations of weld induced residual stress fields and distortion patterns, the influence of various weld process parameters on dynamic performance of the CE rotating bowl assembly. In this regard, the effect of weld speed, heat input and welding sequence and finally the effects of different clamping conditions are considered. Further, the scope and major objectives of this study as follows,

- For evaluation of weld induced residual stresses and distortions, the analysis of heat source fitting to be carried out with heat inputs ranging from 200-500 J/mm to arrive an optimal heat input for obtaining proper weld penetration and heat affected zone (HAZ).
- For a constant heat input, studying the influence of different weld speeds and powers on temperature distribution, residual stresses, weld induced distortion and their distributions.
- Computing the residual stresses on both the inner and outer surfaces as well as along the radial direction. Also investigation of the variation in welding distortions along longitudinal and radial directions of cylindrical components.

- Demonstration of the validity of the temperature distribution, residual stress and distortions obtained from numerical simulation with full scale shop floor welding experiments.
- Studying the dynamic behavior comprehensively through numerical analysis by introducing the obtained distortions on the surface of the bowl after welding for different conditions.
- Characterization of the weld joints and heat affected joint and base metal of welded component using scanning electron microscope.

### **1.7 Thesis Outline**

The dissertation is organized in six chapters and the significant contribution in each chapter can be briefly summarized as follows:

Chapter 1 presents introduction to nuclear fuel reprocessing and various process equipments which are amenable for remote operation followed by welding induced residual stresses and distortions primarily concentrating on residual stress evolution and distortion occurrence in circumferentially welded pipe/cylindrical joints. Based on the importance and detrimental effects offered by welding to the structural integrity and dynamic stability of the structures, motivation for the present research work and in line with scope and objectives of the work are established, followed by the brief description of the all chapters.

Chapter 2 is an overall literature review of the previous work published in various articles related to issues in computational welding mechanics. It comprises of mainly welding simulations and experimental work carried out pertaining to circumferential welding of thin section walled components in detail. Efforts being made to cover the significant contributions focusing on

experimental measurement techniques / prediction of residual stresses in welded structures using wide variety of methods employed are outlined.

Chapter 3 gives the modeling and simulation techniques and material properties used in the present study. It consists of the analytical equations and FE formulation of the welding phenomenon followed by the introduction to physics behind the arc and Goldak's [75] approximation. This chapter also describes about the heat source fitting, elasto-plastic material modeling, modeling of heat transfer modes etc.

The results from a number of numerical and experimental studies based on different welding process parameters are presented in Chapter 4. To investigate the effects of welding process parameters comprising welding heat input and welding speed varied explicitly on the temperature distribution and the corresponding influence on weld induced distortions and residual stresses are monitored. The effect of these deformations in particular to the dynamic performance of the CE rotating bowl is also discussed. Distortions and residual stresses in both longitudinal and hoop direction are also presented through detailed parametric studies. Further, the effects of different weld orientations are also presented in this chapter. The aim of the study is to investigate the most appropriate weld process parameters for circumferentially welded thin-walled cylinders especially CE rotating bowl. The chapter provides an overview of validation strategy for FE models and detailed comparison of FE predicted and experimentally measured data.

Finally, in Chapter 5 significant conclusions and the future scope from the present research work are presented.

## **Chapter 02**

### **AN OVERVIEW OF THE LITERATURE ON WELDING OF THIN SECTIONS**

Welding has a number of detrimental effects on the structural integrity and in-service performance of the weldments. These detrimental effects are due to imperfections induced by the welding in the weldments, of which the structural shape change behavior, residual stresses and the weld solidification cracks that are reported to have very severe degrading effects on the mechanical strength and which may possibly can lead to catastrophic failure. A number of catastrophic failures of high pressure vessels of thin-cylindrical shells and other similar structures due to longitudinal and circumferential welds are reported in the literature. Both weld residual stresses and distortions can significantly affect the performance and reliability of the welded components. Therefore, these must be critically dealt while design and manufacturing phases, to ensure intended in-service use of the welded component.

## 2.1 Introduction

The reliability and high performance of thin-walled cylindrical components are of paramount importance in aerospace, marine, aeronautical structures, pressure vessels and nuclear applications. Welding is the mandatory integrating technique available for joining those components of critical equipments, where the specific strength and cost effectiveness are the major design constraints.

Tremendous efforts have been made in the past few decades by numerous researchers showing a remarkable development in new welding techniques for better quality products capable of excellent in-service performance against thermal and structural load bearing features. Despite of these considerable innovations in high temperature joining techniques, still the problems of weld induced imperfections like residual stresses and distortions are the major challenges for the welding engineers due to the complex nature of the welding phenomena.

Masubuchi [1] and Connor [31] discussed various types of welding induced distortions, residual stresses in thin walled structures and the respective control and mitigation techniques. Distortions are considered as the most common defects that occur during welding, which can adversely affect the dimensional accuracy and thus lead to expensive corrective work. Hence, it is very essential to forecast the distortions in advance in order to minimize the negative effects, so that it helps in improving the quality of welded parts and finally to reduce the manufacturing costs as well. Deo *et al.* [32] presented a panel with angular distortion, that is transverse to the welding direction and caused by shrinking near the fusion zone resulting in a change in the angle of the parts.

Chin-Hyung Lee *et al.* [33] have carried out three dimensional FE analysis to estimate the residual stresses in circumferential welds of steel pipes with inside radius to wall thickness ratio ranging from 10 to 100. They have also illustrated the variation in residual stresses at different circumferential locations and the effects of diameter on residual stress distributions. Shim Y *et al.* [34] considered a ramp heat input and included the effect of moving arc in their analysis. They also investigated the effect of various ramp times and observed that 20% of the actual heat input time is the best ramp time. Liang Wang *et al.* [35] have investigated the effect of laser travel velocities with constant power and the laser powers with constant velocity on the distribution of residual stress during laser welding of thin wall plates. In this study, net heat input during welding process was also varied. Spina *et al.* [36] evaluated the effect of welding speeds on the weld profiles and distortion of the components during laser welding of AA 5083 sheets using numerical simulations. This study revealed that as the welding speed reduced the net heat input increased and vice versa. Brickstad *et al.* [37] numerically simulated a multi-pass circumferential butt-welding of stainless steel pipes using a non-linear thermo-mechanical Finite element analysis (FEA) to study the variation in weld heat inputs. They also studied the variation in the through-thickness of the weld and HAZ on the axial and hoop stresses for austenitic stainless steel pipe welds and their sensitivity against weld parameters. Kazuo Ogawa *et al.* [38] investigated the residual stress in penetration nozzles by considering different nominal heat inputs and weld speeds at constant weld power for different weld passes. Chaowen Li *et al.* [39] carried out three dimensional FEA of temperatures and stresses for increasing weld speeds with constant power on different samples. The above study reveals that increase in weld speed at constant power, increases the net heat input. Kermanpur *et al.* [40] studied the effect of variation in net heat input for a GTAW circumferentially butt welded pipes. The study revealed that

increasing the heat input resulted in a wider weld pool along with a higher maximum temperature in the HAZ. Wu, C.S *et al.* [41-42] used different levels of heat inputs with different welding currents by keeping welding speed and voltage as constant for two different arc welding processes (double sided and plasma) in the numerical simulation. They also carried out numerical analysis to predict the temperature field and weld pool shape as a function of welding speed with constant laser power and current. Gery *et al.* [43] investigated the effect of variable welding speeds and energy inputs on the transient temperature distribution, shape and boundaries of fusion zone and HAZ. Dean Deng *et al.* [44] examined the influences of heat input on the size of HAZ, welding residual stress and distortion during numerical simulation of electro slag welding process. Dean Deng *et al.* [45] performed four different cases of welding simulations with constant weld current, voltage and speed to clarify the influence of phase transformation on the residual stress and welding deformation. Teng *et al.* [46] carried out welding simulations on T-shape fillet welding plate and discussed on buckling strength of welded joints and the effect of flange thickness, penetration depth and restraint conditions on distortions and residual stresses. Long *et al.* [47] predicted the temperature variations, fusion zone and HAZ as well as longitudinal and transverse shrinkage, angular distortion and residual stress for various welding speeds and plate thicknesses. Díaz *et al.* [48] carried out the comparative analysis on distortion of TIG welding of austenitic and duplex stainless steels by considering two different net heat inputs for both the stainless steels. Jiang *et al.* [49] studied the effect of different welding heat inputs and layer numbers on residual stresses and deformation in repair welds of stainless steel clad plate. Yanhong Tian *et al.* [50] investigated the effect of heat input and welding speed on the temperature field, especially on the shape and dimensions of the weld pool. It can be observed from the above detailed literature survey that no focused studies had been undertaken

to study the effect of different conditions of weld speeds and powers with constant heat input on the variation in temperature distributions and residual stresses. Further, literature survey also reveals that no studies have been reported on the variation in longitudinal and circumferential residual stresses along the radial distance from the outer surface as a function of different weld speeds and powers with constant heat input. The relationship between weld speed and power *versus* residual stress and their distributions at constant heat input can be established, through FE modeling. Further, these FE models can be used for optimizing the weld parameters for obtaining sound welds.

There have been numerous investigations that pertain to the numerical analysis with experimental validation to understand the temperature distribution, distortions and the residual stresses. During welding, the weld component may undergo severe thermal cycles because of high concentrated heat source in the region of weld centre, which in turn results in distortion and residual stresses in the weld metal in longitudinal as well as in circumferential directions. There are a few studies that deal with the measurement of thermal cycles and optimizing the important welding process parameters such as welding speed, heat input, weld sequence and clamping conditions etc for butt welding of plate.

Sattari-Far I., *et al.* [51] presented a three-dimensional thermo-mechanical analysis to investigate the effect of welding sequence on welding deformations in pipe–pipe joints and showed that a suitable welding sequence can substantially decrease the amount of welding distortions for a particular geometry. Rybicki E.F., *et al.* [52] developed a mathematical model for predicting transient temperature distributions, residual stresses, and residual deflections for girth-butt welds and compared temperature profiles for a two-pass welded pipe. They validated their predicted residual stresses and residual deflections based on a FE representation against individual passes,

temperature dependent elastic-plastic constitutive behavior with the data obtained from a welded 304 stainless steel pipe.

Goldak *et al.* [53,75] described the deformations and stresses during butt-welding of a pipe from the analytical temperature field during welding. They have adopted a thermo-elastoplastic material model in their FEA. They have included the influence of volumetric changes due to phase transformations on the deformations (radial shrinkage) and the residual stresses. They have compared the radial shrinkage and residual stresses calculated using their model with the experimental values. Dong. Y., *et al.* [54] discussed the three-dimensional FEM of residual stresses in a girth-welded, with a main emphasis on modeling procedures for the global residual stress characteristics. They have suggested the shell element model with a heat source moving along the circumferential joint, which is cost effective and capable of predicting the global residual stress features. They have presented the effects of pipe wall thickness and welding speed on residual stresses as well.

Karlsson. R.I., *et al.* [55] have presented a three-dimensional FEM which can predict the temperatures, stresses, and deformations in a single-pass butt-welded pipe. They have observed the residual compressive hoop stresses in the weld and the residual circumferential stress variations, especially in the beginning and end regions of the weld. Fricke. S. *et al.*, [56] have demonstrated a technique that has been developed for numerical simulation of the welding process and validated with the results of welding on austenitic pipe welds. They have accounted for the effect of inter-pass cooling which causes sensitization of the HAZ, the effect of gap width on the resultant weld residual stresses, or the effect of the ‘last pass heat sink welding’ (welding of the final passes while simultaneously cooling the inner surface with water) producing compressive stresses in the root area of a circumferential weld in an austenitic pipe.

Lundback *et al.* [57] have developed a model for weld deposition which is able to describe the material behaviour over a large strain, strain rate and temperature range in welding. They have validated their model with the physical model by measuring temperature and deformations. The phase changes for optimizing residual stresses and distortions are the concern of recent Investigators. Murugan *et al.*, [58] insisted that in a multipass welding operation, the residual stress pattern developed in the material vary with each weld pass. They have measured the residual stresses after each pass using X-ray diffraction method and compared the peak temperatures attained at different points during weld bead deposition for both carbon steel and stainless steels.

Dean Deng *et al.* [59] employed both experimental and the FE methods to investigate the welding residual stress distribution in medium thick-walled austenitic stainless steel pipe in multiple passes. They have developed a model to simulate the temperature fields there by the welding residual stress field. Lee *et al.* [60] developed a three-dimensional FEM for the accurate simulation of circumferential welding that can incorporate the three-dimensional effects. They have conducted parametric studies with inside radius to wall thickness to investigate the effects of pipe diameter on residual stresses.

Teng *et al.* [61] employs the technique of element birth and death to simulate the weld filler variation with time in T-joint fillet welds using thermal elasto-plastic analysis considering the effects of flange thickness, welding penetration depth, and restraint conditions on the residual stresses and distortions. Chang *et al.* [62] aimed at analyzing the thermo-mechanical behavior and evaluation of the residual stresses in butt-welded joints and presenting the data to confirm the validity of currently employed fabrication processes in welded structures and improving further. Kiyoshima *et al.* [63] develop a method based on variable length heat sources which is

time-effective computational approaches for practice engineering analysis of multi-pass joints. They analyzed a dissimilar metal with J-groove joint with axis-symmetric geometrical shape and discussed the influence of heat source model (type) on welding residual stress and distortion. Chakrapani Basavaraju [64] developed an axisymmetric FE evaluation of hoop shrinkage associated with circumferential butt welds in thin wall stainless steel pipes. Bachorski M.J. *et al.* [65] used linear elastic finite-element modelling technique that has been developed based on shrinkage volume approach to predict post-weld distortion in single V butt welded plates.

Arc welding is an effective joining method to produce high strength welded structures. Due to the non-uniform expansion and contraction of the weld metal and surrounding base metal by heating and cooling cycles during welding, thermal stresses occurs in the weld and the adjacent areas producing significant residual stress fields. These high magnitude residual stresses of the order of yield strength of the material within the HAZ can be a major threat for the in-service structural integrity of welded structures. The strains produced during the heating phase always induce plastic deformation of the metal. The stresses resulting from these strains combine and react to produce internal forces that cause a variety of welding distortions. The problems of reduced strength of the structures in and around the weld zone due to residual stresses and fitment/appearance issues due to poorly fabricated and distorted structures is a major concern of the welding industry for decades. Therefore, precise prediction of stress fields and distortions patterns (transient and residual) is of critical importance to ensure the in-service structural integrity of these welded structures. GTAW and Gas Metal Arc Welding (GMAW) process are the obvious selection in this regard due to excellent weld joint features. In general these welds are commonly produced by single or double "V" joint configuration penetrations and single or multiple pass arc welding processes.

## 2.2 Distortion

One of the most troublesome problems a welding engineer usually encounters is that of welding distortion. Welding, however, induces thermal strains in the weld metal and base metal regions near to the weld, resulting in stresses due to non-uniform heating and cooling cycle, which in turn combine and react to produce internal forces that cause bending, buckling, and rotation. These displacements are termed as welding distortions [1]. During the joining of components by welding, the highly localized thermal gradients from welding result in high magnitude residual stresses of the order of yield strength of the material within and around the weld region, along with significant deformation/distortion of the structures to be welded.

In other way, welding induced distortion can be defined as the change in shape and dimension of a welded assembly after welding; when it is free from any of the external forces of thermal gradients. The interaction of solidifying weld metal with the parent base metal, results in change in dimensions and shape of the weldments, generally referred to as welding distortions. Different types of distortion patterns for plate and pipe in both longitudinal and circumferential welding, the mechanism involved and the factors affecting different types of welding distortions were presented by many researchers in recent years. In circumferential welding of thin pipe, the longitudinal distortion which is transverse to the welding direction and caused by shrinking near the fusion zone resulting in a change in the shape of straight pipe. Fig. 2.1 portrays weld induced distortion in a circumferentially butt welded pipe joint.



**Fig.2.1: weld distortion in a circumferential pipe joint**

In circumferential welding of pipe mainly there are two types of dominating distortions, the axial shrinkage and the radial deflection. In this case, it is possible that the component can have expansion and shrinkage. The shrinkage of the weld in the circumferential direction induces circumferential force, shearing force, and bending moments, to the cylinder, which are the resultants of the residual stresses in both circumferential and axial directions. Thus, the state of stress in a circumferential welded pipe may be quite different of that in the flat plate.

### **2.3 Residual Stress**

In order to analyze the residual stresses and distortions due to welding, a thorough understanding of heat transfer, metallurgical transformations and mechanical fields and the interactions in between them are needed [1]. Of course, the welding is difficult problem to solve mathematically due to the transient temperature distributions, moving heat source design, material deposition, temperature dependent material properties, metal plasticity and elasticity, transient heat transfer and thermo-mechanical coupling etc. Despite of these considerable innovations in high temperature joining techniques, still the problems of weld induced imperfections like residual stresses and distortions are major challenges for the welding engineers due to the complex nature of the welding phenomena.

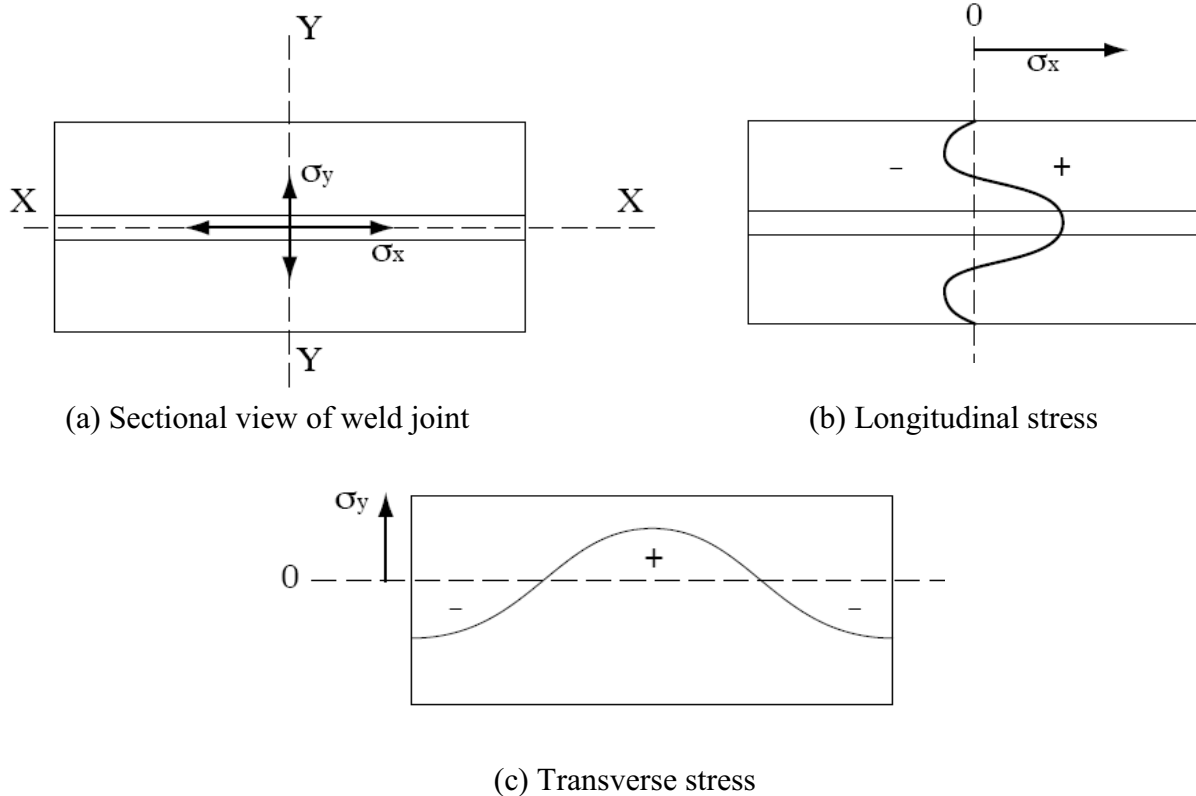
Welding residual stresses are produced in an assembly as a consequence of local plastic deformations introduced by local temperature history consisting of a rapid heating and subsequent cooling phase. During the welding process, the weld area is heated up sharply compared to the surrounding area and fused locally. The material expands as a result of being heated. This expansion is restrained by the surrounding cooler area, which gives rise to thermal stresses. The thermal stresses partly exceed the yield limit, which is lowered at elevated temperatures.

Consequently, the weld area is plastically hot-compressed. After cooling down too short, too narrow or too small compared to the surrounding area, it develops tensile residual stress, while the surrounding areas are subjected to compressive residual stresses to maintain the self-equilibrium.

In case of circumferentially welded pipe joints, there are mainly two types of residual stresses which may develop after welding, which can be classified into axial and hoop stress. The stress normal to the direction of the weld bead is known as the axial stress. In general, compressive and tensile axial stress fields can be observed in and near the weld region on the outer and inner surfaces of the cylinders respectively. Varying shrinkage patterns through the wall thickness on the inner and outer surfaces, due to different temperature gradients results in tensile and compressive residual stress fields on inner and outer surfaces, respectively near the weld line. The stress parallel to the direction of the weld bead is known as the hoop stress. The residual hoop stresses are developed due to the radial expansion and contraction during the heating and cooling sequence of the welding process.

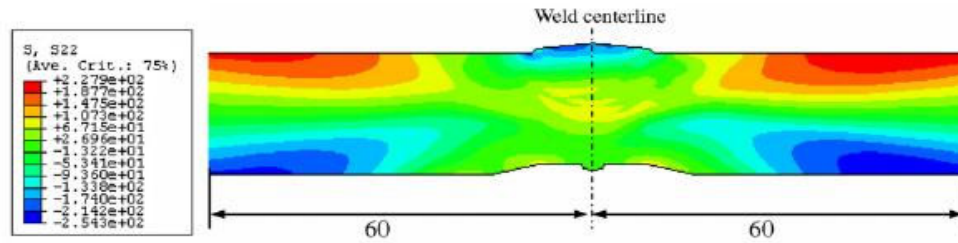
Although, the experimental investigations provide valuable insights into the process of arc welding, many experimental techniques are complex and expensive and some quantities, such as the transient stress/strain development during welding, cannot be measured. Furthermore, traditional trial and error approach based on costly and time consuming welding experiments encounters hindrance to sound welds due to welding process parameters optimization. In order to get an appropriate insight into the process, to extend the application of arc welding process on shop floor level with high reliability and cost effectiveness, it is mandatory to apply appropriate control techniques for both distortion and residual stresses. A synergistic approach involving both FEM and experimental work has proven very useful, which often fails to provide a complete picture of temperature and stress/strain/deformation distribution in the weldment. On the other hand, detailed experimental measurements of the residual elastic strain distributions in welded parts are typically not feasible due to significant resource (man, machine and material) consumption. Mathematical modeling for residual stress evaluation provides a resource effective method in comparison to the experimental methods. However, development of the modeling scheme again demands an experimental data.

Fig.2.2 shows the residual stress distribution of a single pass weld made automatically with no intermediate stops and starts. Measurements of the residual stress in real welds show that this model is quite accurate in predicting the residual stress in single pass welds.



**Fig.2.2: Residual Stresses developed during welding of a butt joint**

A little significant contribution for the welding residual stress distribution and its effects on the performance and structural integrity of circumferentially welded thin-walled cylinders is reported and further investigation is yet to be explored. Therefore, it demands immediate attention and focus of the researchers to ensure the structural integrity of those structures for better product quality and reliability. It is anticipated that the design optimization due to the appropriate weld parameters for thin cylindrical welded shell structures can be the major contributions from this research. It is known that one of the main contributing factors for slow-growing cracking in parts exposed to radioactive environments is the presence of residual tensile stresses near the surface.



**Fig.2.3: Axial stress distribution inside and outside surfaces of circumferential pipe joint considered by (Deng *et al.*[66])**

Teng and Chang [46] presented sequentially coupled thermal stress analysis for the determination of residual stresses. They presented parametric studies based on axis-symmetric FE models to demonstrate the effects of pipe diameter and wall thickness on residual stresses. Temperature dependant material properties were used for elastic-perfectly plastic material model without solid state phase transformations. Their results exhibited self balancing behavior of residual stresses. Both the axial and hoop stresses were tensile on the inner surface near the weld centerline and stress reversal occurred in the regions away from the centerline as shown in Fig.2.3 & 2.4. They used three-dimensional shell element models and analyze welding residual stresses on the same sized pipes to investigate the effect of pipe wall thickness.

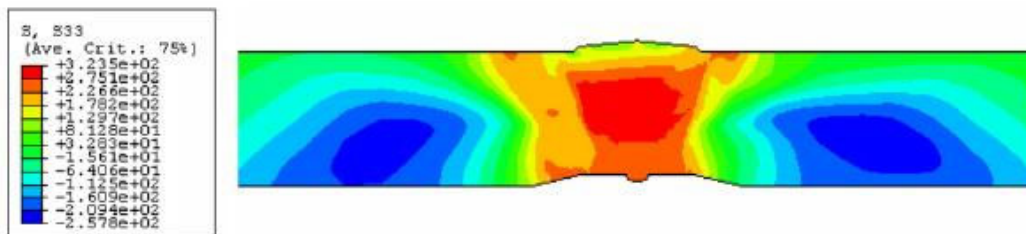


**Fig.2.4: Hoop stress distribution inside and outside surfaces of circumferential pipe joint considered by (Deng *et al.*[66])**

The FE simulations of welding being highly non-linear transient phenomenon is a highly computational power intensive, therefore the use of three dimensional models is limited to the single pass weld only.

Many authors have focused their investigations on weld induced distortion patterns, the influence of various process and geometric parameters on weld induced residual stresses. Few researchers envisaged the effects of tack weld orientation and identifying the optimum welding process sequence and the effects of different clamping conditions on residual stress generation and distortion patterns.

Deng et. al.[66] employed both the experiments and the FEMs to investigate the welding temperature field and the residual stress distribution for a typical medium thick-walled pipe in multi pass welding. Axial and hoop residual stresses distribution contours are shown in Fig. 2.3 and Fig.2.4 respectively.

Further, the study of both in process and post-weld stress mitigation techniques are also important in welding of thin sections. Mainly the above investigations include the geometric parameters comprising of the pipe diameter and wall thickness and process parameters include the variation of heat input. Parametric studies for implementation of best suitable numerical techniques that takes phase changes in to account mainly to analyze the effects of tack weld orientations and selection of feasible structural boundary conditions are the interest of recent investigators.

Efforts were also made to cover the significant contributions focusing on experimental measurement / prediction of residual stresses and distortions in welded structures. Mostly, significant contributions in the field of welding simulations before 2001 are critically reviewed

and discussed by Lindgren L. E *et al.* [67-69]. Mainly their focus is on application of the FE method to predict the thermal, material and mechanical effects of welding by describing appropriate models for heat input and material behavior. Further, Yaghi *et al.* [70] discussed in detail the thin and thick-walled stainless steel pipe welds including pipe diameter effects as well. They have incorporated the effects of solid phase transformations in the simulation of welds. Their investigations include parametric studies and characterization of residual stresses, the effect of material properties on residual stresses, three-dimensional geometric influences etc.

The present study is mainly focused on a three-dimensional transient, non-linear thermo-mechanical simulation of welding of CE rotating bowl assembly followed by the control and mitigation of circumferentially, butt welded thin-walled cylinders. CE which can be classified under thin walled equipment is used in the nuclear spent fuel reprocessing plants of FBR to recover U and Pu leaving highly radioactive fission products [71]. There are three circumferential welds proposed for integration of the CE bowl as a single unit. Therefore adopting proper welding process parameters is extremely important in deciding the dimensions of the final bowl.

Raj *et al.* [72] presented the operational experience and design challenges associated with various equipments / vessels such as fuel dissolvers, evaporators, CE and single pin chopper etc., used in fast reactor fuel reprocessing plants. Natarajan, *et al.*, [73-74] addressed a comprehensive review on the operational experiences in the area of nuclear fuel reprocessing and a brief description of various R&D activities currently being pursued in the CORAL.

The welding process can be modeled using a coupled thermo-mechanical process. However, due to the weak structural to thermal field couplings, sequentially coupled analysis is therefore used

in modeling of welding. In general, welding analysis is carried out by performing a nonlinear transient thermal analysis first, and then applying those results as thermal loads in the nonlinear structural analysis in order to compute distortions and residual stresses.

In this regard, as a first step, the transient temperature history associated with the heat flow during welding can be solved from the thermal analysis. It is generally based on the heat conduction formulation with the moving heat source. The resulting output i.e., temperature history is applied as a thermal load for the stress evolution in the subsequent mechanical analysis. Thermal strains and stresses can be calculated at each time increment by considering the temperature dependent material properties. Also, a plastic yield criterion needs to be followed in evaluating residual stresses that will be accumulated by the thermal strains and stresses induced during welding.

In summary, review of literature shows that there is a wide scope for the future development in the area of thin walled components welding. Generally these thin walled structures are comprising of number of longitudinal and circumferential joints which are the mandatorily integrated by welding. It is evident that a lot of work pertaining to numerical simulation of welding for simplified geometries using two-dimensional analysis by employing symmetry conditions is carried out with certain assumptions due to limited computational cost. To enhance the accuracy of those numerical simulations and closely approach the shop floor welding, the present study aims at developing a fully three-dimensional modeling and simulation technique for material stainless steel (AISI-304) which is being used for manufacturing centrifugal extractors. In this research work, different cases have been verified by varying the weld process parameters to the extent possible validations as well.

## **Chapter 03**

### **NUMERICAL MODELING OF WELDING OF THIN WALLED CYLINDRICAL BOWL AND EXPERIMENTAL**

The welding process is to be modeled using a coupled thermo-mechanical process. However, due to the weak structural to thermal field couplings, sequentially coupled analysis is therefore used in general by performing a nonlinear transient thermal analysis first. Then the results of the thermal analysis will be applied as thermal loads in a nonlinear structural analysis to compute distortions and residual stresses.

#### **3.1 Thermal analysis**

As a first step, the transient temperature history associated with the heat flow during welding can be solved from the thermal analysis. It is generally based on the heat conduction formulation with the moving heat source. The resulting output i.e., temperature history is applied as a thermal

load for the stress evolution in the subsequent mechanical analysis. The governing partial differential equation for the 3-D transient heat conduction, with internal heat generation is given by the thermal equilibrium equation.

### 3.1.1 Thermal Model: Temperature distribution

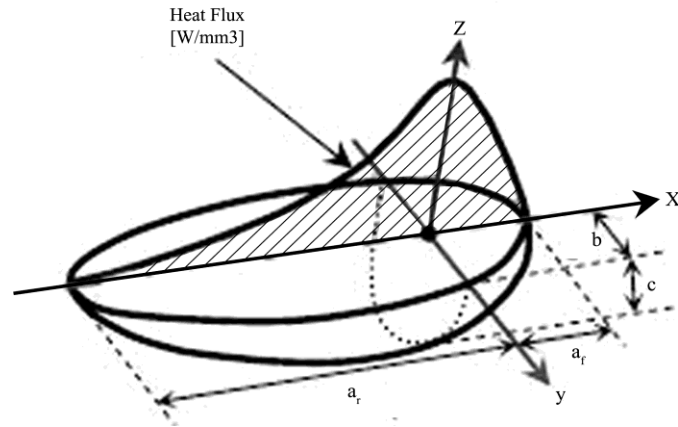


**Fig.3.1: Goldak Double Ellipsoid Heat Source Model [75]**

Generally, the residual stresses are not only dependent on non-uniform temperature distribution generated during the welding but also sensitive to transient temperature distribution because of moving heat source. In this study, the heat from the moving weld source is applied as a volumetric heat source with a double ellipsoidal distribution as proposed by Goldak [75]. This is shown in Fig. 3.1 and can be expressed as

$$\dot{Q}\{x, y, z\} = \dot{Q}_0 \exp - \left\{ \frac{x^2}{a^2} + \frac{y^2}{b^2} + \frac{z^2}{c^2} \right\}, \quad (3.1)$$

where  $\dot{Q}\{x, y, z\}$  represents the net internal volumetric rate of heat generation within the weldment,  $x, y$  and  $z$  are the coordinates in the double ellipsoid reference system. In Fig. 3.2,  $a$  (i.e.  $a_f$  and  $a_r$ ),  $b$  and  $c$  are the lengths which characterize the distribution of energy in heat

source. The heat source is centered at the origin of a frame of reference which moves with the welding torch. The term  $\dot{Q}_0$  is the power of the welding heat source and is defined as

$$\dot{Q}_0 = \frac{2\eta VI}{abc\pi\sqrt{\pi}\operatorname{erf}\left\{\frac{z}{c}\right\}}, \quad (3.2)$$

where  $\eta$ ,  $V$  and  $I$  are weld efficiency, voltage (volts) and current (amperes), respectively. Thereafter, the temperature distribution within the component is modeled by equation of conservation of energy and by non-linear isotropic Fourier heat flux constitutive equation. In the present thermal model, mainly three factors such as heat losses due to radiation and convection, heat transfer in the weld pool and thermal effects during solidification have been considered. Radiation losses dominate at higher temperatures near to and in the weld zone while convection losses dominate at lower temperatures away from the weld zone. This thermal boundary condition is employed for all free boundaries of the cylindrical component. To consider the heat transfer due to fluid flow in the weld pool, a temperature dependent thermal conductivity was used. The thermal effects due to solidification of the weld pool are modeled by taking in to account the latent heat of fusion. The ambient temperature was assumed to be  $T_0 = 20^{\circ}\text{C}$ . Therefore the initial conditions for this study are  $T(x, 0) = T_0$ , accordingly all the thermal and mechanical properties are considered corresponding to room temperature. In this investigation, a sequentially coupled thermal-metallurgical-mechanical analysis was performed. The term ‘sequentially coupled’ means that the transient temperatures at each node and phase fractions are first computed in a coupled thermal-metallurgical analysis. The thermal histories and its corresponding phase fractions are then applied as a predefined field in the mechanical analysis.

### 3.1.2 Thermo elastic-plastic mechanical Model: Distortions and Residual stresses

In the mechanical analysis, the temperature history obtained from the thermal analysis can be used input as a thermal loading for the structural analysis [76]. The thermal strains and stresses can be calculated at each time increment by considering the temperature dependent material properties to account for the thermal effects. Also, the thermal state effects the plastic yield criterion results in residual stresses that will be accumulated by the thermal strains and stresses.

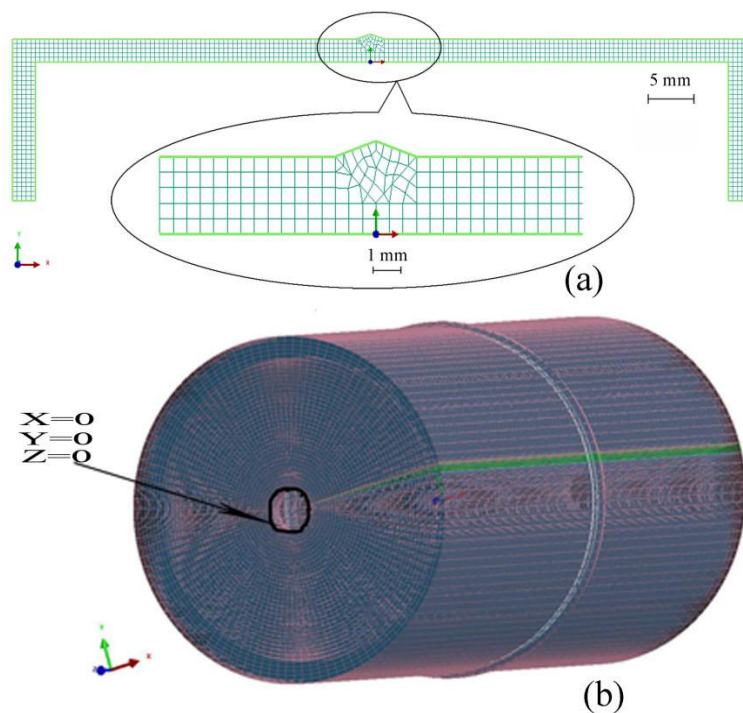


**Fig.3.2: Finite element model (a) 2-D mesh and (b) 3-D mesh with boundary conditions**

Analysis was carried out to evaluate the distortion and state-of-stress induced during welding, referred as mechanical analysis, using the same FEM, which is used in the thermal analysis. The 2-D mesh and 3-D mesh are shown in Figs. 3.2 (a) and (b), respectively. The details of boundary conditions used in the analysis and dimensions of the components for simulation model are given in Fig. 3.4. With boundary conditions such as  $U_X = U_Y = U_Z = 0$ , the component is constrained at

both ends in  $X$ ,  $Y$  and  $Z$  directions. The mechanical analysis was carried out using the temperature histories that were obtained by the thermal analysis.

The constitutive laws relating stress, strain, and temperature are nonlinear in the theory of plastic deformation of solids. There are two basic sets of equations that are used in the mechanical analysis i.e., the equilibrium equation and the constitutive equation, are as follows:

The governing equilibrium equation is 
$$\sigma_{ij} + \rho b_i = 0 \tag{3.3}$$

Where,  $\sigma_{ij}$  is the stress tensor and  $b_i$  is the body force. The stress tensor is symmetrical, i.e.  $\sigma_{ij} = \sigma_{ji}$ .

The corresponding constitutive behavior can be modeled using a Rate-independent elastic–plastic material model considering any elasto-plastic yield criterion like either the Von Mises yield criterion or the other, the temperature-dependent mechanical properties and the linear isotropic hardening rule.

The residual stresses arise due to incompatible strains caused by thermal gradients and microstructural changes, and therefore it is necessary to consider thermo-elasto-plastic formulation. Hence, the total strain ( $\epsilon$ ) can be expressed as

$$\epsilon = \epsilon_e + \epsilon_p + \epsilon_{th} + \epsilon_{tp} \tag{3.4}$$

Here  $\epsilon_e$  is the elastic strain,  $\epsilon_p$  is the plastic strain,  $\epsilon_{th}$  is the thermo-metallurgical strain and  $\epsilon_{tp}$  is that due to phase transformation. To calculate the thermo- metallurgical strain, the strains that

arise due to thermal expansion and phase change were incorporated. This strain  $\varepsilon_{th}$  is given as

$$\varepsilon_{th} = \sum f_i \varepsilon_{th_i}(T), \quad (3.5)$$

where  $\varepsilon_{th_i}(T)$  is the thermo-metallurgical strain corresponding to phase  $i$  at temperature  $T$  and  $f_i$  is the phase proportion of phase  $i$ . Though during welding it is known that the solid state phase transformation can give rise to  $\varepsilon_{tp}$ , for the investigated AISI 304 stainless steel, the  $\varepsilon_{tp}$  component is negligible and is thus not considered.

The elastic strain component is computed knowing Young's modulus  $E(T)$  and a constant Poisson's ratio ( $\nu=0.33$ ) for an isotropic material. The dependence of  $E(T)$  with temperature was used while evaluating the elastic strain. The plastic strain component due to large thermal gradients during heating and cooling was computed following the plastic model which is for the case of isotropic hardening. The employed model further had the features of Von-Mises yield surface and temperature dependent mechanical properties.

### 3.2 Finite element formulation

The corresponding finite element equations for both thermal and mechanical analysis are obtained by choosing a form of interpolation function representing the variation of the field variables, namely temperature,  $T$  and displacement,  $U$ .

For isotropic material, 3-D temperature distribution can be written as.

$$\rho C \frac{\partial T}{\partial t} = \frac{\partial}{\partial x} \left( K \frac{\partial T}{\partial x} \right) + \frac{\partial}{\partial y} \left( K \frac{\partial T}{\partial y} \right) + \frac{\partial}{\partial z} \left( K \frac{\partial T}{\partial z} \right) + Q \quad (3.6)$$

Matrix form of the above equations can be written as

$$\rho C \frac{\partial T}{\partial t} = (L)^T (D \{L\} T) + Q \quad (3.7)$$

Where,

$$L = \begin{bmatrix} \frac{\partial}{\partial x} \\ \frac{\partial}{\partial y} \\ \frac{\partial}{\partial z} \end{bmatrix} \text{ and } D = \begin{bmatrix} K & 0 & 0 \\ 0 & K & 0 \\ 0 & 0 & K \end{bmatrix}$$

Finite element equation including boundary condition may be written as follows

$$[C]\{T\} + [K]\{T\} = \{F_E\}, \quad (3.8)$$

in which,

$$[C] = \int_V C [N][N]^T dv \quad \text{Specific heat matrix} \quad (3.9)$$

$$[K] = \int_V ([B]^T [D] [B]) dv + \int_A h_f [N][N]^T dA \quad \text{Thermal conductivity matrix} \quad (3.10)$$

$$\{F_E\} = \int_V Q [N] dv + \int_A h_f T_B [N] dA \quad \text{Heat generation \& convection matrix} \quad (3.11)$$

Where:

$\rho$  is the density ( $\text{kg/m}^3$ ),

$C$  is the specific heat ( $\text{J/kg.K}$ ),

$K$  is the conductivity ( $\text{W/m.K}$ ),

$h_f$  is the convective heat transfer coefficient ( $\text{W/m}^2.\text{K}$ ),

$Q$  is the rate of internal heat generation per unit volume ( $\text{W/m}^3$ ),

[N] is the matrix of element shape functions,

[B] is the matrix of shape functions derivative, and

{T} is the vector of nodal temperature.

The temperature fields obtained by solving the above equations from thermal analysis will be further used as input for structural response (stress / strain fields) in mechanical (structural) analysis. The finite element equation for mechanical analysis may be written in the incremental form as

$${}^{i+1}[K_1]\{\Delta U\} - {}^{i+1}[K_2]\{\Delta T\} = {}^{i+1}\{R\} - {}^i\{R\} \quad (3.12)$$

in which:

$$[K_1] = \int_V [B]^T [D^{ep}] [B] dV, \quad (3.13)$$

$$[K_2] = \int_V [B]^T [C^{th}] [M] dV, \quad (3.14)$$

$$\{R\} = \int_S [N]^T \{p\} dS + \int_V [N]^T \{f\} dV, \quad (3.15)$$

$$[D^{ep}] = [D^e] + [D^p]. \quad (3.16)$$

Where,

{Δ U} is the incremental of nodal displacement,

{Δ T} is the incremental of nodal temperature,

[B] is the matrix of strain-displacement,

$[D^e]$  is the matrix of elastic stiffness,

$[D^p]$  is the matrix of plastic stiffness,

$[C^{th}]$  is the matrix of thermal stiffness,

$[M]$  is the temperature shape function,

$\{P\}$  is the vector of traction or surface force,

$\{f\}$  is the vector of body force, and

' $i$ ' is the current step of analysis.

The vector of nodal displacement at  $(i+1)^{th}$  time step could be obtained from:

$${}^{i+1}\{U\} = {}^i\{U\} + \{\Delta U\} \quad (3.17)$$

Finally, the stress in the structure can be updated using the following stress-strain

$${}^{i+1}\{\sigma\} = {}^i\{\sigma\} + \{\Delta\sigma\}, \quad (3.18)$$

$$\{\Delta\sigma\} = [D^{ep}][B]\{\Delta U\} + [C^{th}][M]\{\Delta T\} \quad (3.19)$$

In order to solve the above equation, commonly, the iterative numerical solvers implemented based on Newton-Raphson (or) Runge-Kutta methods can be used.

### 3.3 Material properties

While performing weld simulation, it is important to consider the variation of thermo-physical and thermo-mechanical properties of AISI 304 SS material with temperature. Thermo-physical properties such as thermal conductivity, specific heat capacity and density were considered. The thermo-mechanical properties that were taken in to account include Young's modulus, yield

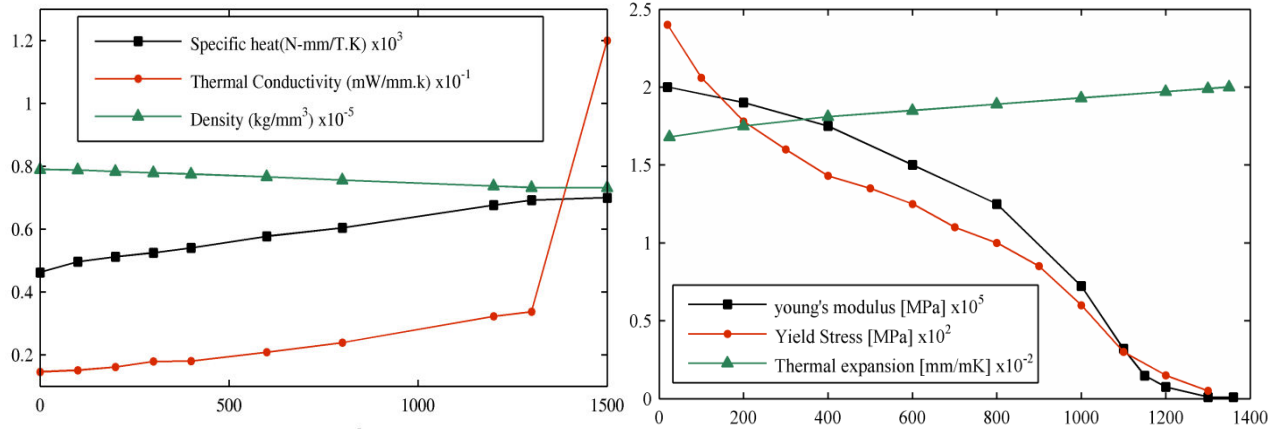


**Fig.3.3(a): Temperature dependent thermo-physical properties** and **Fig.3.3(b): Temperature dependent thermo-mechanical properties** stress and coefficient of thermal expansion. The various properties of AISI 304 SS for the FE simulation are taken from Farid et al., [77] and the thermo-physical and thermo-mechanical properties are shown in Figs. 3.3(a) and 3.3(b) respectively. The solidus and liquidus temperatures were considered as 1360<sup>0</sup>C and 1450<sup>0</sup>C respectively and the value of latent heat of fusion is taken as 260 KJ/Kg. The chemical composition of 304 SS used in the present investigation is given in Table 3.1 and the temperature independent material properties and constants such as Poisson's ratio, convection heat transfer coefficient, Stefan-Boltzmann constant and emissivity are listed in Table 3.2 [78]. The isotropic hardening model with linear strain hardening behavior was assumed for the FE analysis. In this investigation, four different cases of heat input were taken to study the distribution of molten zone and HAZ area. These four

different cases are listed in Table 3.3. Temperature distributions for all cases of heat source fitting are described in the section 4.1.

**Table 3.1 Chemical composition (in Wt %) of AISI 304 stainless steel**

<b>C</b>	<b>Cr</b>	<b>Mn</b>	<b>Ni</b>	<b>Si</b>	<b>S</b>	<b>P</b>	<b>Fe</b>
0.07	16-18	1.1-1.3	8.4-9.4	≤ 1	≤ 0.03	≤ 0.045	Bal

**Table 3.2 Material properties used for FE simulation**

<b>Property</b>	<b>Value</b>
Poisson's ratio	0.33
Convection heat transfer coefficient	25 W/m <sup>2</sup> K
Stefan-Boltzmann constant	5.670*10 <sup>-8</sup> W/m <sup>2</sup> K <sup>4</sup>
Emissivity	0.8

**Table 3.3 Welding process parameters used for heat source fitting**

<b>Case</b>	<b>Power=V*I (W)</b>	<b>Weld speed S (mm/s)</b>	<b>Heat input (J/mm)</b>
<b>a</b>	200	1	200
<b>b</b>	300	1	300
<b>c</b>	400	1	400
<b>d</b>	500	1	500



### 3.5 Rotating bowl assembly

In the present work, a synergistic approach is followed involving both FEM and experimental work which has proven to be effective way of design and optimization. As the design of the bowl demands stringent tolerances and critical process parameters, a TIG welding is selected which has not only the capability of controlling the heat input to the weldment but also gives excellent weld joint features as well.

In order to get an appropriate insight into the actual process, so as to optimize the welding process parameters a numerical simulation is carried out using a FE based commercial software package called “SYSWELD” which improves the CE rotating bowl stability by giving high reliability and cost effectiveness weld. It can also measure the quantities such as transient stress/strain development during welding which cannot be measured through experiments.

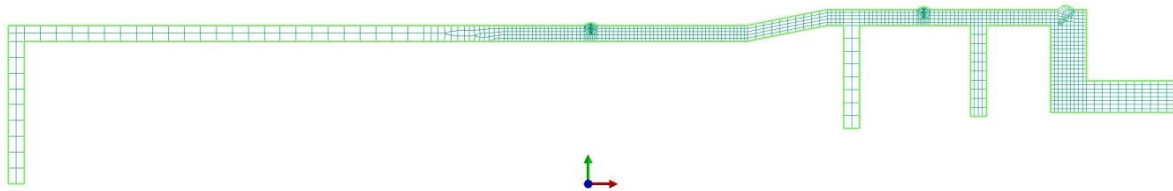


**Fig.3.5: 2D Finite element mesh of rotating bowl.**

A 3D FE mesh has been created based on the geometry of weld panel (2D mesh extruded by 360°) with profile of real weld shape as shown in Fig.3.5. Mesh near the weld bead has been further refined to preserve or reproduce the weld geometrical and metallurgical characteristics in and around the bead and hence to make the important prediction within the HAZ. Welding process is supposed to be modeled using a coupled thermo-mechanical process. However, due to the weak structural to thermal field couplings, sequentially coupled analysis is performed by carrying out a nonlinear transient thermal analysis first, followed by structural analysis to

compute distortions and residual stresses. The material properties of 304L stainless used in the FEA computation is taken from the Metals Handbook of Brown et al. [79] and related articles of Kim et al.[80] and Zhu et al.[81]

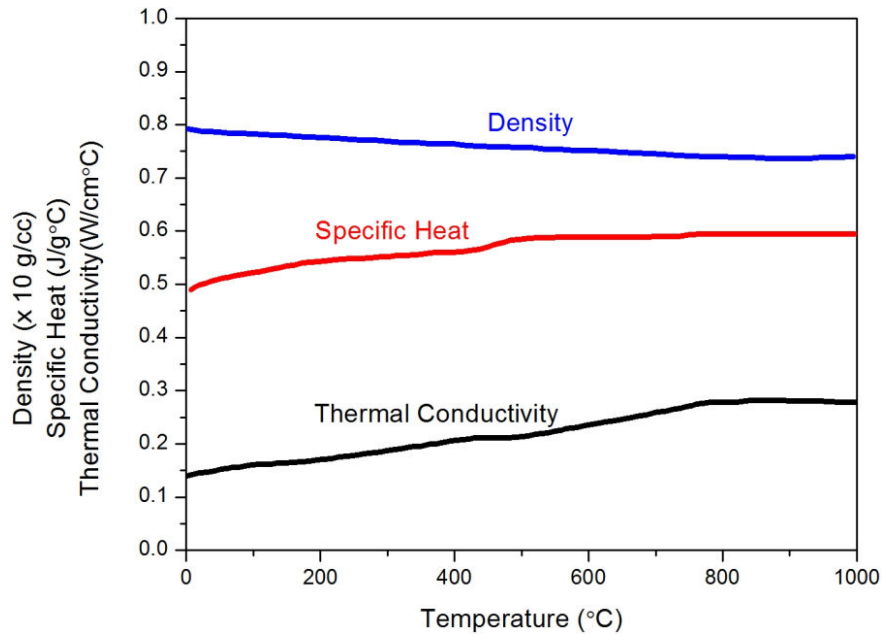


**Fig. 3.6(a): Variation of thermal properties against temperature of SS 304L**

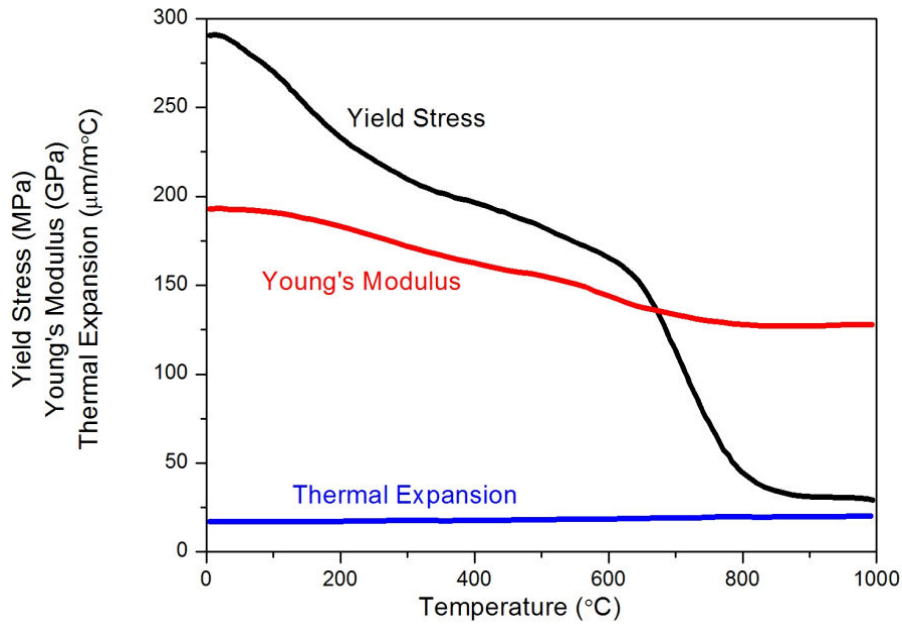


**Fig. 3.6(b): Variation of mechanical properties against temperature of SS 304L**

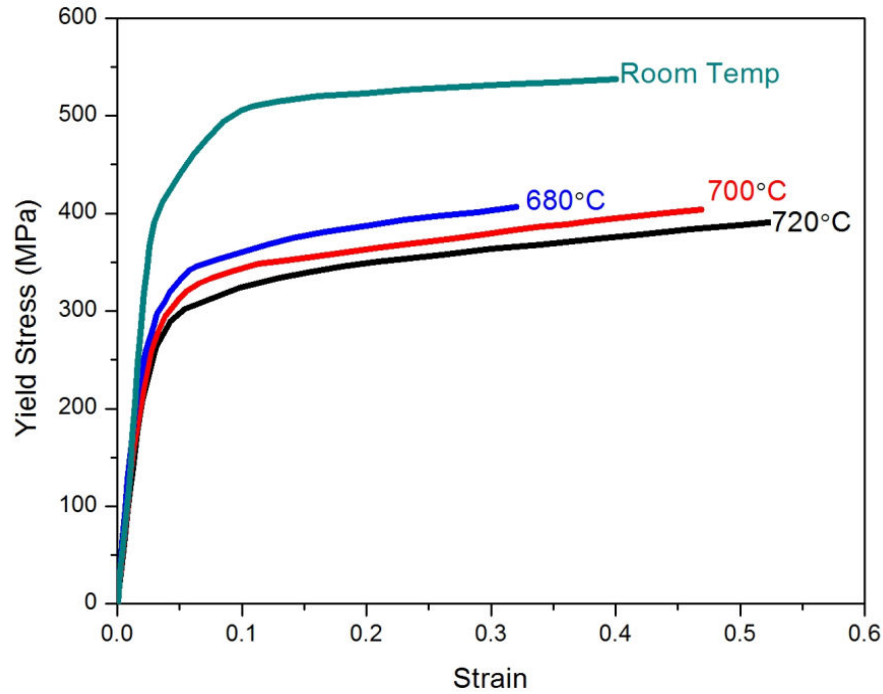


**Fig. 3.6(c): True Stress vs strain curve for SS 304L**

The thermal and mechanical properties are depicted in Fig. 3.6 (a) and (b), respectively. The temperature dependent stress–strain curves of SS 304L stainless for temperatures ranging from room temperature to 720°C obtained experimentally are given in Fig. 3.6 (c).

### 3.5.1 Welding fixtures

The structural boundary conditions used for arresting certain degrees of freedom the welding component using welding fixtures will highly affects the residual stresses developed during welding in addition to the significant effects on the structure deformations [82]. The type of restraint on the weldments determines the control of distortions and residual stress fields. Generally low restraint structure produces significant deformations and low residual stress fields may leads to degraded misaligned welded structures. On the other hand when a work piece is

rigidly fixed will result in significant residual stresses and low deformations. The converse is also true for the welded parts that are not clamped (free-free condition in the present case).

Consequently in most of the over clamping conditions, weld crack phenomenon is dominant, therefore, a distinction has to be made between various clamping conditions that not only keep the residual stresses low, but also reduce the final distortions in the weldment as well. In the present study the rotating bowl assembly is firmly fitted and aligned in a fixture for tack welding as shown in Fig.3.7. Similarly for the circumferential welding of the bowl, a specially designed fixture has been made to minimize the welding induced distortions and residual stresses in the component as shown in Fig.3.8.

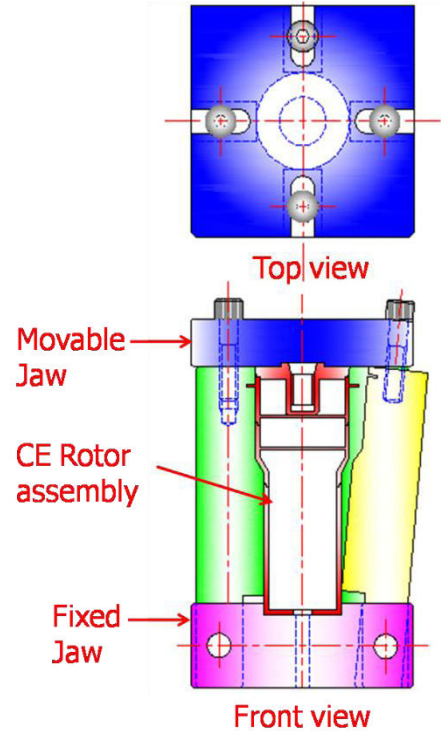


**Fig. 3.7: Fixture for tack welding**

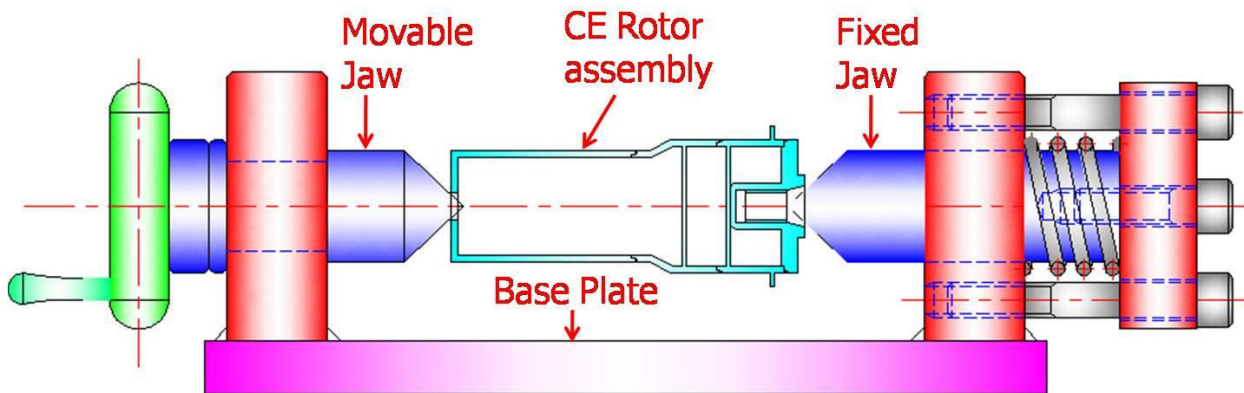


**Fig. 3.8: Special fixture for welding**

In this regard, selection of proper numerical model for predicting the distortion and residual stresses due to welding is essential for improving the performance of thin walled CE rotor.

Therefore, computational methodology and techniques based on FEA for the prediction of temperature profiles and subsequent weld induced residual stress fields and distortion patterns in GTA welded thin-walled cylinders are described in this chapter. It describes the modeling, simulation techniques and material properties used in the present study, which consists of the analytical equations and FE formulation of the welding phenomenon followed by the approximation of subsequent quantities. This chapter also describes about the heat source fitting, elasto-plastic material modeling, modeling of heat transfer modes etc,. Further, the details of specially designed weld fixtures used for the welding of CE rotor are also presented in this chapter. Therefore, the above mentioned formulations and the issues associated with the modeling of welding of thin walled components provided in this chapter will be taken care and further implemented in the next chapter.

## **Chapter 04**

### **RESULTS AND DISCUSSIONS**

The localized non-uniform heating and subsequent cooling can causes complex thermal gradient across it, which may lead to stress and strain fields [1]. These strains produced in the component mainly during the heating phase lead to the plastic deformation of the metal. The stresses resulting from these strains will produce internal forces that cause a variety of welding distortions. Still, the problems of reduced strength of the structures in and around the weld zone due to residual stresses and accurate alignment issues due to poorly fabricated and distorted structures is a sever concern in the welding industry for decades [83-85]. Therefore, accurate prediction of those stress fields and distortions patterns (transient and residual) is of paramount importance to ensure the strength and there by in-service structural integrity of these welded structures.

In Numerical modeling of the welding, the appropriate heat input which gives the desirable weld penetration and HAZ can be arrived based on the analysis of heat source fitting with different heat inputs on trial and error basis, according to the type of welding [86].

#### ***4.1 Heat source fitting***

The amount of heat from the welding process and subsequent cooling controls the weld penetration and the HAZ. The amount of heat input plays an important role as it affects the mechanical properties and metallurgical structure of the weld and the HAZ [87-88]. The heat input required for welding mainly depends on the base metal thickness, thermal conductivity and melting point of the base metal. In arc welding, energy is transferred from the welding electrode to the base metal by an electric arc. During welding both the base metal and the filler metal are melted to create the weld. This melting is possible only if sufficient amount of power and energy density is supplied to the electrode. Heat input in GTAW is a measure of energy transferred per unit length of weld. The heat input ( $Q$ ) in J/mm is the ratio of power and weld speed

$$Q = \frac{\eta VI}{S}, \quad (4.1)$$

Where  $\eta$  = weld efficiency,  $V$  = voltage,  $I$  = current and  $S$  = welding speed (mm/min).

In this investigation, four different cases of heat input were taken to study the distribution of the molten zone and the HAZ area. These four different cases are listed in Table 3.3. Temperature distribution for all cases of heat source fitting is shown in Fig. 4.2. For case-a, with 200 J/mm as

heat input (Fig. 4.2(a)), improper weld penetration and HAZ is observed since maximum temperature of  $1407^{\circ}\text{C}$  was not sufficient for melting the base metal. For case-c and case-d (with

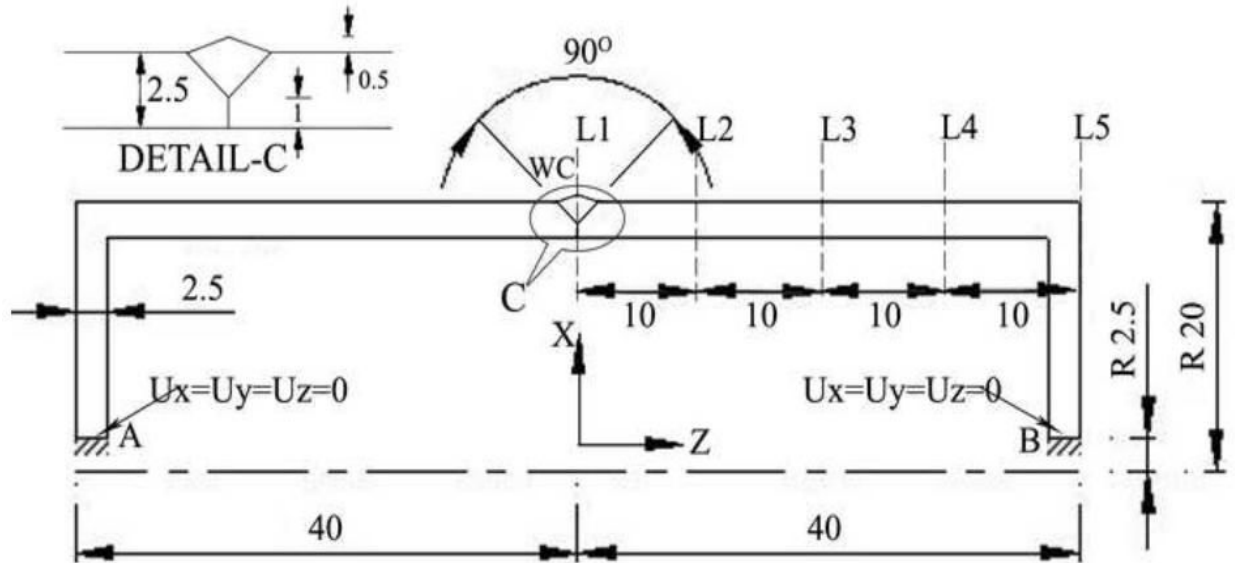


**Fig. 4.1: Schematic 2-D line diagram of cylindrical work piece with boundary condition.**

400 J/mm and 500 J/mm heat input), molten zone and HAZ are broadly spread. Maximum temperatures for case-c and case-d are noticed as  $2521^{\circ}\text{C}$  and  $3007^{\circ}\text{C}$  respectively, which may result in high welding distortions and residual stresses.

During experiments, wire feed rate was 5 to 6 mm/sec to obtain the proper bead quality. The macroscopy of the weld bead shape obtained with 37 A current and 10 V voltage was compared with the predicted weld pool shape as shown in Fig. 4.3. The parameters such as weld heat input, velocity and the double ellipsoidal heat source model which were considered during numerical simulations are saved to an in-built function database for further use in the prediction of thermal and stress fields during welding process simulation.

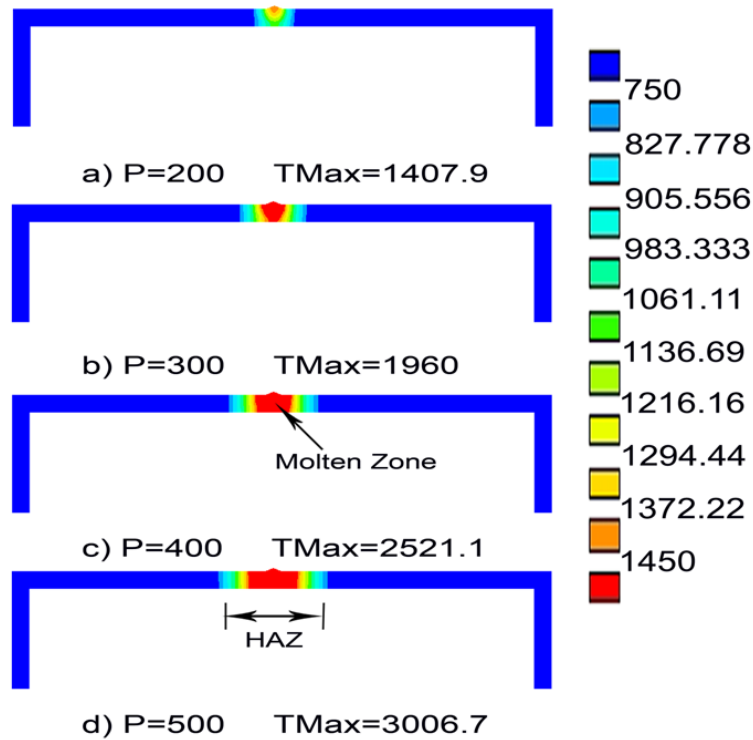


**Fig. 4.2: Temperature distribution for different cases of heat source fitting**

Among the four, case-b (i.e. 300 J/mm heat input) was found to give better weld penetration with controlled molten zone and HAZ at the maximum temperature of 1960<sup>0</sup>C. For this heat input (i.e. 300 J/mm), the Gaussian parameters for double ellipsoid heat source as suggested by Goldak [86] are given in Table 4.1. The experimental weld pool shape and the predicted weld HAZ are shown in Fig. 4.3, and it could be seen that the results are in good agreement with each other. Further, the HAZ was found to be comprised of series of contours that ranged from 700 to 1450<sup>0</sup>C (Fig. 4.3). The above observation directed us to study in detail the temperature distribution and the residual stresses for different combination of weld speed and power giving constant heat input of 300 J/mm. The results obtained based on simulation are discussed in the following section.

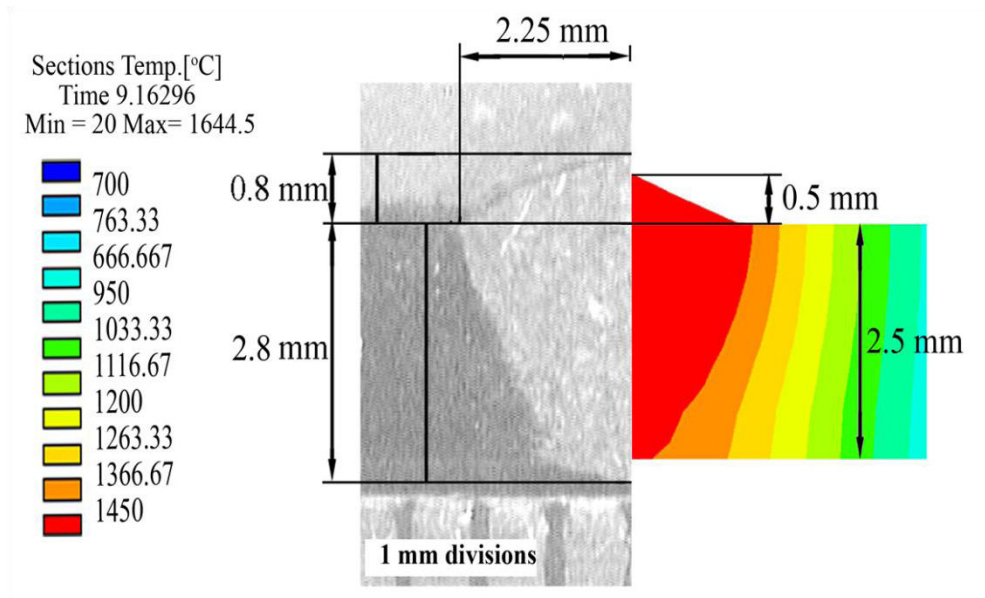


**Fig. 4.3: The weld pool shapes obtained by experiments and FE simulation.**

**Table 4.1: Heat source characteristic parameters**

Parameter	Value
$Q_f$ (W/mm <sup>3</sup> )	42.16
$Q_r$ (W/mm <sup>3</sup> )	42.16
$a_f$ (mm)	1.2
$a_r$ (mm)	1.2
$b$ (mm)	1.2
$c$ (mm)	1.15

In the present study, for different combinations of weld speed and power with constant heat input of 300 J/mm, the temperature distributions have been obtained are described below. Fig. 4.4 & 4.5 shows the three dimensional temperature distributions on the outer surface at 59.6 sec and 85.9 sec respectively for the simulation condition of weld speed = 1mm/sec and power = 300 watts.

Fig. 4.6(a) shows four temperature distributions on the outer surface for four different combinations of weld speed and power as mentioned in Table 4.2. The temperature distribution is taken at 5 mm along the Z coordinate and at 180° section from weld start position during welding. It is observed that the temperatures are attaining near to the peak values at 180° section from weld start position when heat source crosses the section. For example, in case of Fig. 4.6 (a) with weld speed of 1 mm/sec, when the weld torch travels around a circumference of  $\pi \times D$  ( $3.14 \times 40 = 125.6$  mm), weld torch reaches the 180° section at 62.8 sec. Hence, the temperature close to peak is observed at 62.8 sec with 1 mm/sec weld speed. The effect of weld speed and power for the condition of constant heat input is that the peak temperature increases with increase of weld speed and power.

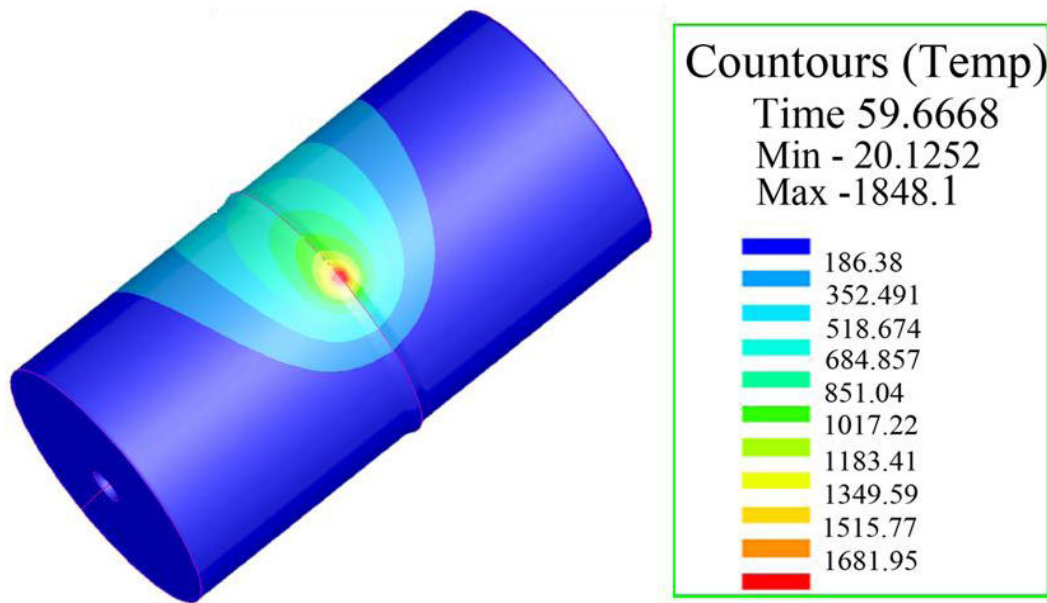


**Fig. 4.4: 3-D Temperature profile on the outer surface**

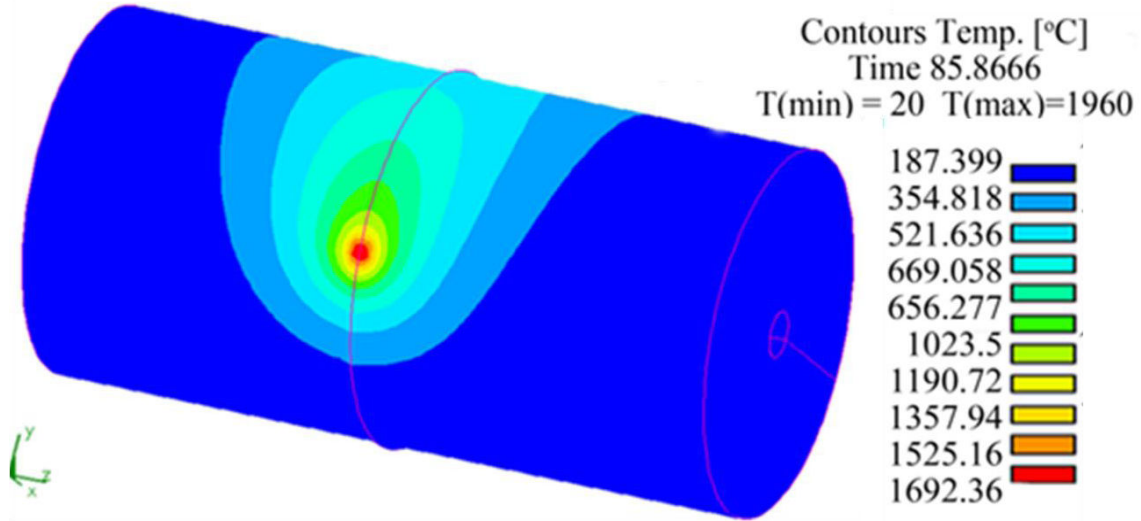


**Fig. 4.5: 3-D Temperature profile on the outer surface**

**Table 4.2: Summary of different combinations of weld speed and power**

	Weld speed S (mm/s)	Power = V×I (W)	Heat input (J/mm)
1	0.5	150	300
2	1	300	300
3	2	600	300
4	3	900	300

#### ***4.2 Welding temperature characteristics - Thermal analysis:***

FE simulation of the welding process, for the constant heat input of 300 J/mm at different combinations of weld speed and power, has been carried out for predicting the temperature characteristics at various locations away from weld. A typical result of the simulation is presented in Fig. 4.5, which depicts three dimensional temperature profile on the outer surface at 85.87 s for the simulation condition mentioned in case-2 of Table 4.2. The elliptically shaped

temperature distribution is observed on the external surface of the component and these are in agreement with the presented literature. Figs. 4.6 (a)-(e) shows the temperature distribution on the outer surface during the welding for five different locations along the Z coordinate at  $180^{\circ}$  section (i.e., mid of the circumference) from the weld start position. These five locations are shown in Fig. 4.1. The temperature distribution profiles are shown in the Figs. 4.6 (a)-(e) for different combination of the weld speed and power as mentioned in Table 4.2. As anticipated, peak temperatures are at the weld location (WL) as shown in Fig. 4.6 (a). From Figs. 4.6(b)-(e), it is apparent that peak temperatures are found to decrease with the measurement locations longitudinally away from the WL.

The peak temperature and temperature distribution profile at each location are observed to be in good agreement with the welding process in practice. It is clear that the temperatures at  $180^{\circ}$  section from the weld start position are high when the heat source crosses the section. For instance, in case of Fig. 4.6(a) with the weld speed of 0.5 mm/s, when the weld torch travels around a circumference of  $\pi D$  ( $3.14 \times 40 = 125.6$  mm), weld torch reaches the  $180^{\circ}$  section after 125.6 s. Hence, the peak temperature is observed at 125.6 s for 0.5 mm/s weld speed. Similarly, peak temperature is observed at 62.8 s for 1mm/ s weld speed. Due to forward heat flow from the weld torch, a preheating action occurs and also temperature falls slowly when the torch crosses the section.

The effect of weld speed and power on temperature distribution for various locations away from the weld is presented in Figs. 4.6(b)-(e). It is observed that the peak temperature increases at the weld centre (WC) with increasing weld speed and power as shown in Fig. 4.6(a). It is discerning to note (Figs. 4.6 (b)-(e)) that the difference in peak temperatures also gets reduced for locations longitudinally away from the WL. The possible reason for such an observation could be that with

increasing weld speed and power, the rate of heat input is higher than the rate of heat dissipation. This also would result in localized heating at the fusion zone.

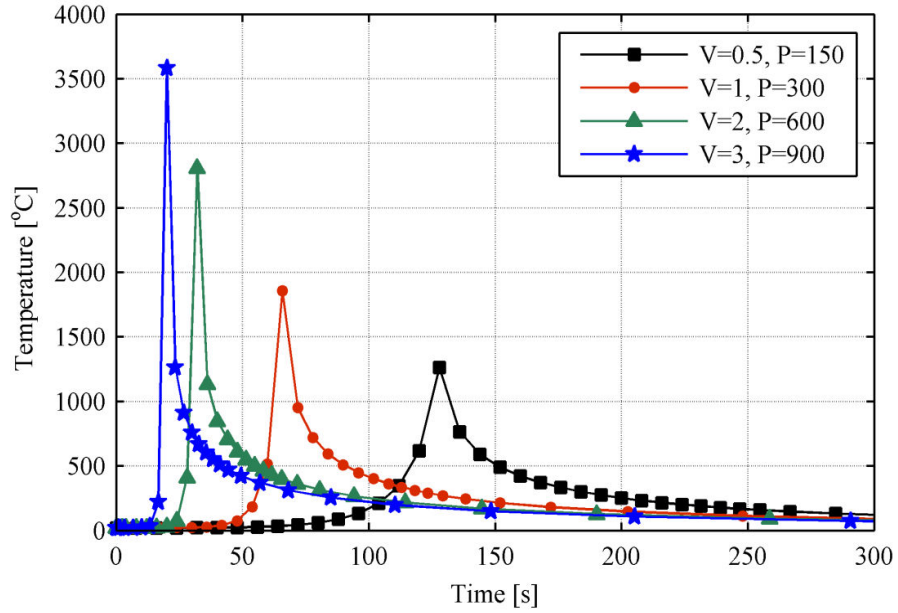


**Fig. 4.6(a): Simulated transient thermal cycles at the weld centre.**

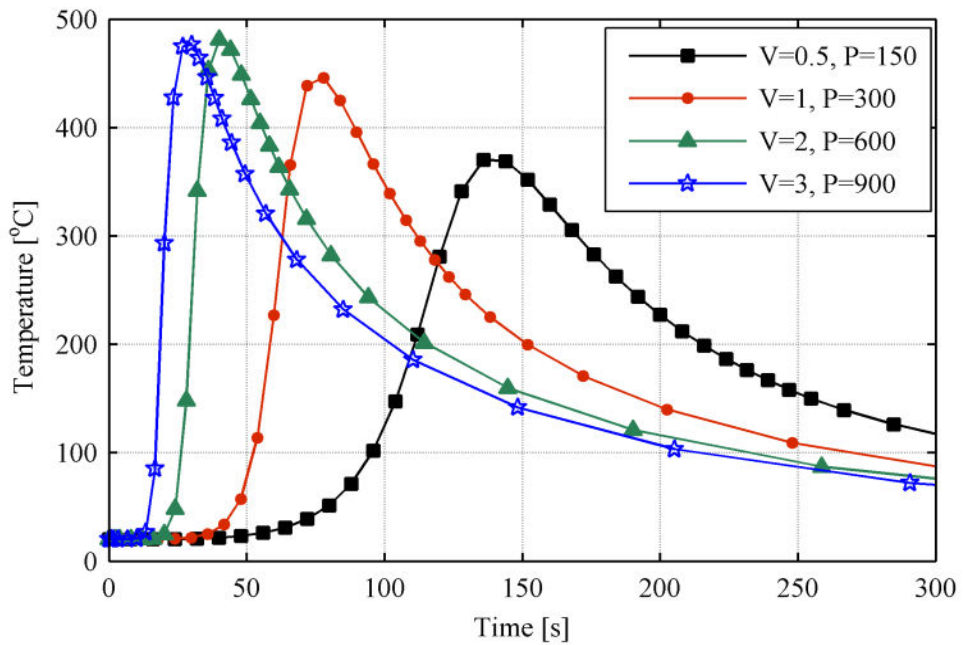


**Fig. 4.6(b): Comparison between simulated transient thermal cycles for four different cases at different locations longitudinally 10 mm away from weld centre.**

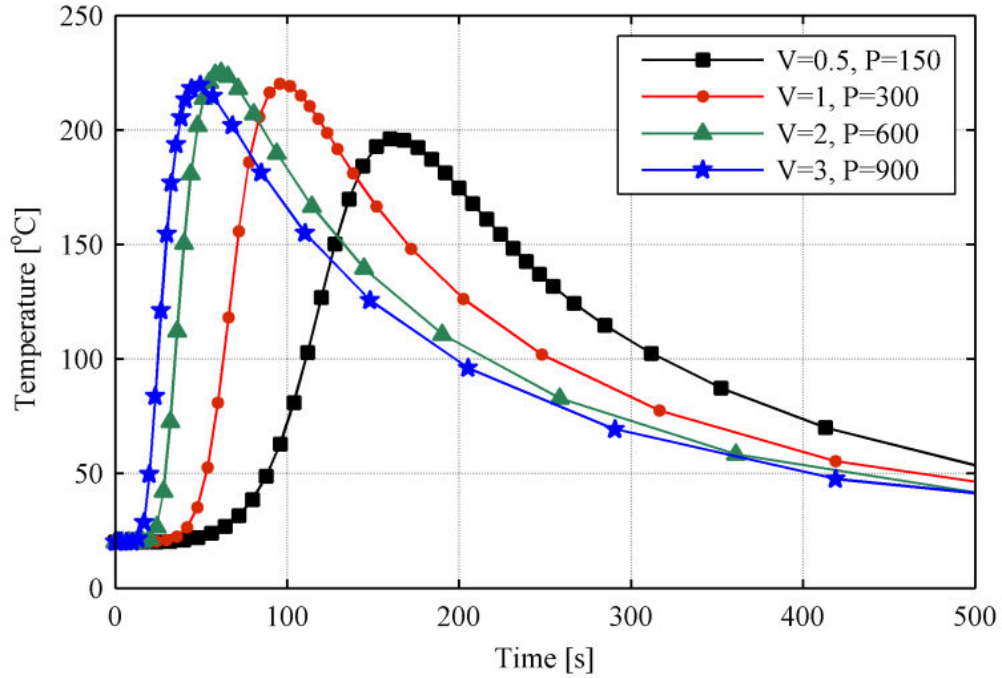


**Fig. 4.6(c): Comparison between simulated transient thermal cycles for four different cases at different locations longitudinally 20mm away from weld centre.**

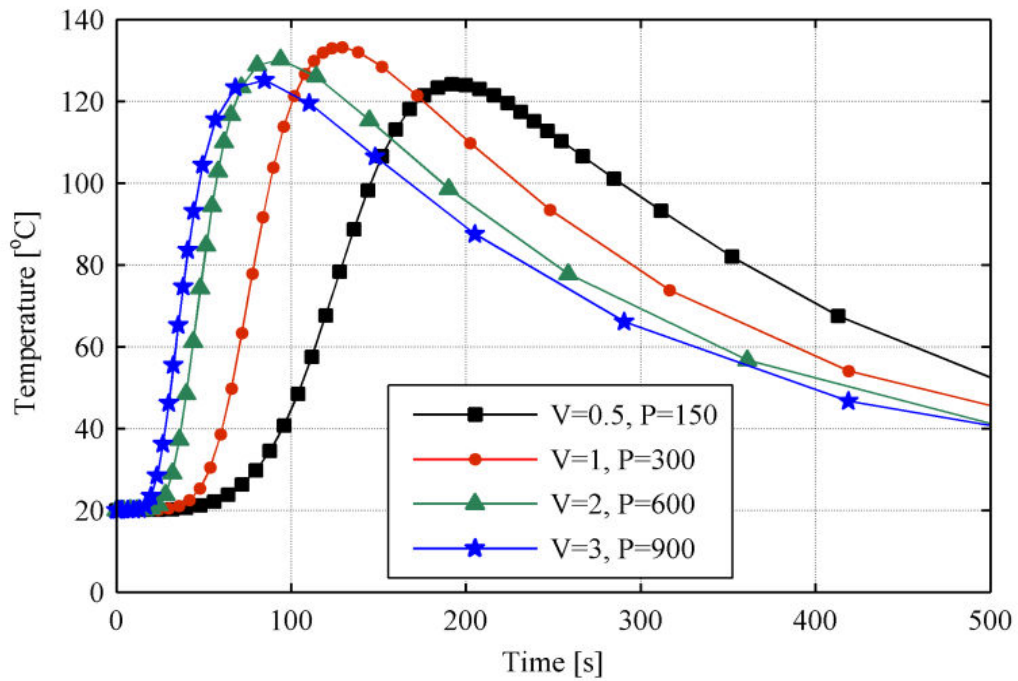


**Fig. 4.6(d): Comparison between simulated transient thermal cycles for four different cases at different locations longitudinally 30mm away from weld centre.**

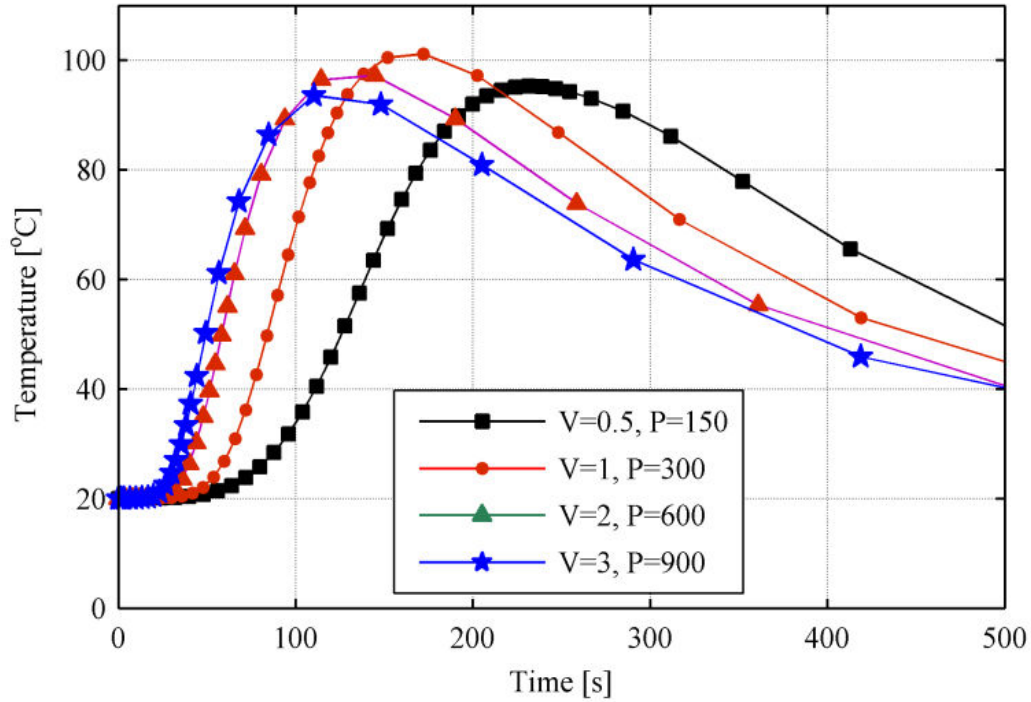


**Fig. 4.6(e): Comparison between simulated transient thermal cycles for four different cases at different locations longitudinally 40mm away from weld centre.**

#### ***4.2.1 Influence of the weld speed and power on temperature distribution***

The effect of the weld speed and power on the temperature distribution for various locations away from the weld is presented in Figs. 4.6(a)-(e). It is observed that the peak temperature increases at the weld centre (WC) with increasing weld speed and power as shown in Fig. 4.6(a). It is discerning to note (Figs. 4.6(a)-(e)) that the difference in peak temperatures also gets reduced for the locations longitudinally away from the WL. The possible reason for such an observation could be that with an increase in the weld speed and power, the rate of heat input is higher than the rate of heat dissipation. This also would result in localized heating at the fusion zone.

### 4.3 Distortions

In the mechanical analysis, the radial distortions and longitudinal distortions along the longitudinal direction (Z coordinate) were simulated on the inner surface and outer surfaces for four different combinations of the weld speed and power with constant heat input of 300 J/mm. These distortion values were taken at 180° section from the weld start position. Figs.4.7(a)-(b) show the radial distortions along the longitudinal direction (Z coordinate) on the inner and outer surfaces respectively. Figs.4.8(a)-(b) show the longitudinal distortions along the longitudinal direction (Z coordinate) on the inner and outer surfaces respectively.

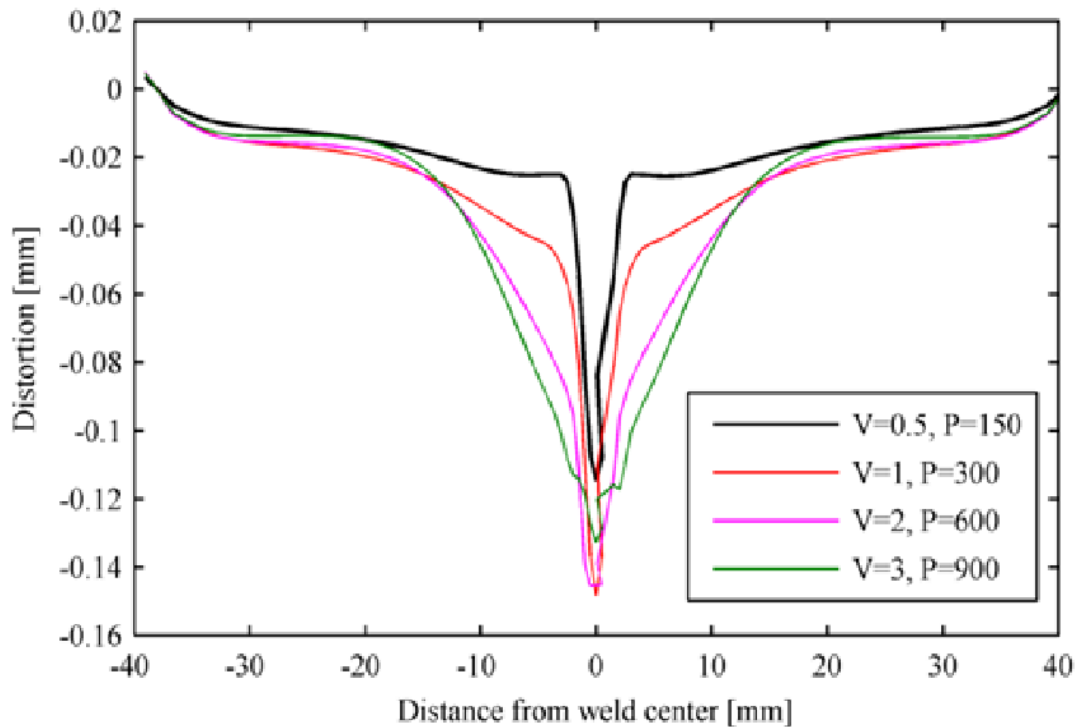


Fig. 4.7 (a): Radial distortions along the longitudinal direction (Z coordinate) on the inner surface

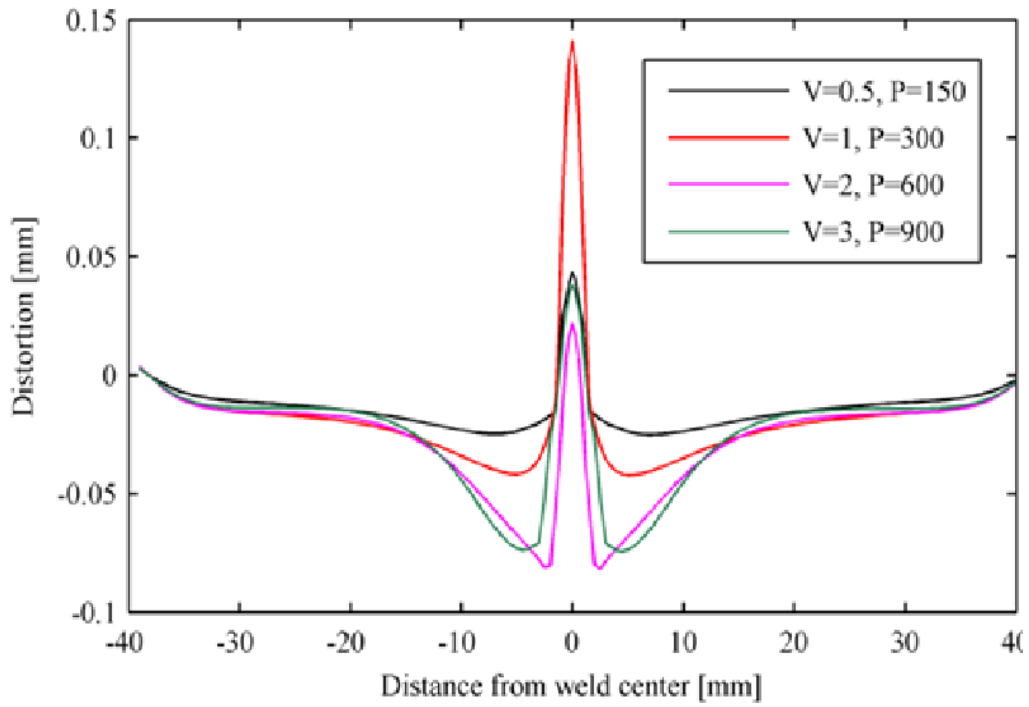


Fig. 4.7 (b): Radial distortions along the longitudinal direction (Z coordinate) on the outer surface

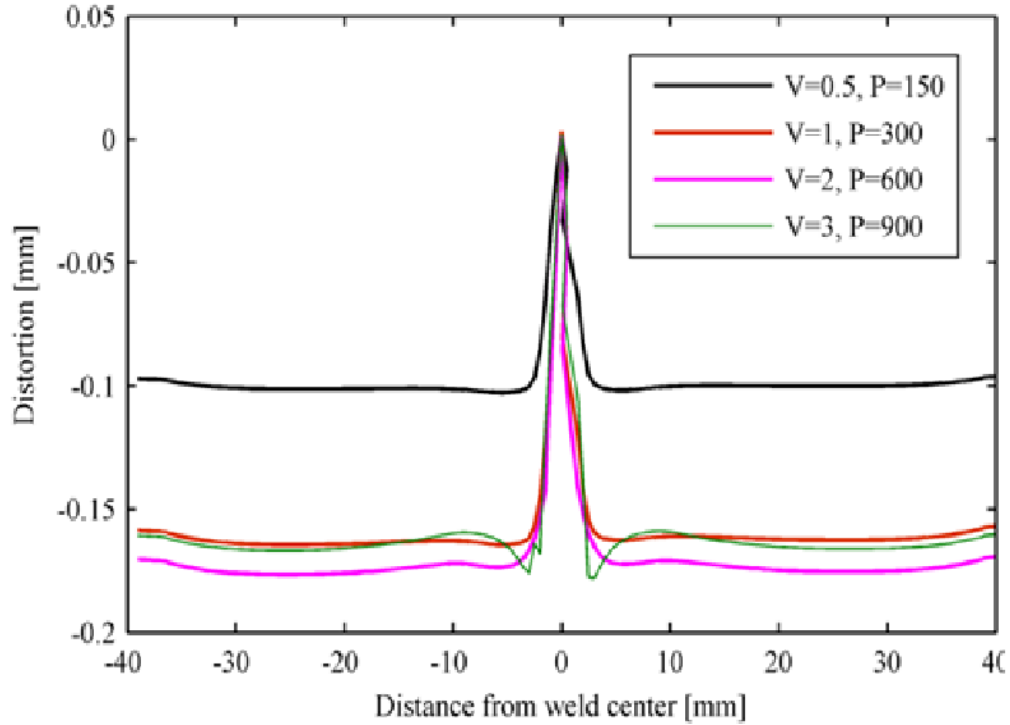
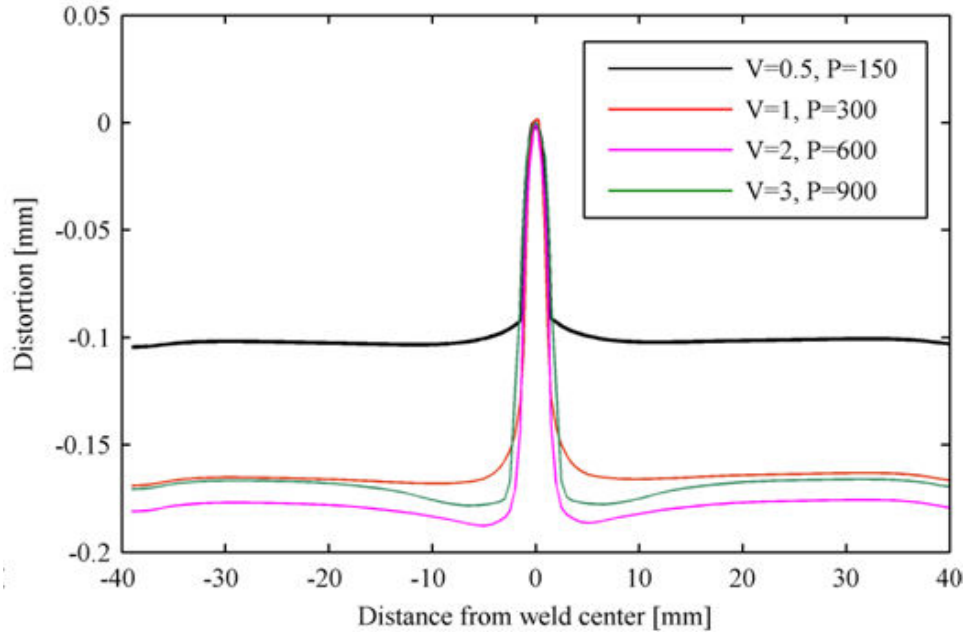


Fig. 4.8 (a): Longitudinal distortions along the longitudinal direction (Z coordinate) on the inner surface



**Fig. 4.8 (b): Longitudinal distortions along the longitudinal direction (Z coordinate) on the outer surfaces**

**4.3.1 Radial distortions along longitudinal direction (Z- coordinate)**

Figs.4.9(a),(b) shows the distortion distribution and its magnitudes. On the inner surface, negative distortions are observed along the Z coordinate. It can be seen that the considerable variation in distortions within 20 mm adjacent to weld on both sides. As the weld speed and power increases for the condition of constant heat input, distortions adjacent to weld ranges from 0.02 mm to 0.12 mm. Similarly on the outer surface for varying weld speed and power with constant heat input, distortions are varying from 0.01 mm to 0.075 mm. This indicates that on the inner surface, the diameter of the component in the weld metal region and its vicinity reduces after welding. Whereas on the outer surface, the diameter of the component increases within the weld metal and adjacent to the weld, the diameter reduces. This bending deformation in the component generates stresses through the component thickness.

The observations and the trends seen on the inner surface in this study were found to be in agreement with the results reported in the literature. An important observation in this study is, no expansion/contraction of wall thickness is observed in radial direction beyond the weld bead. The same trend is shown in Fig. 4.8.

#### ***4.3.2 Longitudinal distortions along longitudinal direction (Z coordinate)***

On the inner surface and outer surface, negative distortions are observed along the Z coordinate. This is due to shrinkage of weld metal. The noticeable variation in distortion was observed within 4 mm adjacent to WC on both sides, whereas, the longitudinal distortions are observed to be constant beyond 4 mm from WC.

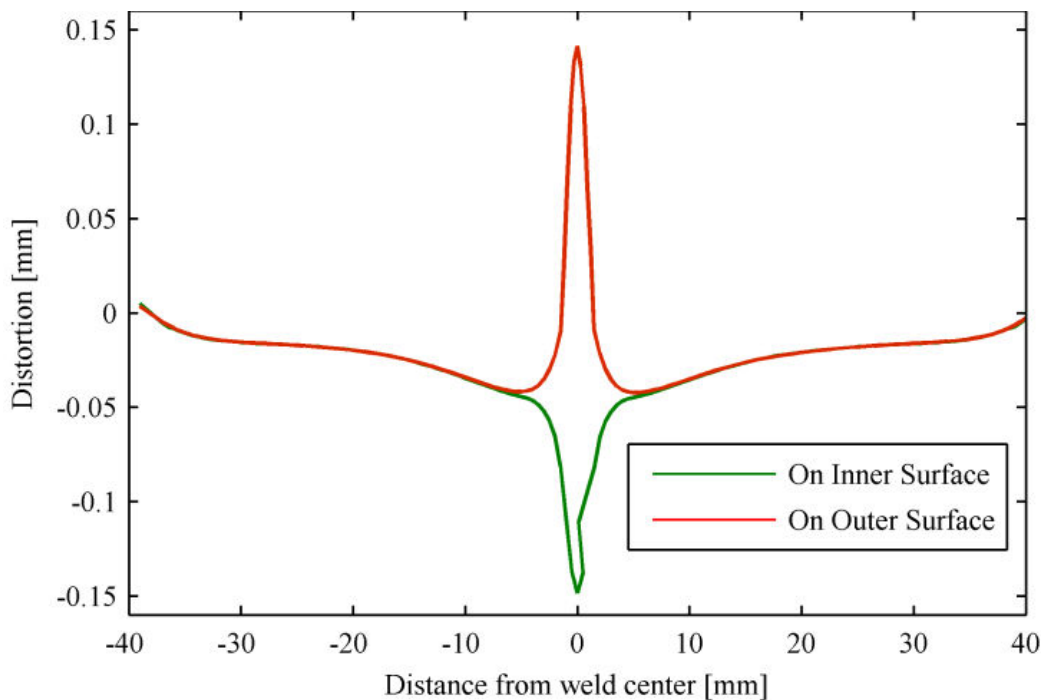


**Fig. 4.9 (a): Variation of wall thickness along the radial direction**

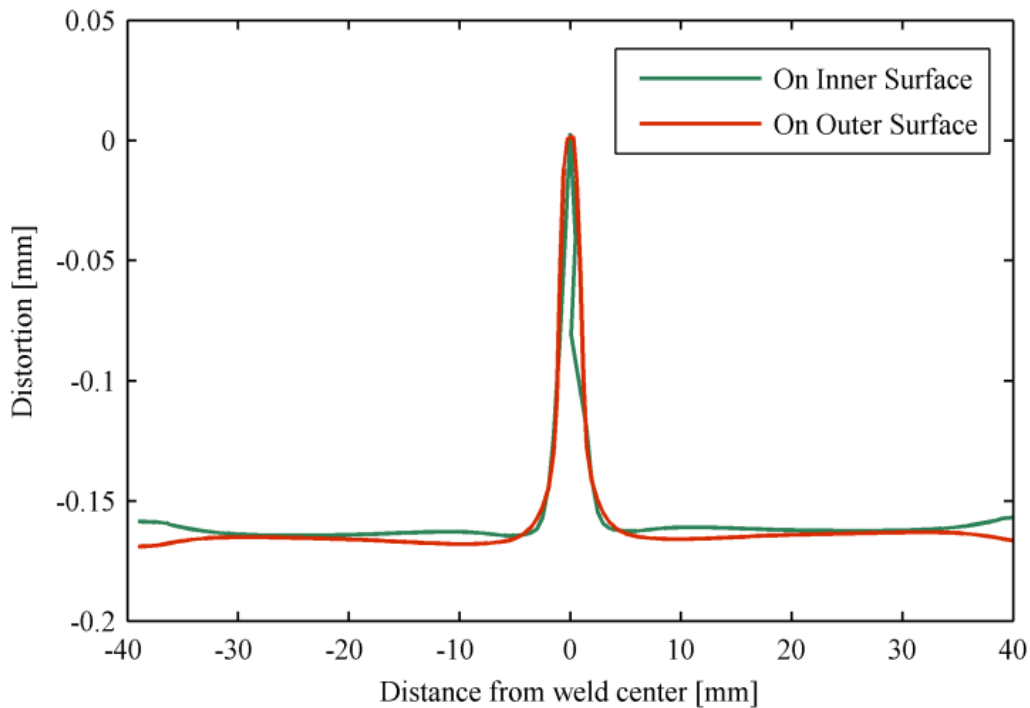


**Fig. 4.9(b): Variation of component length along the longitudinal direction (Z coordinate).**

On both the surfaces, the longitudinal distortions are ranging from 0.1 mm to 0.18 mm as the weld speed and power increases for the condition of constant heat input. The length of the component becomes smaller, due to radial shrinkage. Fig 4.9(b) shows that the longitudinal shrinkage is uniform along the Z coordinate on the inner and outer surfaces.

#### ***4.4 Distortion on 3-plane circumferential butt joint***

As the process of welding is highly nonlinear and complex in nature, for the purpose of validation a GTAW experimental test rig has been setup with a special purpose fixtures as shown Fig.4.10.

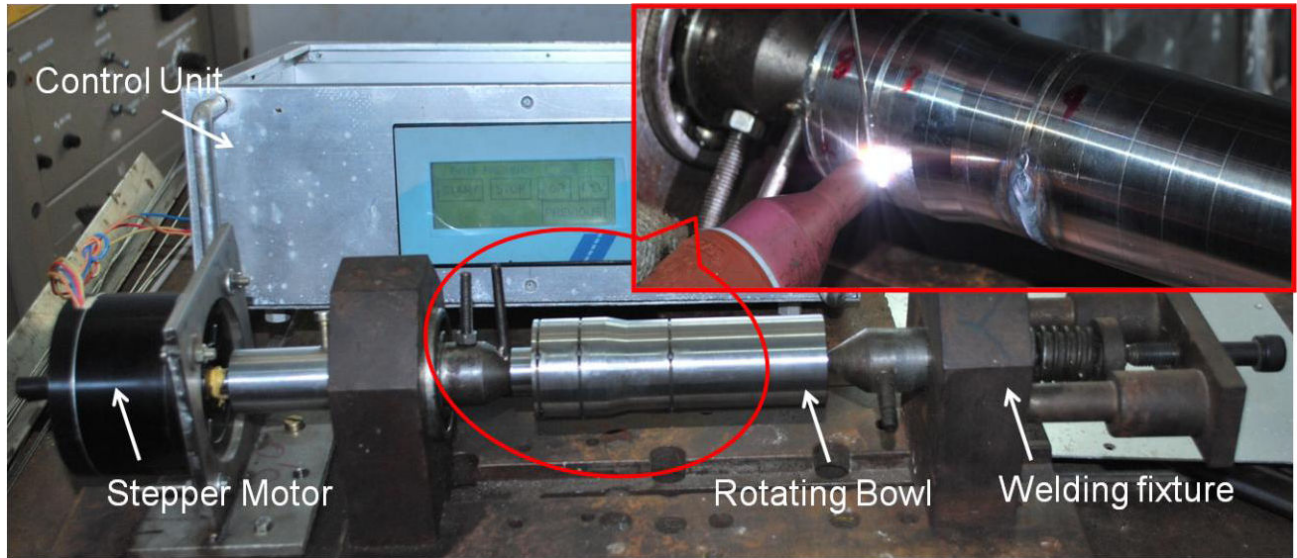


**Fig. 4.10: Experimental set up used for welding of 3-plane circumferential butt joint.**

In the numerical analysis the nodal temperature distributions from the thermal analysis will be used as an input for the coupled structural analysis. Therefore experimental data correlation for the HAZ dimensions and the nodal temperature data and there by validation for accurate predictions of subsequent stress fields and distortion patterns is a prerequisite. In the present study K- type thermocouples with computer interface data acquisition system is chosen for the thermal model validation. Thermocouples at seven different locations along its length and three locations over the circumference spacing  $120^\circ$  between each a total of 21 thermocouples are placed and temperature is recorded through the data logger with an interval of 0.12 seconds for comparison with numerical results. The arrangement of thermocouples on the surface of rotating bowl is shown in Fig.4.11. Further details of those locations are given in Table. 4.3.

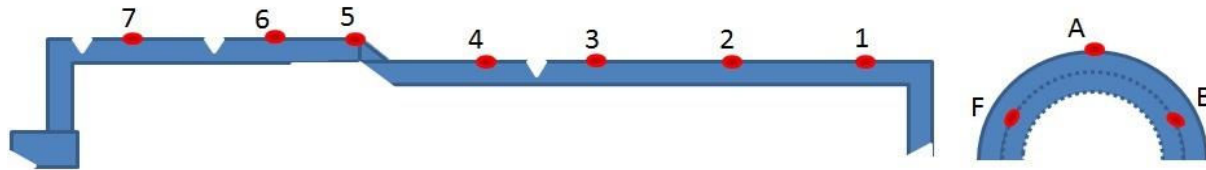


**Fig. 4.11: Measurement locations of thermocouples on the rotating bowl assembly surface.**

**Table.4.3: Measurement locations of thermocouples on the rotating bowl assembly surface**

<b>Thermocouple location</b>	<b>T1A</b>	<b>T1C</b>	<b>T1E</b>	<b>T2B</b>	<b>T2D</b>	<b>T2F</b>	<b>T3A</b>	<b>T3C</b>	<b>T3E</b>	<b>T4B</b>	<b>T4D</b>
<b>Distance from WL (mm)</b>	54	54	54	32	32	32	8	8	8	-8	-8
<b>Angle from weld start</b>	0	120	240	60	180	300	0	120	240	60	180
<b>Thermocouple location</b>	<b>T4F</b>	<b>T5A</b>	<b>T5C</b>	<b>T5E</b>	<b>T6B</b>	<b>T6D</b>	<b>T6F</b>	<b>T7A</b>	<b>T7C</b>	<b>T7E</b>	
<b>Distance from WL (mm)</b>	-8	8	8	8	-8	-8	-8	8	8	8	
<b>Angle from weld start</b>	300	0	120	240	60	180	300	0	60	120	

Measurement of the welding-induced distortions in the present study is performed to provide the dimension comparison of the welded component before and after welding and also to provide the actual data for examining the accuracy of the numerical predictions. The distortions at the critical points on the surface of the rotating bowl assembly are measured before start of welding and after the parts were cooled to room temperature and released from the fixture using a dial gauge indicator.

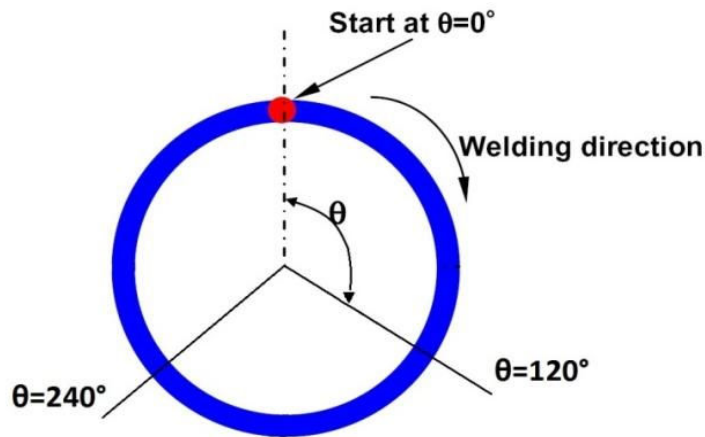


**Fig. 4.12: Direction of Welding along its circumference.**

There are fourteen such different locations along its length and six locations over the circumference spacing  $60^\circ$  between each point, collectively a total of 84 locations around the bowl surface as shown in Fig.4.14. The details of measurement locations are given in Table 4.4. The run-outs have been checked for nine nos. of such bowls, against three different clamping conditions, four different speeds and three different sequences for a single pass. In order to compare the effect of multi-pass welding against single pass, the same has been also checked for one case as well.

In total there are three circumferential welds required to complete each bowl, and it is necessary to provide the weld joint totally from outside. It is proposed to divide in to three segments spacing  $120^\circ$  each as shown in Fig.4.12 & 4.13. The welding input parameters and the bead geometry details of the joint are furnished in Table 4.5. A quantitative comparison of measured and predicted transient temperatures at three thermocouple locations starting at  $0^\circ$  and ending

120° is presented in Fig. 4.16(a). A typical result of thermal simulation is presented in Fig. 4.15, in which the 3D temperature profile on the outer surface at 100 s.

**Table.4.4: Longitudinal and transverse distortion measurement locations on the surface of rotating bowl assembly**

<b>Measuring location</b>	<b>L1</b>	<b>L2</b>	<b>L3</b>	<b>L4</b>	<b>L5</b>	<b>L6</b>	<b>L7</b>
<b>Distance from Bottom (mm)</b>	2	13	24	35	46	57	68
<b>Measuring location</b>	<b>L8</b>	<b>L9</b>	<b>L10</b>	<b>L11</b>	<b>L12</b>	<b>L13</b>	<b>L14</b>
<b>Distance from Bottom (mm)</b>	76	84	96	104	123	131	137
<b>Measuring location</b>	<b>A</b>	<b>B</b>	<b>C</b>	<b>D</b>	<b>E</b>	<b>F</b>	
<b>Angle from weld start position (in degrees)</b>	0°	60°	120°	180°	240°	300°	

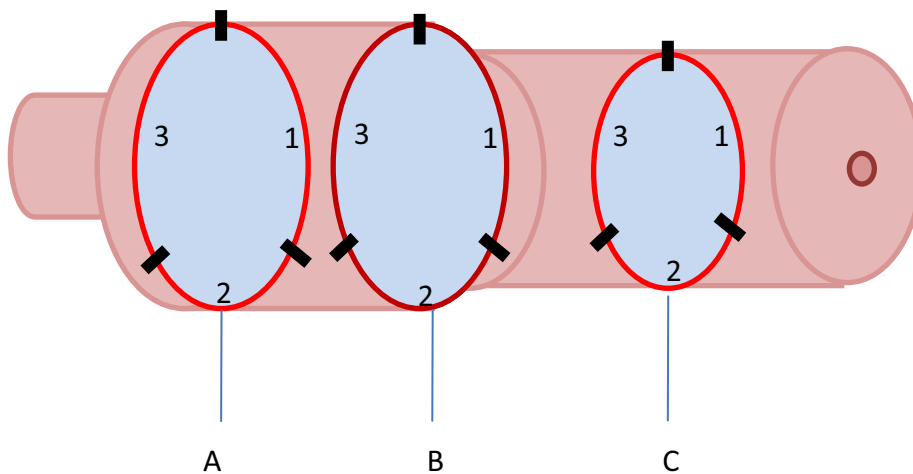


**Fig. 4.13: Segments of Welding used in sequential welding.**

**Table.4.5: Weld input parameters and weld bead geometry details**

Welding Input Parameters		Bead Geometry	
Current (I)	45-50A	Root Gap	0.1mm
Voltage (V)	14V	Depth of penetration	1-1.5mm
		Bead width	0.8mm
		V-groove	70°

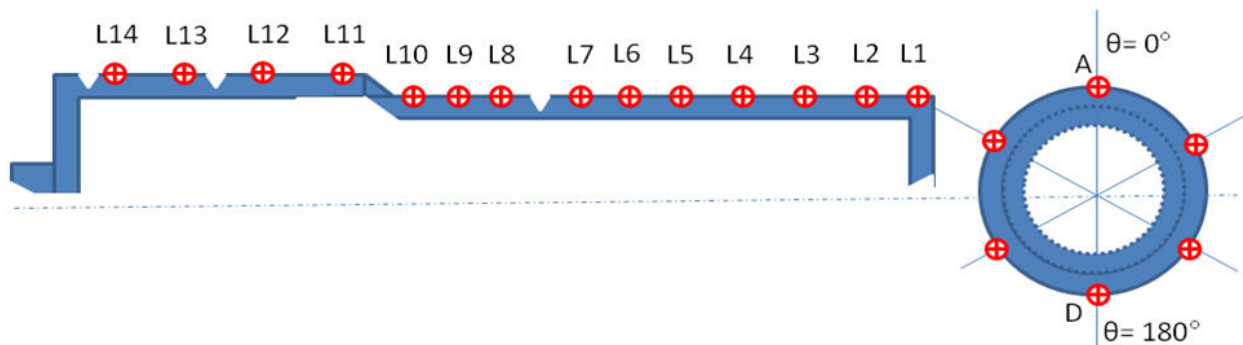


**Fig. 4.14: Longitudinal and transverse distortion measurement locations on the surface of rotating bowl assembly.**

These thermocouples show a close agreement with the FE data. Similarly during welding of the second segment in addition to those three thermocouple previous thermocouple data (which is at 90° from weld starting point) is also plotted as shown in Fig. 4.16(b). The comparison of numerical results to those experiments before and after welding is presented in Fig. 4.17 showing reasonably a good agreement between them. Fig. 4.18 shows a typical contour of longitudinal distortion of the bowl cooled to room temperature after welding.

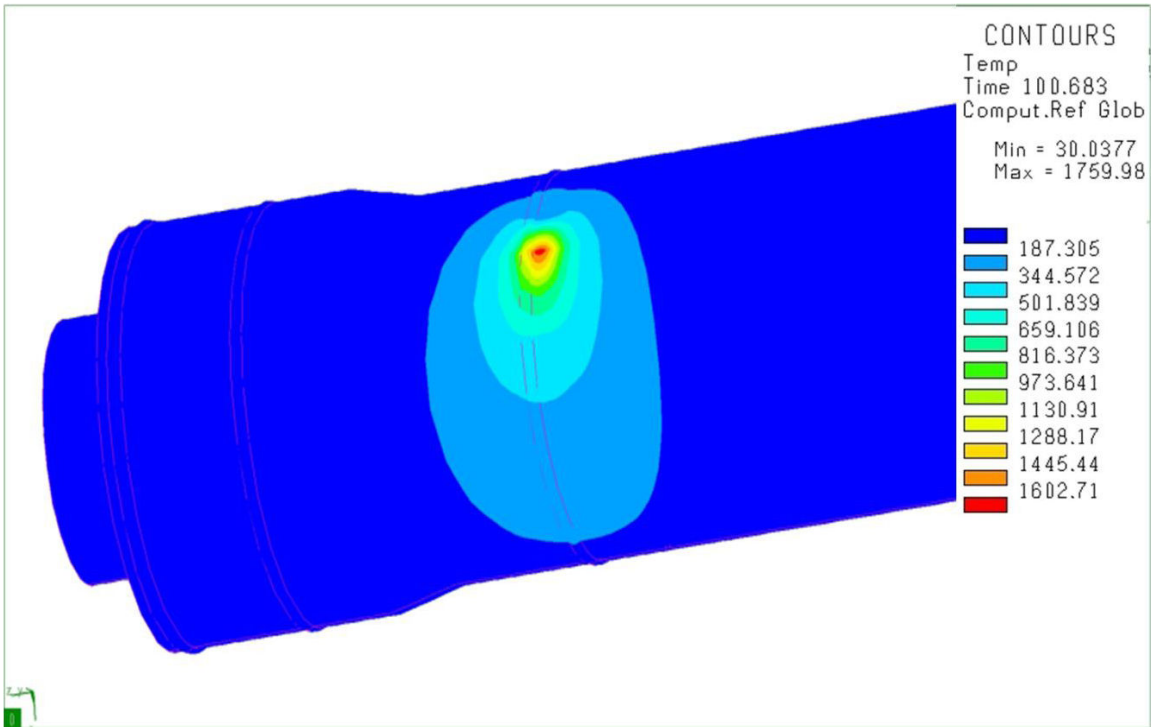


**Fig. 4.15: Typical temperature Contour on the outer surface of rotating bowl at 100sec.**

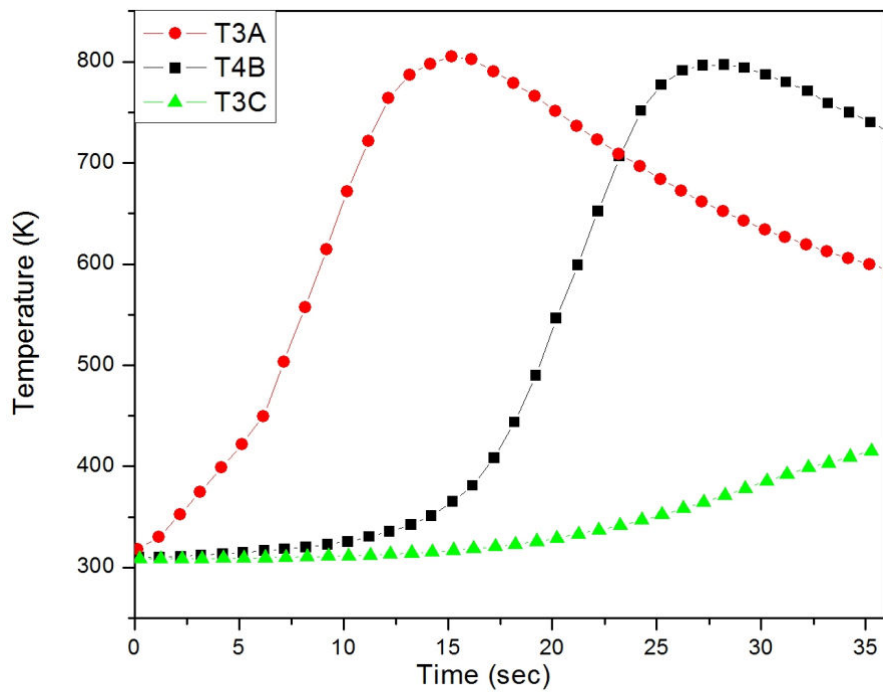


**Fig. 4.16(a): Temperature distribution along its length of the weld for the First sector.**

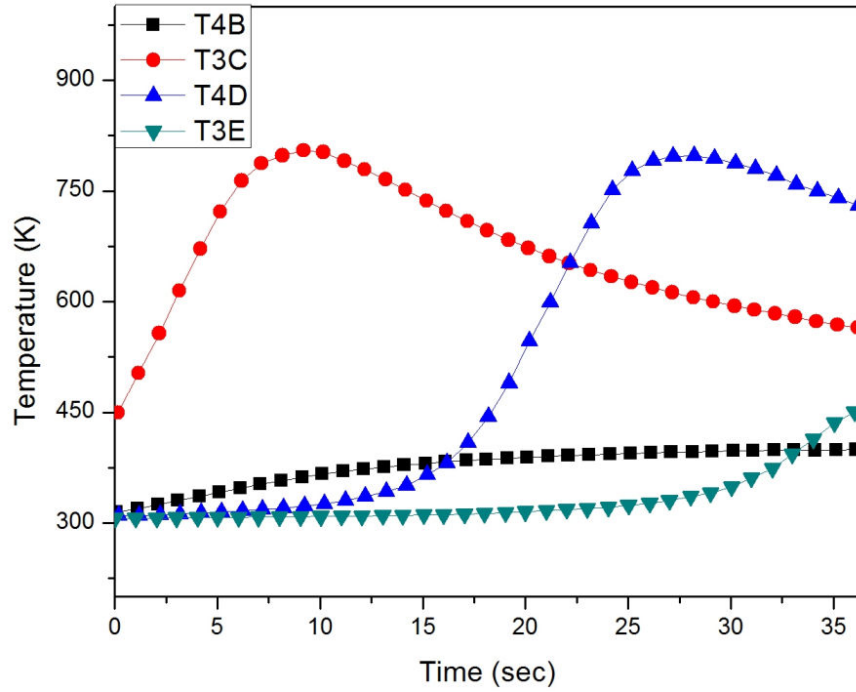


**Fig. 4.16(b): Temperature distribution along its length of the weld for the second sector .**

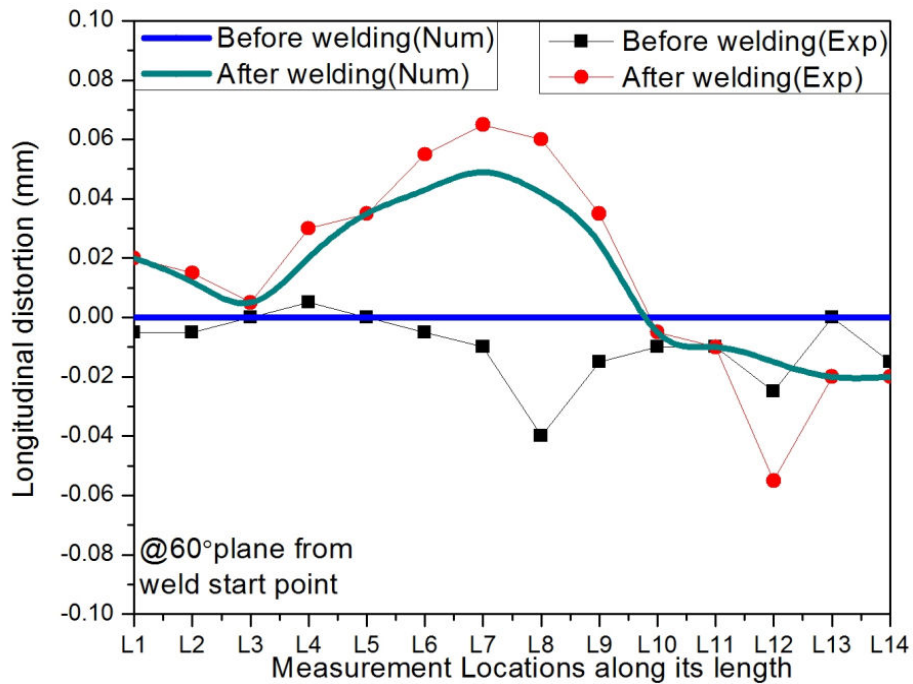


**Fig.4.17: Longitudinal distortions along its length of the bowl at angle 60° from the weld start position before and after welding.**

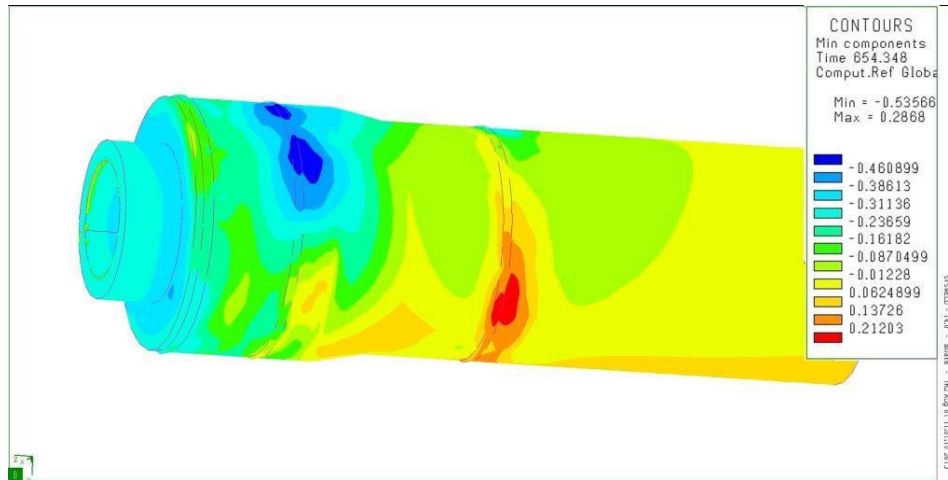


**Fig 4.18: Contour of Longitudinal distortions of the bowl at room temperature after welding.**

It can be observed from Fig.4.19 that the distortions are high at higher welding speeds for an optimum sequence and clamping conditions. It is obvious from Fig. 4.21 that free-free clamping condition which is fully unconstrained produce high distortions. In practice, one would run through a number of weld sequences with the model until the desired solution is obtained which will be time consuming and costly. Experience suggests three possible common sequences which have been checked for the same. In contrast, the distortions were significantly reduced after using an optimum sequence of welding for the same conditions as shown in Fig.4.20. The effect number of passes on distortion is depicted in Fig. 4.22.

At present, however, there is no process that completely eliminates distortion. Many distortion control techniques and weld design optimization procedures such as prestraining, weld sequencing and precambering were developed by experience. Even though it is possible to design weld processes such that the final distortion is close to zero, with some probabilistic variation around the undistorted shape, it leads to the development of residual stress within the weld components.

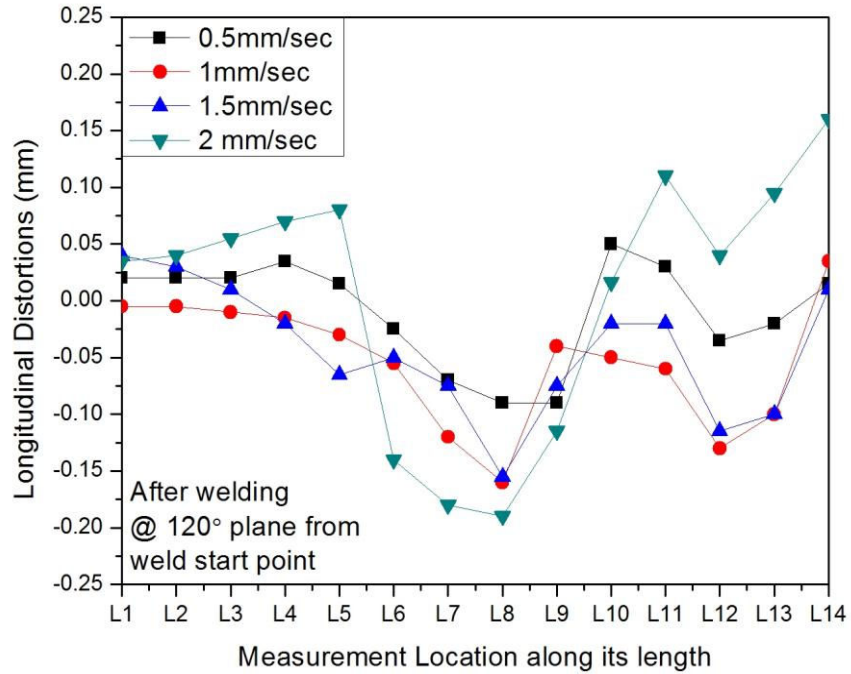


**Fig.4.19: Longitudinal distortions along its length of the bowl at angle 120° from the weld start position for different weld speeds.**

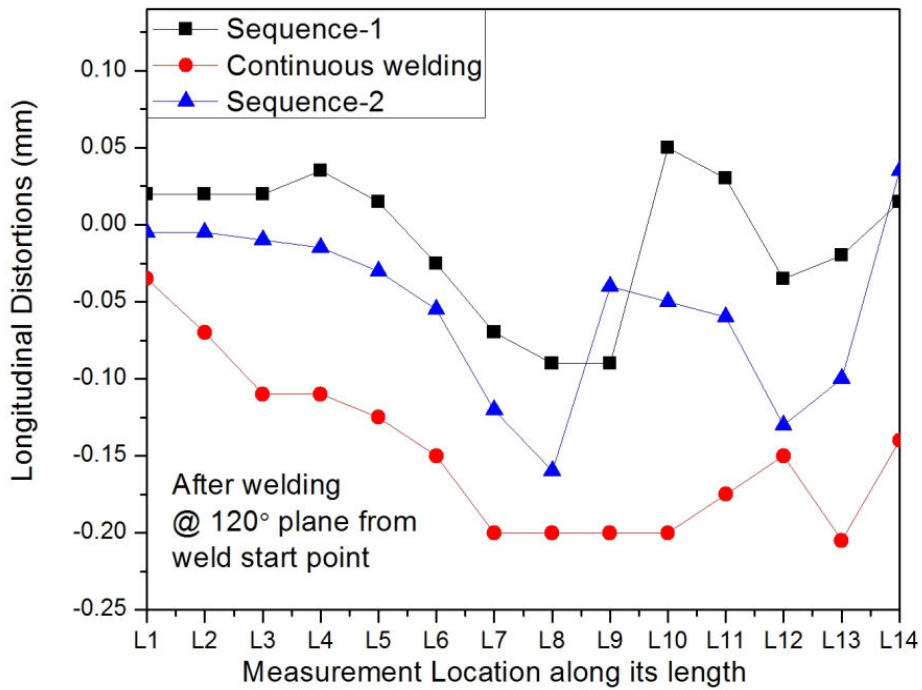


**Fig.4.20: Longitudinal distortions along its length of the bowl at angle 120° from the weld start position for different sequences of welding.**

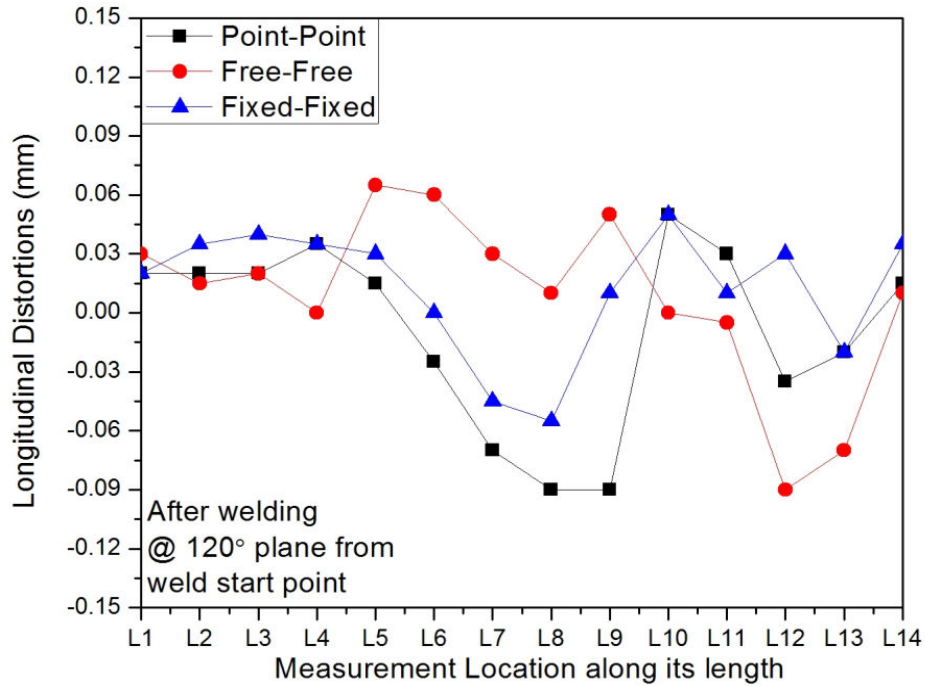


**Fig.4.21: Longitudinal distortions along its length of the bowl at angle 120° from the weld start position for different clamping conditions.**

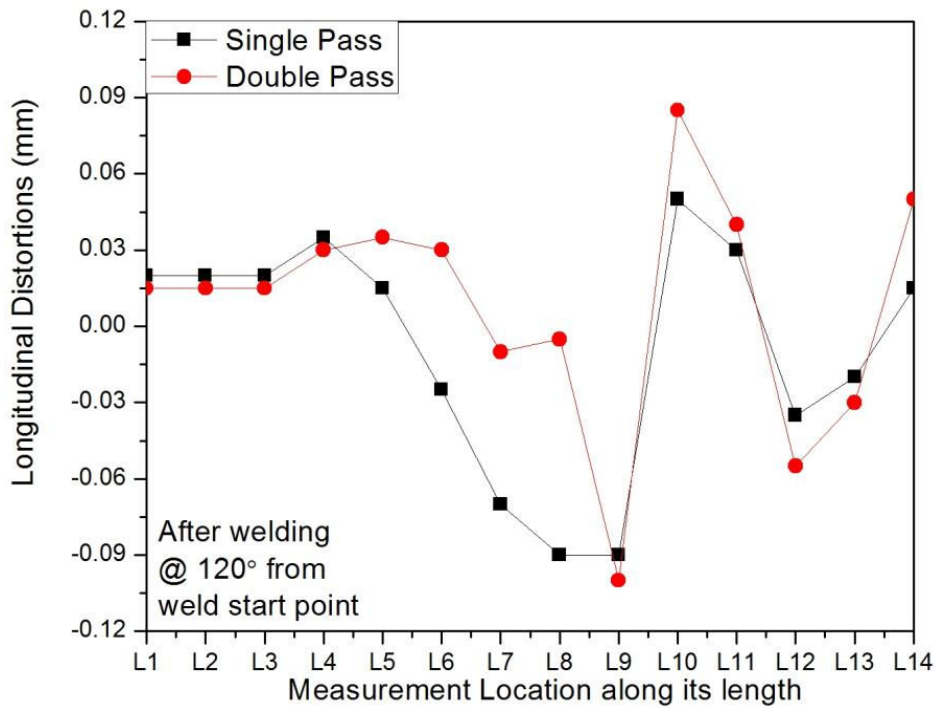


**Fig.4.22: Longitudinal distortions along its length of the bowl at angle 120° from the weld start position for varying number of passes**

## 4.5 Micro structure

In general during the welding, the thermal gradients are very large which is the motive force for the changes in mechanical and material fields. As the simulations that are concerned with the mechanical effects of the welding require both the computation of thermal and mechanical fields, the material behavior due to the change in microstructure depends on the temperature and deformation histories in addition to the chemical composition of the material. The influence of microstructure is mainly observed in the heat affected and fusion zone of the weld which may influence residual stress and deformation fields considerably.

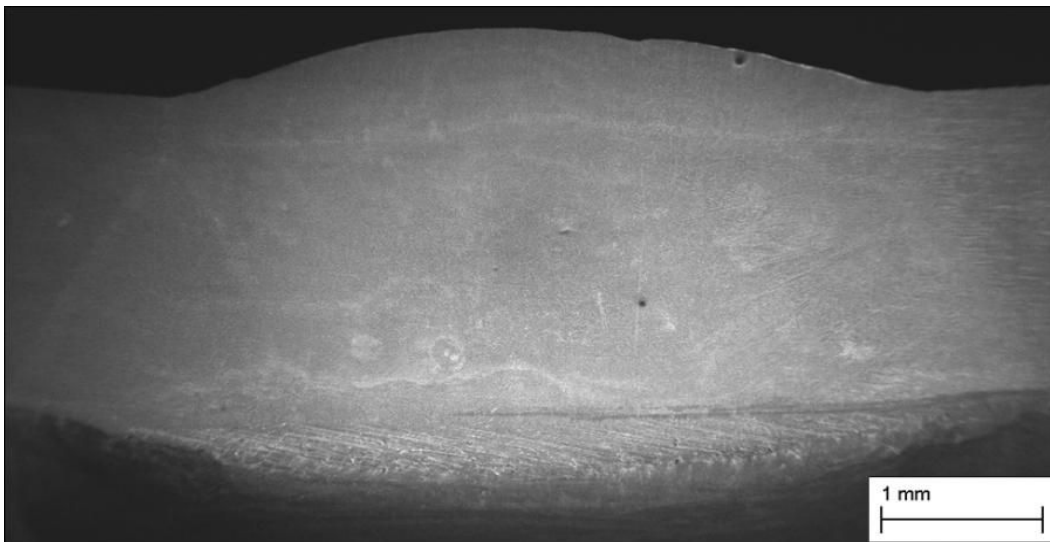


**Fig.4.23: Microstructure of the Weld zone and the HAZ of TIG welded component.**

Detailed study of weld pool characteristics may, however, be a separate research field due to the level of refinement as the temperature field and weld bead geometry are difficult to be predicted and subsequently accounted in a macroscopic context [88]. However, in this study the physics of weld pool impact on the microscopic effect of the welding is neglected, but the quality of TIG welding is assessed by micro structure examination. Metallography of the weld sample has been

studied and the microstructure of the weld sample in both the base metal, HAZ and Weld zone (WZ) are shown in Fig.4.23 and 4.24.

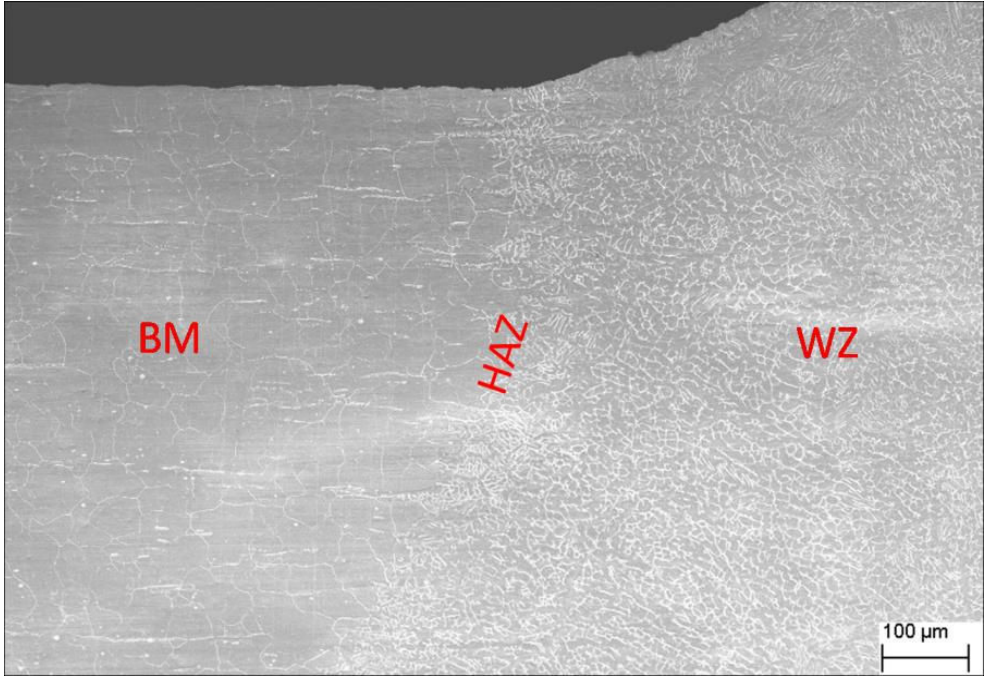


Figure 4.24: Microstructure of the TIG welded component of 2mm thick sample.

4.6 Dynamic Analysis

To study the dynamic behavior a dynamic model of rotating bowl assembly, a 2D geometric model (see Fig 4.25) of the bowl is modeled using a commercial software package called

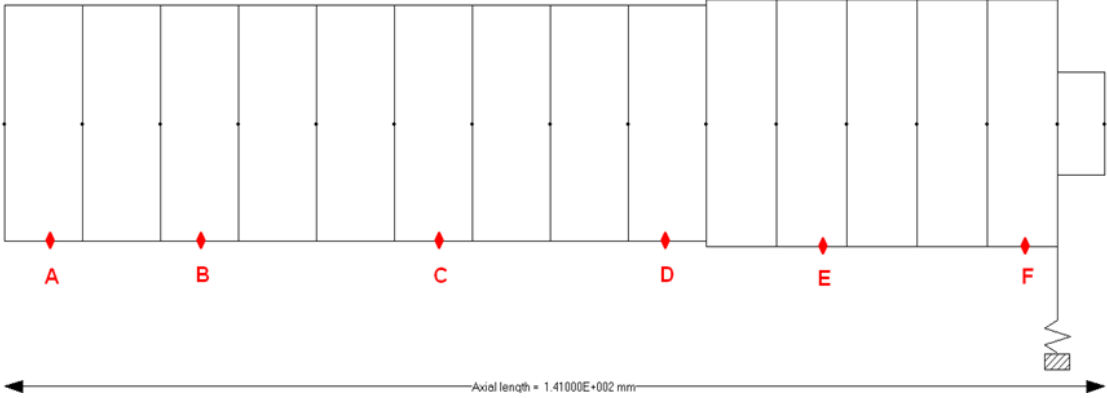


Fig.4.25: 2D model of Rotating bowl assembly

Advanced Rotating Machinery Dynamics (ARMD). Generally welding induced distortion in these straight bowls may cause eccentricity, which results in unbalanced mass, when operated at higher speeds. The following is the dynamic equation and the characteristic solution used to solve for the mode shapes and frequencies

$$[M]\ddot{x} + ([C] + \omega[G])\dot{x} + [K + K']x = \{Q\} + \{F_i\} \quad (4.2)$$

where, [M],[C],[G] and [K] are the mass, damping, gyroscopic and stiffness matrices of the bowl respectively and {Q} and {F<sub>i</sub>} is the gravity force and imbalance force, respectively. [K'] is the stiffness matrix due to the eccentricity in the rotating bowl.

Mainly the unbalanced mass is an important parameter which affects vibration and stability of rotor-bearing systems. Numerical simulation is performed at n = 3000 rpm with different values mass unbalance resulting from the distortions by keeping other physical parameters remain constant.

Certainly, it is understood from Fig. 4.26 that the effect of higher modes can be ignored because there is no significant contribution of the coupling to these modes as the difference between the second and fourth natural frequencies is very high. In addition, Fig. 4.27(a) shows the variation in critical speeds and indirectly system stability for different weld speeds which decreases with the increase in speed. This is because the higher speeds which results in large distortions as well as it reduces the stiffness and damping effects. Fig. 4.27(b) shows the variation of different welding sequences against bearing stiffness.

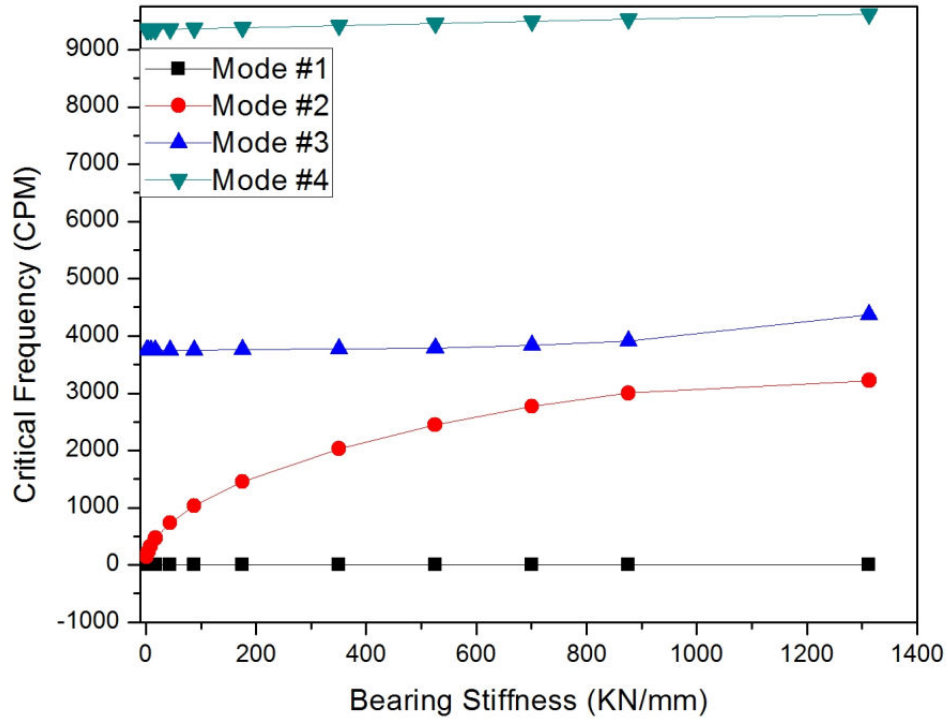


**Fig. 4.26: Motor critical speed map.**

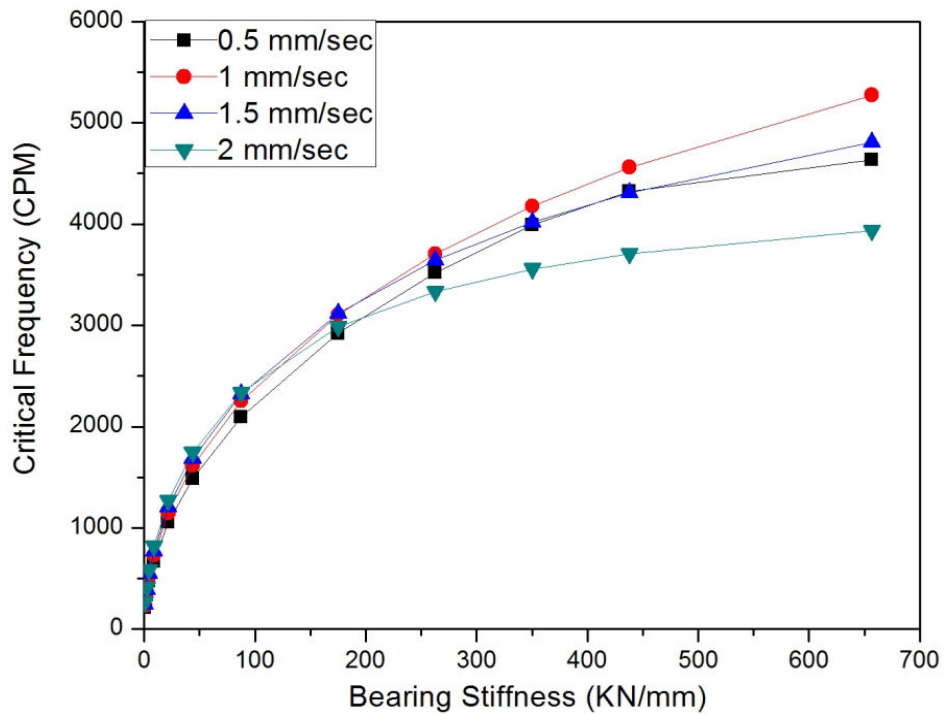


**Fig. 4.27 (a): Variation of critical speeds against bearing stiffness for different weld speeds.**

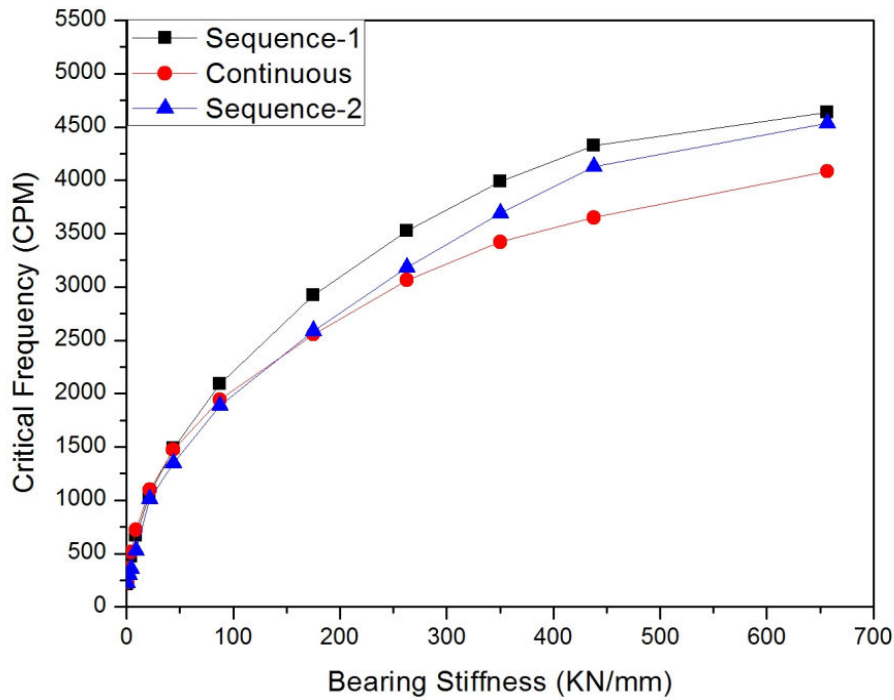


**Fig. 4.27(b): Variation of critical speeds against bearing stiffness.**

#### ***4.7 Welding residual stress (Mechanical analysis)***

Based on simulation, residual stresses in the longitudinal, circumferential and radial directions were obtained on the inner surface, outer surface and along the radial distance from the outer surface for varying weld speed and power with constant heat input of 300 J/mm and are presented in Figs. 4.28(a)-(d) respectively. It is to be noted that these residual stress values correspond to 180° section from the weld start position as mentioned earlier. Detailed analysis has been carried out on the above results to understand the characteristics and the influence of varying weld speed and power on these residual stresses and these are discussed in the following sections.

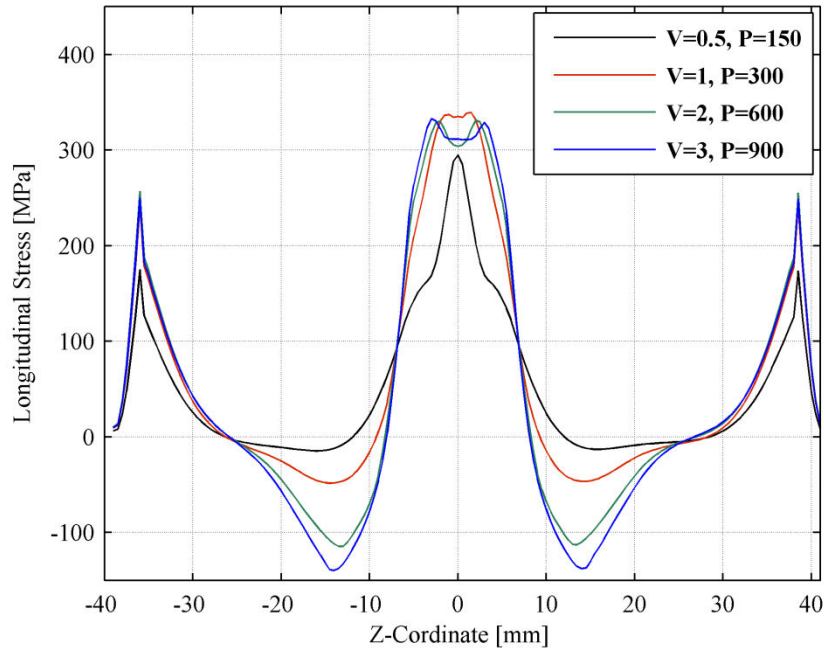


**Fig.4.28(a): Comparison between longitudinal residual stresses for different cases at 180<sup>0</sup> section from the weld start position on the inner surface.**

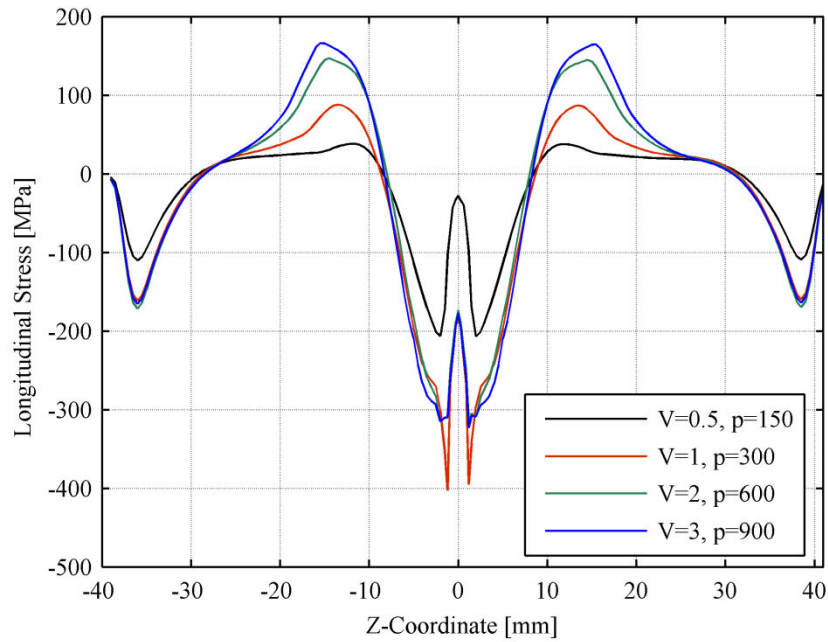


**Fig. 4.28(b): Comparison between longitudinal residual stresses for different cases at 180<sup>0</sup> section from the weld start position on the outer surface.**

#### ***4.7.1 Longitudinal stress***

The longitudinal stresses, normal to the direction in the circumferential joint of weld bead, are shown in Figs 4.28(a)-(d). In these figures, the stress distribution was analyzed for the inner and outer surfaces, as well as the stresses along the radial direction from outer surface at 3 mm and 14 mm away from WC. It can be seen that the stresses were both tensile and compressive which arise due to temperature gradients, variable shrinkage patterns and the type of boundary condition imposed in this simulation work. Fig. 4.28(a) reveals that on the inner surface, the longitudinal tensile stresses show a peak at the weld line (WL) and then decrease to compressive stresses. Further, stress reversal from compressive to tensile can be seen on both sides of WC. The tensile to compressive reversal is found to occur at around 8 mm from the WC, whereas compressive to tensile at around 25 mm from the WC (Fig. 4.28(a)).

On the other hand, the results on the outer surface showed the opposite trend, i.e. compressive to tensile and then tensile to compressive. The transition from compressive to tensile was obtained at around 8 mm and that from tensile to compressive at around 34 mm on both sides of WC (Fig. 4.28(b)). The observations and the trends seen on the inner and outer surfaces in this study were found to be in agreement with those obtained by other investigators [16, 24 and 66]. It was also noticed (Figs. 4.28(a) and (b)) that the variation in the stress is maximum at locations of 3 mm and 14 mm longitudinally away from the WC. The results corresponding to these locations are shown in Figs. 4.28(c) and (d), respectively.

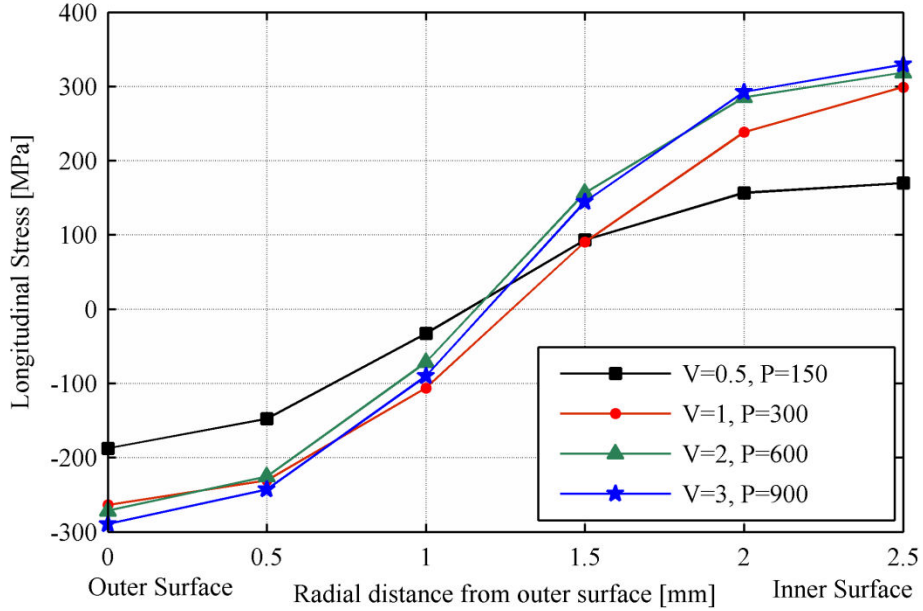


**Fig. 4.28(c) : Comparison between longitudinal residual stresses for different cases at 180° section from the weld start position along the radial direction from outer surface at 3 mm away from WC.**

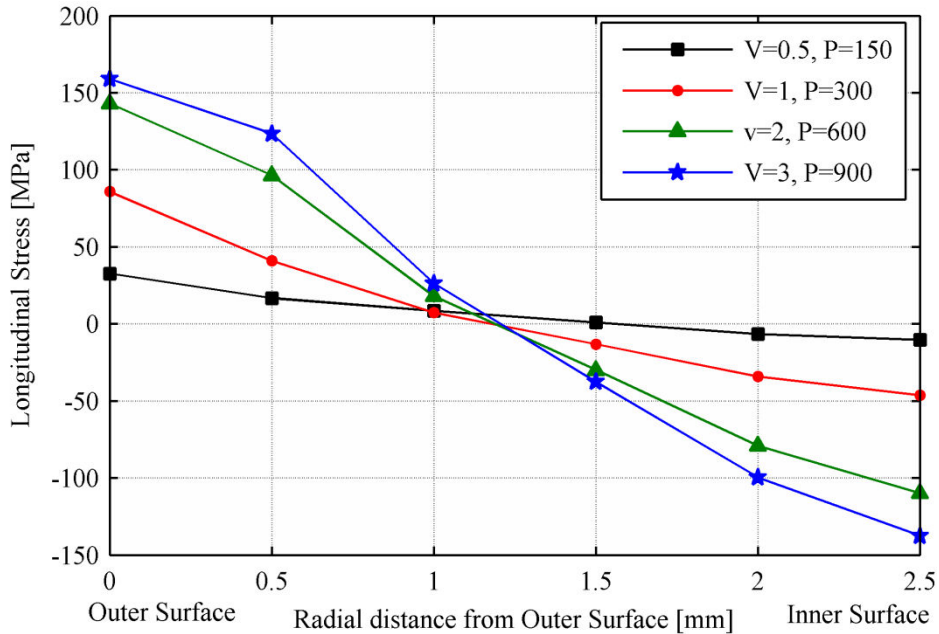


**Fig.4.28(d): Comparison between longitudinal residual stresses for different cases at 180° section from the weld start position along the radial direction from outer surface at 14 mm away from WC.**

#### ***4.7.1.1 Influence of the weld speed and power***

It can be seen in Fig. 4.28(a) and (b) that the stress values increase with increasing weld speed and power irrespective of locations along the Z coordinate. This increase in stresses for the location of 3 mm away from the WC was found to be significant with increase in tensile stresses as 150 MPa on the inner surface, and that for compressive stresses as 100 MPa on the outer surface (Fig. 4.28(c)). Further, for the Z coordinate beyond 8 mm from the WC, the same increasing trend in compressive (Fig. 4.28(a)) and tensile stresses (Fig. 4.28(b)) was observed. It is noticed that peak tensile residual stresses occur within the fusion zone on the inner surface. At 3 mm longitudinally away from WC, the magnitude of peak tensile residual stress is found to be 330 MPa which is greater than the yield stress (i.e. 265 MPa) of the material. The presence of such high tensile residual stresses needs to be minimized as they cause fatigue damage, SCC depending under combination of certain material and environment leading to material failure. Whereas on the outer surface, the peak tensile residual stresses were found to be lesser than yield stress.

Figs. 4.28(a) and (b) reveal that the nature of residual stress, changes with respect to increasing Z coordinate. The results shown in Fig. 4.28(c) for 3mm from WC reveal that with increasing radial distance from outer surface, the compressive stresses change over to tensile stresses at 1.25 mm. Whereas, it is interesting to note that for 14 mm as shown in Fig. 4.28(d) that the transition from tensile stresses to compressive occurs also at 1.25 mm distance radially from the outer surface i.e. mid section between the outer and inner surfaces.

### 4.7.2 Circumferential stress

The expansion and contraction in radial direction during thermal cycling can result in circumferential stresses that are along the direction of the weld. The analysis of variation of circumferential stresses with Z coordinate and along the radial direction for various weld speed and power are shown in Figs. 4.29 (a)-(c). The results obtained on the inner (Fig. 4.28(a)) and outer (Fig. 4.29(b)) surfaces can be summarized as follows. While on the inner surface, the tensile residual stresses observed at WL change over to compressive stresses, the reverse trend is observed for those on the outer surface. The transition in stress reversal was found to occur at 7 mm from WC for the inner surface, whereas it was at 15mm for the outer surface. The nature of compressive stress beyond 7 mm was wavy (Fig. 4.29(a)), whereas on the outer surface, it was zig-zag in pattern near the HAZ (Fig. 4.29(b)). The characteristics of the circumferential stress along the radial direction for location of 4 mm in the Z coordinate are shown in Fig. 4.29(c). The trends for circumferential stresses also concur well with the previous research.

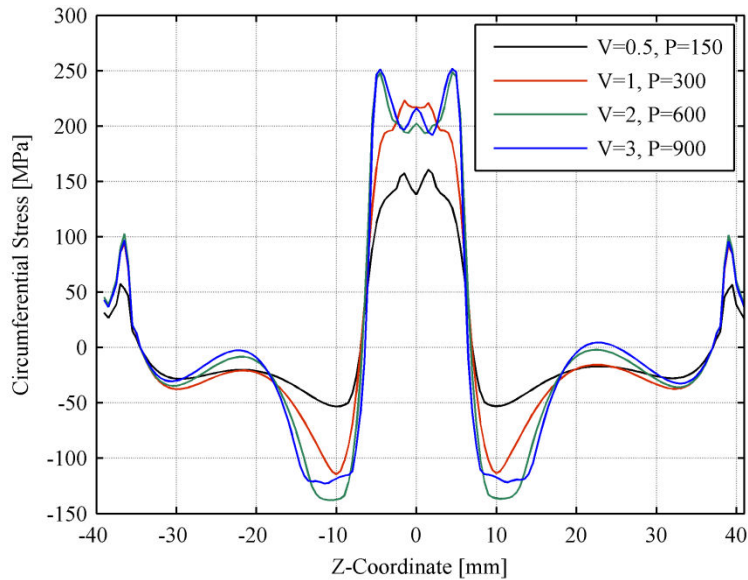


**Fig.4.29(a): Comparison between circumferential residual stresses for different cases at 180° section from the weld start position on the inner surface**

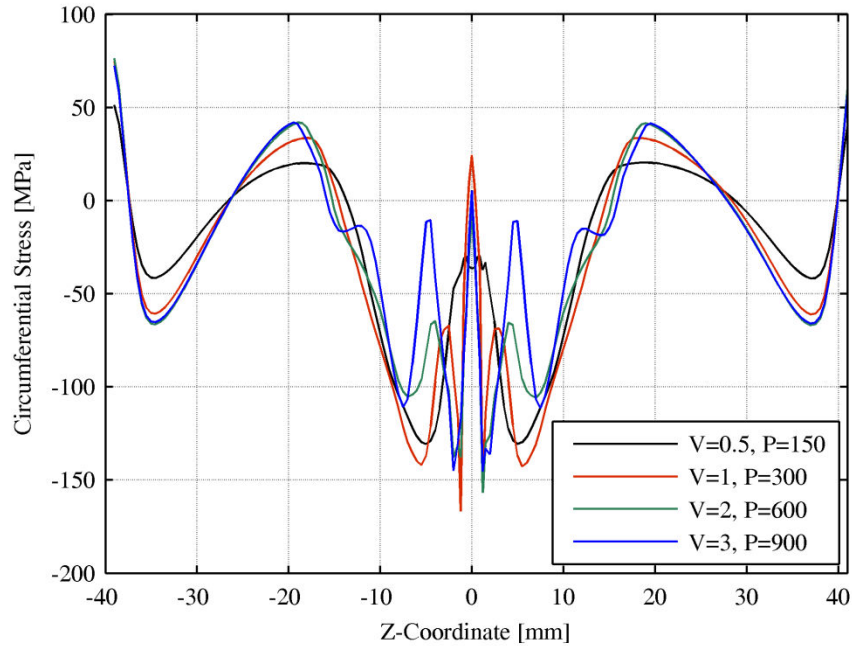


**Fig.4.29(b): Comparison between circumferential residual stresses for different cases at  $180^{\circ}$  section from the weld start position on the outer surface**

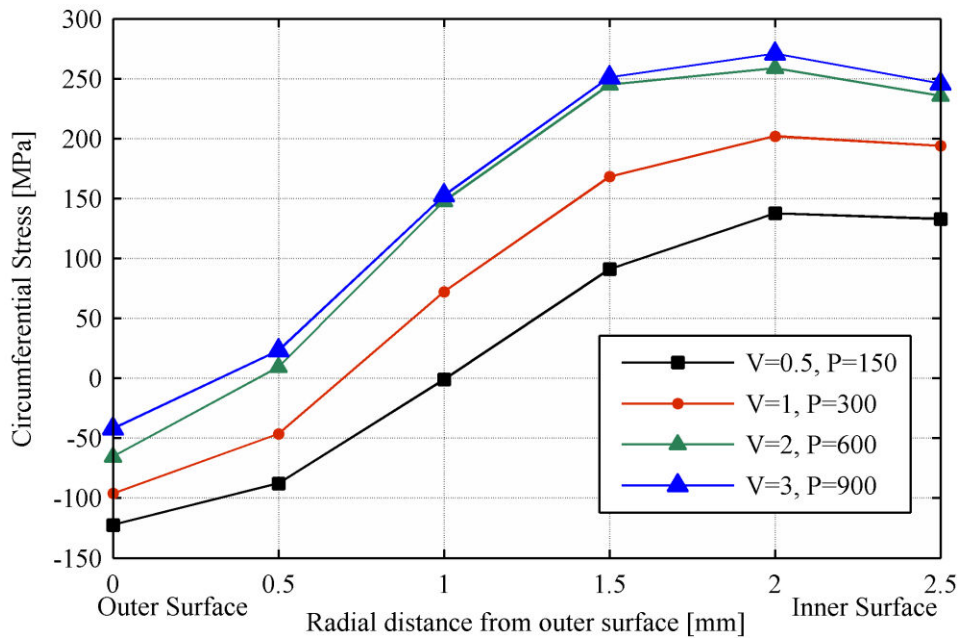


**Fig.4.29(c): Comparison between circumferential residual stresses for different cases at  $180^{\circ}$  section from the weld start position along the radial direction from outer surface at 4mm away from the WC**

#### ***4.7.2.1 Influence of weld speed and power***

It was observed that with the increase in weld speed and power, the circumferential stress increased and this increase was found to be significant. For the location of 4 mm from WC (Fig. 4.29(c)), the magnitude of increase in tensile residual stresses was  $\approx 120$  MPa on the inner surface, whereas it was  $\approx 100$  MPa for compressive stresses on the outer surface. It is important to notice that the peak tensile residual stress of  $\approx 250$  MPa observed could be reduced to  $\approx 130$  MPa by decreasing the weld speed (i.e. 0.5mm/s) and power (i.e. 150 W) as shown in Fig. 4.29(c). This reduction in residual stress is much less than that of the yield stress (i.e. 265 MPa), which is beneficial to improve the service life of the component. The results on the circumferential residual stresses along the radial direction revealed that the transition from compressive to tensile stresses occurs at a distance between 0.5 and 1mm radially from the outer surface as shown in Fig. 4.29(c).

#### ***4.7.3 Radial Stress***

The radial residual stresses on both sides of WL are generated because of the variable shrinkage patterns. The variable shrinkage patterns are caused due to the temperature gradients across the wall thickness in the component during welding. The results of these radial stresses are presented in the following. Figs. 4.30 (a) and (b) exhibit the radial stress distribution on the inner and outer surfaces, respectively and these are for  $180^\circ$  cross-section from the weld start position. An interesting observation to note is that unlike the longitudinal and circumferential stresses, the radial stresses were not influenced by the weld speed and power. It can also be seen that the stresses were negligible on both sides of WL along the Z coordinate except at 40 mm distance on the inner surface (Fig. 4.30 (a)) and at WL on the outer surface (Fig. 4.30 (b)).

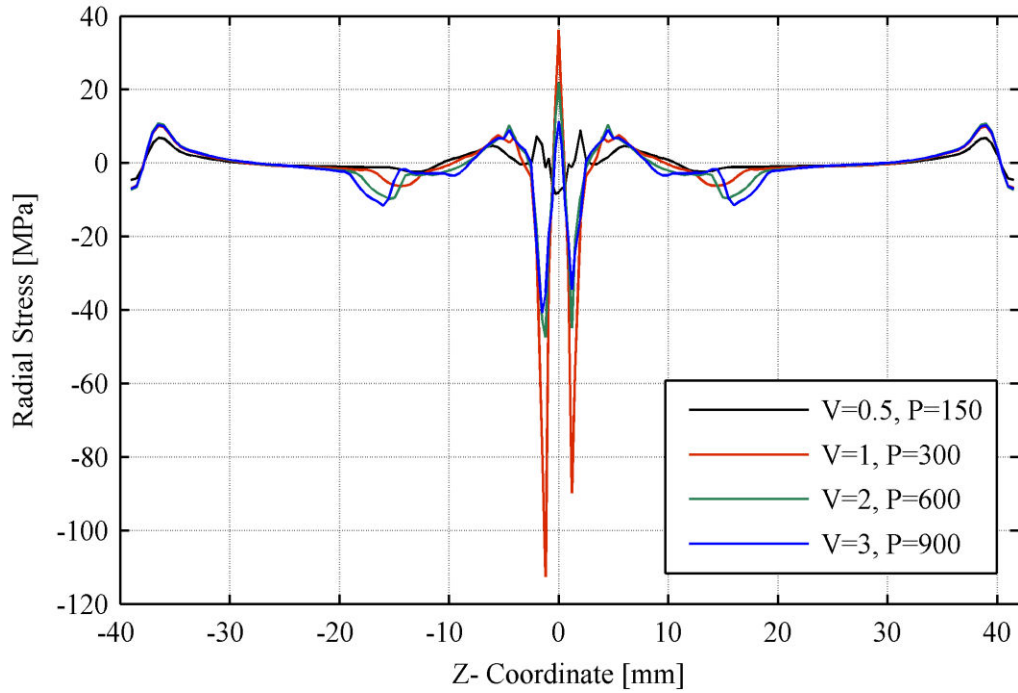


**Fig. 4.30 (a): Comparison between radial residual stresses for different cases at 1800 section from the weld start position on the inner surface.**

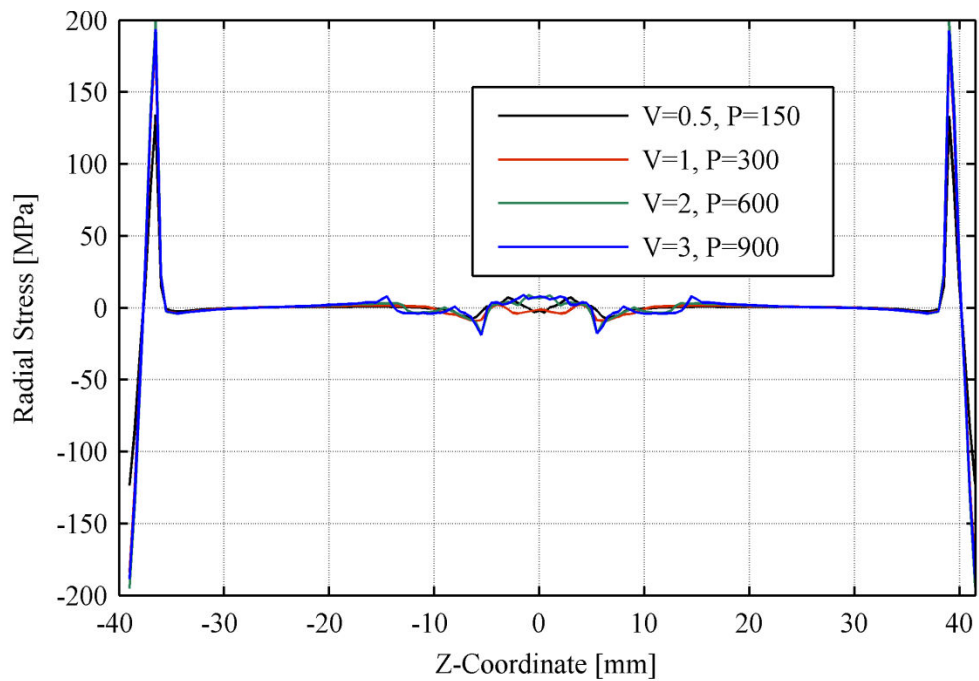


**Fig. 4.30 (b): Comparison between radial residual stresses for different cases at 1800 section from the weld start position on the outer surface.**

Further, it is evident that the nature of the stress was tensile (i.e. at 40 mm) on the inner surface, whereas it was tensile to compressive in the HAZ on the outer surface. The peak tensile stress observed at 40 mm along the Z coordinate (Fig. 4.30 (a)) may be attributed to reasons such as boundary condition imposed during welding and the geometric configuration employed in this study. Based on the above observations, it can be concluded that the influence of weld parameters i.e. investigated weld speed and power can be ignored for the analysis of radial stress distribution.

#### ***4.8 Experimental validation***

The results obtained from the numerical simulation were validated with experiments conducted using GTAW process with SS 308 as the filler material having diameter of 0.8 mm. The experiments were performed only at a particular weld speed of 1mm/s with similar geometric dimensions as shown in Fig. 4.31.

Fig. 4.31(a) and (b) show the schematic of the experimental setup and the welding setup, respectively. The welding setup was equipped with automated speed control through a stepper motor to maintain the constant weld speed of 1 mm/s. The two cylinders were initially joined by tack weld at four locations (each  $90^{\circ}$  apart). Temperature was measured using Chromel-Alumel (K- type) thermocouples connected at twelve locations at the outer surface by silver brazing. The weld start position, weld direction and the location of thermocouples are shown in Fig. 4.32. The thermocouples were located at  $90^{\circ}$ ,  $180^{\circ}$  and  $270^{\circ}$  from weld start position. The transient thermal cycles were recorded with the data acquisition system for time interval of 1S. For welding, 37 A and 10 V were chosen to supply the heat input of about 300 J/mm as used in the simulation.

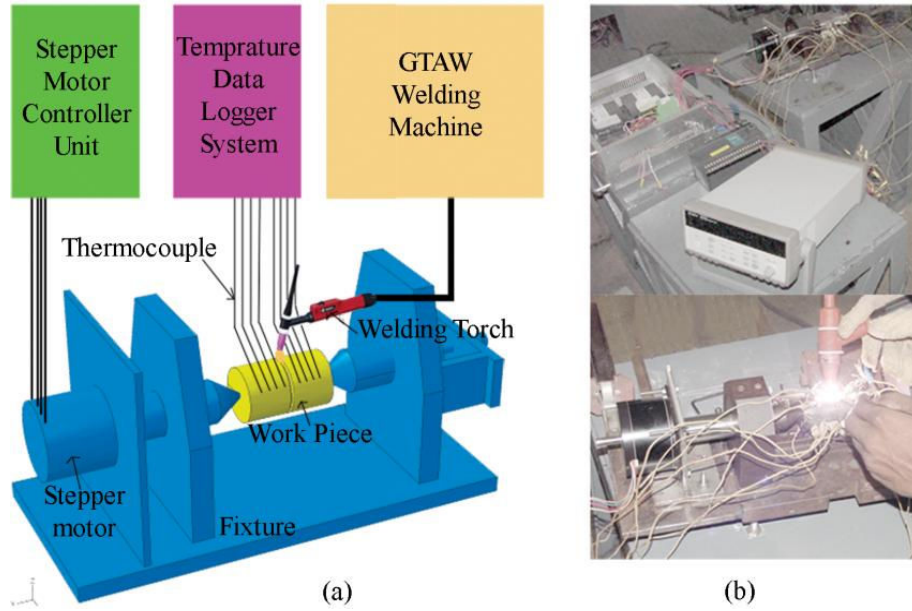


**Fig. 4.31: Experimental setup used (a) schematic diagram and (b) welding setup with clamping fixture and data logging system**

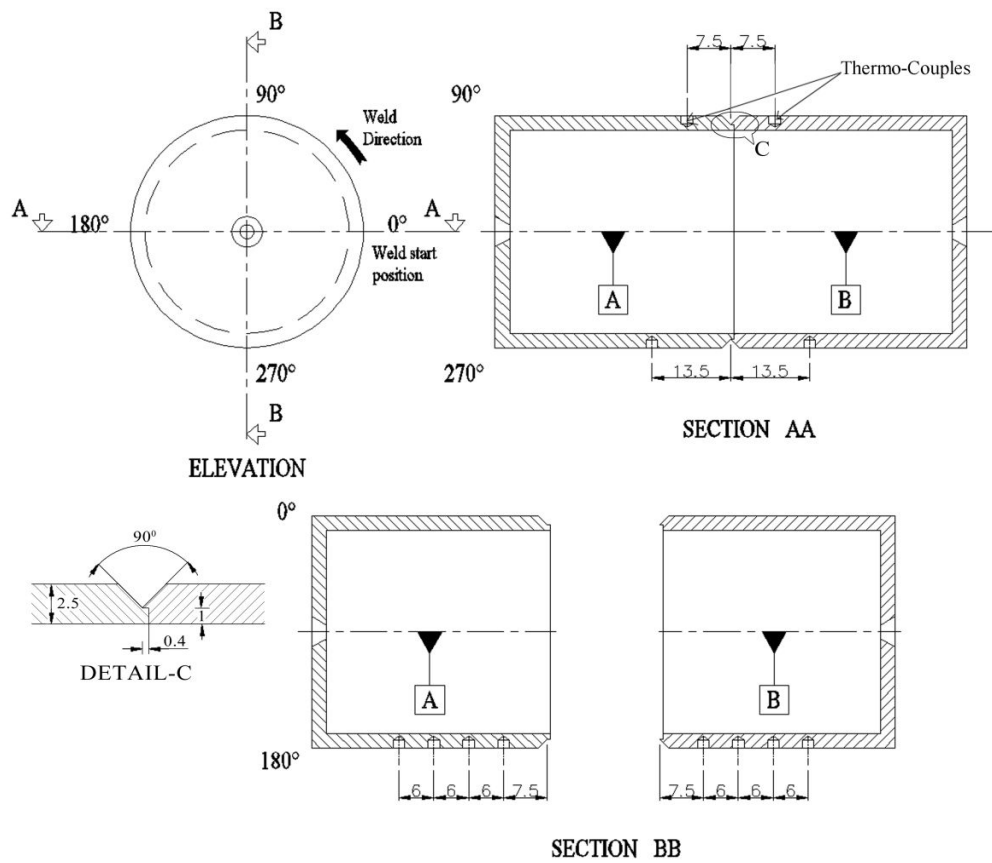


**Fig. 4.32: Location of thermocouples and weld direction.**

Following Eq. (5), it can be easily seen that these process parameters with process efficiency,  $\eta = 0.8$  gives the heat input of 296 J/mm. It is important to emphasize that the experimental data presented correspond only to a particular heat input i.e. case 2 in Table 4.1. The temperature profiles reported were for the 180° section (i.e. 8 locations) shown as section 'BB' in Fig. 4.32 and the values are the average of those obtained on both sides of the WL. The transient temperature profiles obtained experimentally and their comparison with those from simulation for different locations are shown in Fig. 4.33(a). It could be observed that the experimental and simulated FE results match well at locations of 7.5 and 13.5 mm longitudinally away from the WC. Whereas, for 19.5 and 25.5 mm locations, the experimental values were marginally higher than that of FE results. The maximum difference in peak temperatures between experimental and FE simulation was observed to be 9.4% at 25.5 mm location. The rate of increase in temperature also was in correspondence with each other. However, during cooling the experimental values were slightly higher than that of FE results and this would imply that the heat losses during experiments would be a little different from those predicted by simulation.

X- ray diffraction technique [89-90] was employed for measuring the residual stresses on the external surface. It may be mentioned that in this technique, the estimated strains which are measured by the shift in the position of diffraction peak are then converted into stresses. The details pertaining to the determination of residual stresses using X-ray diffraction technique are given by James M.R [91]. Since FE simulation did not reveal any remarkable variation of radial stresses, the longitudinal and circumferential stresses only are considered. The longitudinal stresses were measured at seven different locations, viz. at the WC and at 5, 10 and 20 mm away from the WC on the both sides of weld. The locations for the circumferential stresses were at the WC, and at 5 and 10 mm away from WC on the both sides of weld. The experimental results

along with those from FE simulation are plotted in Fig. 4.33 (b) with error bars for the experimental data. It could be seen that in addition to the close match of trend, the results are in reasonable agreement with each other. The experimental validation of FE results typically obtained for the case of weld speed = 1 mm/s and power = 300 W (i.e. heat input = 300 J/mm) signifies that the computational procedure followed in this investigation can be used for studying the distribution of temperature and residual stresses in a GTAW welded single plane circumferential butt joint.

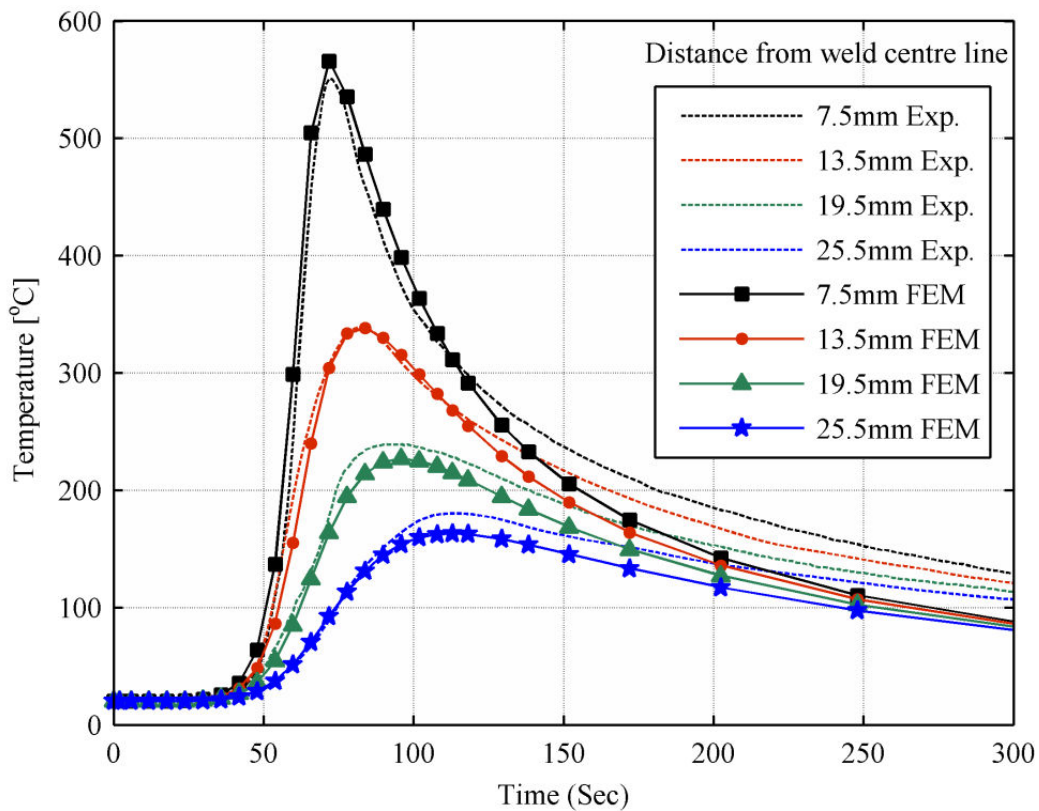


**Fig. 4.33 (a): Comparison of experimentally obtained temperature profiles with FE simulation for different locations**

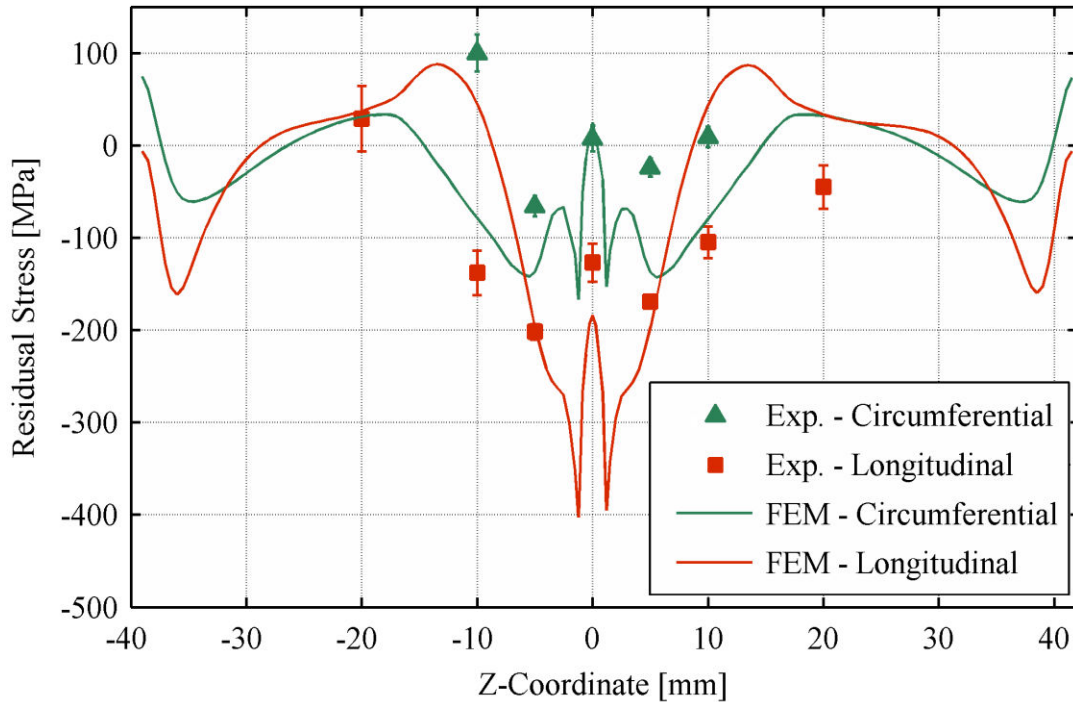


**Fig. 4.33 (b): Comparison of experimentally obtained Residual stresses with FE simulation for different locations**

For validating the predictions by numerical simulation, experimental work was carried out on two thin cylinders with similar geometric dimensions as shown in Fig. 4.34. The two cylindrical components were tack welded together at four locations (each  $90^{\circ}$  apart), before commencing the welding. Considering the weld speed of 1mm/sec and an arc efficiency ( $\eta$ ) of 0.8 for GTAW process, the heat input per mm length of weld is 296 J/mm (by using (2)) which is almost equal to the heat input that is used in FE simulation of case 2 in Table 4.1. For the validation of mechanical analysis, radial distortions are measured on the external surface at some specified locations. Experimental radial distortions measurement was conducted by holding the component centre to centre as shown in Fig. 4.34(b).

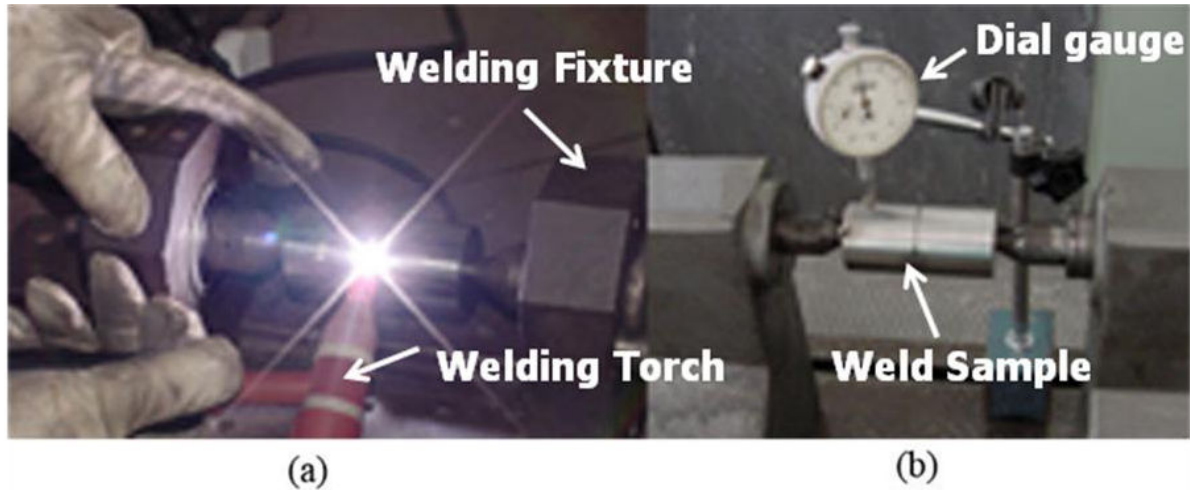


**Fig. 4.34: Experimental setup used (a) Component welding process (b) Dial gauge measurements for distortions.**

Radial distortions are measured at nine specified locations, i.e. at WC, 10mm, 20mm, 30mm and 40mm longitudinally away from WC on both sides of the weld. The quantitative comparison of measured and simulated nodal distortions at same distances in longitudinal direction is shown in Fig. 4.35. It is evident that the simulated results of radial distortions are in good agreement with the experimental data. Thus the numerical simulations are experimentally validated.

In a nut shell, the results from a number of numerical and experimental studies based on different welding process parameters are presented in this Chapter. To investigate the effects of welding process parameters comprising welding heat input and welding speed varied explicitly on the temperature distribution and the corresponding influence on weld induced distortions and residual stresses are observed. The effects of these deformations in particular to the dynamic performance of the CE rotating bowl are also discussed. Residual stresses in both longitudinal and hoop directions on thin walled pipe are also presented through detailed parametric studies. Further, the effects of different weld orientations are also presented in this chapter. In present

research, mostly parametric studies are conducted to investigate the effects of various parameters on structural response of circumferentially arc welded thin-walled cylinders. So, the chapter provides a comparison of FE predicted and experimentally measured data where ever is applicable.

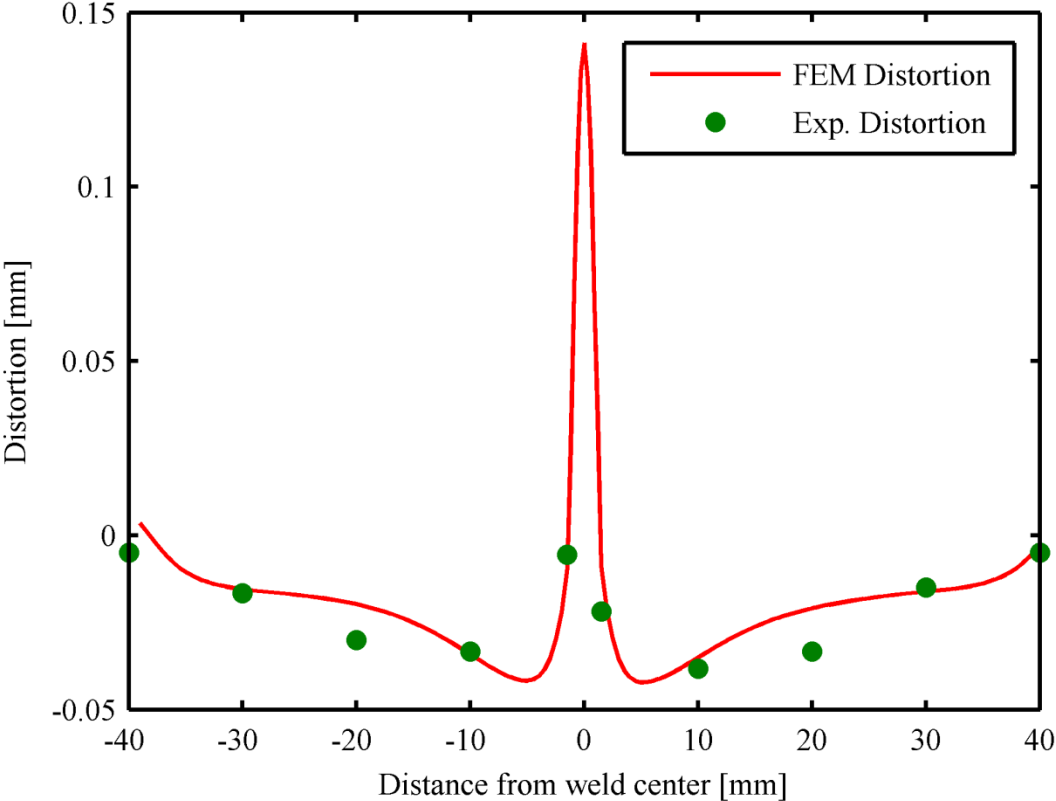


Fig. 4.35: Comparison of distortion obtained experimentally with those from FE simulation

## **Chapter 05**

### **CONCLUSIONS AND FUTURE SCOPE**

#### **CONCLUSIONS:**

Numerical methodology and techniques based on FEA for the prediction of temperature profiles and subsequent weld induced distortion patterns and residual stress fields in GTA welded thin-walled cylinders of stainless steel are developed and implemented successfully in close agreement with the experimental investigations. Detailed results and discussion pertaining to distortions, residual stress fields and there by the dynamic characteristics are presented. The following are the major conclusions from the present investigations.

- The analysis of heat source fitting revealed that the heat input of 300 J/mm results in a proper weld penetration and HAZ. For this heat input, a considerable increase in temperature distribution was observed with increase in weld speed and power.

- The FE analysis of longitudinal and circumferential stresses performed on the inner and outer surfaces as well as along the radial direction revealed a considerable increase with weld speed and power. For the case of 3 mm location away from the WC, the increase in tensile stress was found to be 150 MPa on the inner surface, whereas the increase in compressive stress was 100 MPa on the outer surface. The transition from tensile to compressive and vice-versa was found to occur at 1.25 mm depth (i.e. at the mid section) through wall thickness from the outer surface.
- The circumferential residual stress distribution also exhibited the similar trend with the magnitude of increase in tensile stresses as 120 MPa on the inner surface, while it was 100 MPa for compressive stresses on the outer surface. The transition from tensile to compressive and vice-versa occurred at the radial distance from the outer surface which was found to be between 0.5 and 1.0 mm.
- The results of FE simulation revealed that the radial residual stresses were found to be negligible and were not influenced by the variation in weld speed and power.
- The results of longitudinal, circumferential stresses, radial and longitudinal distortions from FE simulation were compared with those obtained experimentally for a typical condition of weld speed = 1 mm/s and power = 300 W i.e. heat input = 300 J/mm and revealed reasonable agreement with each other.
- For a specific heat input, an increase in peak temperature was observed with the increase in weld speed and power. Similarly the distortions are found to be less with lower weld speed and power against constant heat input.

- The radial distortions adjacent to weld are ranging from 0.02 mm to 0.12 mm on the inner surface and the radial distortions varying from 0.01 mm to 0.075 mm on the outer surface as the weld speed and power increases for the condition of constant heat input.
- The longitudinal distortions are ranging from 0.1 mm to 0.18 mm on both the surfaces as the weld speed and power increases for the condition of constant heat input
- A special experimental welding arrangement consists of special fixtures and stepper motor unit with data logging system is made available to monitor the temperature along the components during welding for different cases.
- The results of radial and longitudinal distortions from FE simulation were compared with the experimental measurements for a condition of weld speed = 1mm/s and power = 300 W, i.e. heat input = 300 J/mm and revealed good agreement with each other.
- For a particular location at 68 mm from the bottom of CE bowl the longitudinal distortions along its length of the bowl at angle 60° from the weld start position after welding is found to be maximum which is 66 microns and the numerical analysis predicted it as 50 microns.
- Distortions for different weld speeds ranging from 0.5mm/sec to 2mm/sec show a maximum value of 200 microns at 2mm/sec and 75 microns at 0.5mm/sec.
- Similarly in continuous welding it is observed a maximum distortion of 210 microns. Maximum distortion value for the case of single pass welding is about 90 microns where as for double pass it is about 95 microns.

- A relative comparison for different weld parameters directly on the distortions of rotating bowl assembly reveals that the number of passes is less significant as compared to the weld speeds and clamping conditions, as the wall thickness is less.
- The effect of welding speeds on the critical speed can be easily identifiable from the modal analysis, which shows for a given operating speed, higher the welding speed implies large distortion which in turn requires high bearing stiffness.

### **FUTURE SCOPE:**

The major concern in the welding domain is the analysis of arc welded thin walled cylindrical components for the study of weld induced imperfections. This research work has considerably contributed towards this requirement, related to the optimization of weld process parameters for welding of thin walled components using both simulation and experimental validation. It is strongly recommended to implement the presented research work for analyzing the important welding parameters and structural boundary conditions for better performance of the CE rotating bowl. The prediction of weld induced imperfections for such critical components is essential before the start of actual welding process. The selection of particular welding process may depend on several parameters in addition to the nature and requirements of the application i.e. the setting parameters, fixed parameters, geometric parameters, structural boundary conditions etc. Further, the future scope is discussed in the following.

1. It is further proposed to study the metallurgical aspects pertain to phase transformations, grain size and hardness profiles in conjunction with different weld speeds and powers with constant heat input per unit length.

2. To determine the peak cyclic stress and the non-linear through-thickness stress distributions and studying the influence of various weld parameters on the assessment of the fatigue crack initiation life of the component due to the welding induced tangential residual stresses using strain-life methodology.
3. The above methodology based on FEA can also be applied for the analysis of other steel materials like SS304L and P91 etc., mainly by incorporating the temperature dependent material properties such as Young's Modulus and thermal conductivity of model with necessary experimental validation.
4. The above studies which have been carried out for TIG welding can be further extended to other welding processes such as Submerged Arc Welding, Electron Beam Welding, and Laser beam welding etc. This is mainly to compare the nature of the HAZ and weld pool size and other heat source parameter requirements of the process.

## References

- [1] . K. Masubuchi., Analysis of Welded Structures, Pergamon Press, London 1980. ISBN 0-08-022714-7.
- [2] . *Welding Handbook*, American Welding Society, Vol. I, 8th edition, Miami, Florida, 1987.
- [3] . Liang. T., Peng-Hsiang Chang, Three Dimensional Thermo-mechanical Analysis of Circumferentially Welded Thin Walled Pipes. *International Journal of Pressure Vessels and Piping*, 1998, 75 : 237-247.
- [4] . Cheng W, Finnie I. A Method for the Measurement of Axis-symmetric Axial Residual Stresses in Circumferentially Welded Thin Walled Cylinders. *Journal of Engineering Material Technology*. 1985, 107: 181 – 185.
- [5] . Popelar CH, Barber T, Groom J., A Method for Determining Residual Stresses in Pipes. *Journal of Pressure Vessel Technology*, 1982 , 104: 223 – 228.
- [6] . Maddox, S.J., "Influence of Tensile Residual Stresses on the Fatigue Behavior of Welded Joints in Steel", *American Society for Testing and Materials*, 1982, 776: 63-96.
- [7] . Toribio J., Residual stress effects in stress-corrosion cracking, *Journal of Materials Engineering and Performance*, 1998, 7 (2):173-182.
- [8] . P. Dong, F.W. Brust,, Welding residual stresses and effects on fracture in pressure vessel and piping components: A Millennium Review and Beyond [J]. *Trans. ASME Journal of Pressure Vessel Technology*, 2000, 122: 329-338.
- [9] . S. Vaidyanathan, A.F. Todato and I. Finnie., Residual Stress Due to Circumferential Welds. *ASME Journal of Engineering Material and Technology* 1973; 95: 233-237.

- [10] . Brand, P.C., Keijser, TH. H. de, Ouden Gen. G, Residual stresses and plastic deformation in GTA-welded steel. *Welding Journal*. 1993,72(3):93-100.
- [11] .Radaj, D., Heat Effects of Welding – temperature Field, Residual Stress, Distortion. *Berlin: Springer-Verlag*,1992.
- [12] .Lindgren, L.E., Numerical modelling of welding, *Computer Methods in Applied Mechanics and Engineering*, 2006, 195(48-49): 6710-6736.
- [13] .H Runnemalm, S Hyun, Three-dimensional welding analysis using an adaptive mesh scheme, *Computer Methods in Applied Mechanics and Engineering*, 2000, 189(2): 515-523.
- [14] .Goldak, J. and M. Akhlagi, Computational Welding Mechanics., *Springer*, 2005.
- [15] .C.S. Wu, H.L. Wang, Y.M. Zhang., Numerical analysis of the temperature profiles and weld dimension in high power direct-diode laser welding. *Computational Materials Science*, 2009, 46 : 49-56.
- [16] .Dean Deng, Hidekazu Murakawa, Numerical simulation of temperature field and residual stress in multi-pass welds in stainless steel pipe and comparison with experimental measurements, *Computational Materials Science*, 2006, 37( 3): 269-277.
- [17] .Goldak, J.A., et al., Computer Modelling of Heat Flow in Welds. *Metallurgical Trans B*, 1986, 17B: 587-600.

- [18] .P.V. Venketakrishnan, J. Philip and R. Krishnamurthy., An Assessment of Stresses in Thin Walled Welded Tubes through Hole-Drilling and Sectioning Methods. *Journal of Materials Processing Technology* 2007, 185(1-3): 228-232.
- [19] . A.N. Lari, J. Lu and J.F. Flavenot. Measurement of Residual Stress Distribution by the Incremental Hole-Drilling Method. *Journal of Mechanical Working Technology* 1985,11(2):167-188.
- [20] .Lundback, A., H. Runnemalm, Validation of three dimensional finite element model for electron beam welding of Inconel 718 , *Science and Technology of Welding & Joining.*, 2005, 10(6):717–724.
- [21] .W. Suder, S. Ganguly, S. Williams, A.M. Paradowska, P. Colegrove Comparison of joining efficiency and residual stresses in laser and laser hybrid welding, *Science and Technology of Welding & Joining*, 2011, 16(3):244–248.
- [22] .Dong P, Residual stresses and distortions in welded structures: a perspective for engineering applications, *Science and Technology of Welding & Joining*, 2005, 10(10):389–398.
- [23] .M.E. Kartal, C.D.M. Liljedahl, S. Gungor, L. Edwards, M.E. Fitzpatrick, Determination of the profile of the complete residual stress tensor in a VPPA weld using the multi-axial contour method, *Acta Materialia*, 2008, 56(16): 4417-4428.
- [24] .Malik AM, Ejaz M. Qureshi, Naeem Ullah Dar, Iqbal Khan. Analysis of circumferentially arc welded thin-walled cylinders to investigate the residual stress fields. *Thin-Walled Structures*, 2008,46(12):1391-1401.

- [25] .B.L. Josefson, Residual stresses and their redistribution during annealing of a girth-butt welded thin-walled pipe, *ASME J. Pressure Vessel Technology*,1982,104:245-250.
- [26] .A.K. Dhingra, C.L. Murphy, Numerical simulation of welding-induced distortion in thin-walled structures, *Science and Technology of Welding & Joining*, 2005, 10 (5) : 528–536.
- [27] .Bhabha, Homi J and N B Prasad, “A Study of the Contribution of Atomic Energy to a Power Programme in India,” *Proceedings of the Second United Nations International Conference on the Peaceful Uses of Atomic Energy*, Geneva,1958:89-101.
- [28] .Natarajan, R., Fast reactor fuel reprocessing technology in India, *Journal of Nuclear Science and Technology*, 2007, 44(3):393-397.
- [29] . Natarajan. R, Baldev Raj, Fast Reactor Fuel Reprocessing Technology: Successes and Challenges, *Energy Procedia*, 2011,7:414-420.
- [30] .Natarajan, R., Challenges in Fast Reactor Fuel Reprocessing, *Indian Association of Nuclear Chemists and Allied Scientists Bulletin*, 1998,14 (2):27-32.
- [31] .Connor, L.P. , Welding handbook-welding processes American Welding Society, vol. 2, 8 edition, 1991.
- [32] .M.V. Deo and P. Michaleris. Mitigation of welding-induced buckling distortion using transient thermal tensioning. , *Science and Technology of Welding & Joining*,2003, 8(1): 49–53.

- [33] .Chin-Hyung Lee, Kyong-Ho Chang. Three-dimensional finite element simulation of residual stresses in circumferential welds of steel pipe including pipe diameter effects. *Mater Sci Eng. A*, 2008, 487 (1-2) : 210-218.
- [34] .Shim Y, Feng Z, Lee S, Kim D, Jaeger J, Papritan JC, Tsai CL. Determination of residual stresses in thick-section weldments. *Welding Journal* .,1992,71(9):305–312.
- [35] .Liang Wang, Sergio D. Felicelli, Phillip Pratt. Residual stresses in LENS-deposited AISI 410 stainless steel plates. *Mater Sci Eng A*, 2008,496(1-2):234–241.
- [36] .R. Spina, L. Tricarico, G. Basile, T. Sibillano. Thermo-mechanical modeling of laser welding of AA5083 sheets. *J Mater Process Tech*, 2007,191:215-219.
- [37] .B. Brickstad, B. L. Josefsonb. A parametric study of residual stresses in multi-pass butt-welded stainless steel pipes. *International Journal of Pressure Vessels and Piping*, 1998,75:11-25.
- [38] .Kazuo Ogawa, Dean Deng, Shoichi Kiyoshima, Nobuyoshi Yanagida, Koichi Saito. Investigations on welding residual stresses in penetration nozzles by means of 3D thermal elastic plastic FEM and experiment. *Computational Materials Science*, 2009,45:1031-1042.
- [39] .Chaowen Li, Yong Wang, Huanxiao Zhan, Tao Han, Bin Han, Weimin Zhao. Three-dimensional finite element analysis of temperatures and stresses in wide-band laser surface melting processing. *Materials & Design*, 2010,31:3366-3373.

- [40] .Kermanpur, M. Shamanian, V. Esfahani Yeganeh. Three-dimensional thermal simulation and experimental investigation of GTAW circumferentially butt-welded Incoloy 800 pipes. *J Mater Process Tech*, 2008,199:295–303.
- [41] .C.S. Wu, J.S. Sun. Numerical analysis of temperature field during double-sided arc welding of thick materials. *Computational Materials Science*, 2002, 25:457-468.
- [42] .C.S. Wu, H.L. Wang, Y.M. Zhang. Numerical analysis of the temperature profiles and weld dimension in high power direct-diode laser welding. *Computational Materials Science*, 2009, 46:49-56.
- [43] .D. Gery, H. Long, P. Maropoulos. Effects of welding speed, energy input and heat source distribution on temperature variations in butt joint welding. *J Mater Process Tech*, 2005; 167:393–401.
- [44] .Dean Deng, Shoichi Kiyoshima. Numerical simulation of welding temperature field, residual stress and deformation induced by electro slag welding, *Computational Materials Science*, 2012, 62:23–34.
- [45] .Dean Deng. FEM prediction of welding residual stress and distortion in carbon steel considering phase transformation effects. *Materials & Design*, 2009, 30:359-366.
- [46] .Tso-Liang Teng, Chin-Ping Fung, Peng-Hsiang Chang, Wei-Chun Yang, Analysis of residual stresses and distortions in T-joint fillet welds, *International Journal of Pressure Vessels and Piping*, 2001,78(8):523-538.

- [47] .H. Long, D. Gery, A. Carlier, P.G. Maropoulos. Prediction of welding distortion in butt joint of thin plates. *Materials & Design*, 2009,30:4126-4135.
- [48] .J.J. del Coz Díaz, P. Menéndez Rodríguez, P.J. García Nieto, D. Castro-Fresno. Comparative analysis of TIG welding distortions between austenitic and duplex stainless steel s by FEM. *Appl Therm Engg*. 2010,30:2448-2459.
- [49] .W.C. Jiang, B.Y. Wang, J.M. Gong, S.T. Tu. Finite element analysis of the effect of welding heat input and layer number on residual stress in repair welds for a stainless steel clad plate. *Materials & Design*, 2011,32:2851-2857.
- [50] .Yanhong Tian, Chunqing Wang, Danyang Zhu, Y. Zhou. Finite element modeling of electron beam welding of a large complex Al alloy structure by parallel computations. *J Mater Process Tech*, 2008,199:41-48.
- [51] .I. Sattari-Far, Y. Javadi, Influence of welding sequence on welding distortions in pipes, *International Journal of Pressure Vessels and Piping*, 2008, 85(4):265-274.
- [52] .E.F. Rybicki, D.W. Schmueser, R.W. Stonesifer, J.J. Groom and H.W. Mishaler, A Finite Element model for residual stresses and deflections in girth-butt welded pipes, *ASME Journal of Pressure Vessel Technology*.1978, 100:256–262.
- [53] .Goldak J. et al., Computer modeling of heat flow in welds, *Metall. Trans. B*, 1968, 17(B):587–600.

- [54] .Dong, Y., Hong, J.K., Tsai, C.L. and Dong, P., Finite Element Modeling of Residual Stresses in Austenitic Stainless Steel Pipe Girth Welds, *Welding Journal*, 1997, 76(10):442-449.
- [55] .Karlsson, R.I. and Josefson, B.L, Three Dimensional Finite Element Analysis of Temperature and Stresses in a Single-Pass Butt-Welded Pipe, *ASME Journal of Pressure Vessel Technology*,1990, 112:76-84.
- [56] .Fricke, S., Keim, E. and Schmidt, J., Numerical Weld Modeling - A Method for Calculating Weld-Induced Residual Stresses, *Nuclear Engineering and Design*, 2001, 206:139-150.
- [57] .Andreas Lundbäck, Lars-Erik Lindgren, Modelling of metal deposition, *Finite Elements in Analysis and Design*, 2011, 47(10):1169-1177.
- [58] .Murugan S, Rai SK, Kumar PV, Jayakumar T, Baldev Raj, Bose MSC. Temperature distribution and residual stresses due to multipass welding in type 304 stainless steel and low carbon steel weld pads. *International Journal of Pressure Vessels and Piping*, 2001,78:307–317.
- [59] .Dean Deng, Hidekazu Murakawa. Numerical simulation of temperature field and residual stress in multi-pass welds in stainless steel pipe and comparison with experimental measurements. , *Computational Materials Science*, 2006, 37(3):269-277.
- [60] .C. H. Lee and K. Chang, “Three-dimensional Finite Element Simulation of Residual Stresses in Circumferential Welds of Steel Pipe Including Pipe Diameter Effects,” *Material Science and Engineering:A*, 2008, 487(1-2) :210-218.

- [61] .Teng. T.L. and Chang, P.H., Three-Dimensional Thermo-mechanical Analysis of Circumferentially Welded Thin-Walled Pipes, *International Journal of Pressure Vessels and Piping*, 1998,75:237-247.
- [62] .P.H. Chang and T.L. Teng, Numerical and experimental investigation on the residual stresses of the butt-welded joints, *Computational Material Science*.,2004, 29(4) :511-522.
- [63] .Shoichi Kiyoshima, Dean Deng, Kazuo Ogawa, Nobuyoshi Yanagida, Koichi Saito, Influences of heat source model on welding residual stress and distortion in a multi-pass J-groove joint, *Computational Materials Science*, 2009 , 46(4): 987-995.
- [64] .Basavaraju, C., Simplified Analysis of Shrinkage in Pipe-Pipe Butt Welds, *Nuclear Engineering and Design*,2000,197:239-247.
- [65] .Bachorski, M.J. Painter, A.J. Smailes and M.A. Wahab - Finite-Element Prediction of Distortion During Gas Metal Arc Welding Using the Shrinkage Volume Approach- *J Mater Process Tech*,1999, 92(93):405-409.
- [66] .Dean Deng, Hidekazu Murakawa and Wei Liang, Numerical and experimental investigations on welding residual stress in multi-pass butt-welded austenitic stainless steel pipe, *Computational Material Science*, 2008, 42:234-244.
- [67] .Lindgren, L.E., Finite Element Modeling and Simulation. Part 1: Increased Complexity, *Journal of Thermal Stresses*, 2001, 24:141-192.
- [68] .Lindgren, L.E., Finite Element Modeling and Simulation. Part 2: Improved Material Modeling, *Journal of Thermal Stresses*, 2001, 24:195-231.

- [69] .Lindgren, L.E., Finite Element Modeling and Simulation. Part 3: Efficiency and Integration, *Journal of Thermal Stresses*,2001, 24:305-334.
- [70] .A. Yaghia, T.H. Hydea, A.A. Becker, W. Suna and J.A. Williams, Residual stress simulation in thin and thick-walled stainless steel pipe welds including pipe diameter effects, *International Journal of Pressure Vessels and Piping*. 2006, 83(11-12) :864-874.
- [71] .Natarajan, R., Challenges in Fast Reactor Fuel Reprocessing, *Indian Association of Nuclear Chemists and Allied Scientists Bulletin*, 1998,14 (2):27-32.
- [72] .Baldev Raj, Materials and Manufacturing Technologies for Sodium Cooled Fast Reactors and Associated Fuel Cycle: Innovations and Maturity, *Energy Procedia*, 2011, 7:186-198.
- [73] .Natarajan, R., Fast reactor fuel reprocessing technology in India, *Journal of Nuclear Science and Technology*, 2007, 44(3):393-397.
- [74] .Natarajan. R, Baldev Raj, Fast Reactor Fuel Reprocessing Technology: Successes and Challenges, *Energy Procedia*, 2011, 7: 414-420.
- [75] .Goldak J, Gu M, Karlsson L. "Numerical aspects of modelling welds". *ASM Handbook Weld*. 1993, 6:1131–1140.
- [76] .Murugan S., Gill T.P.S., Kumar P.V., Raj B. and , Bose M.S.C., "Numerical modeling of temperature distribution during multipass welding of plates" *Science and Technology of Welding and Joining*, 2000 , 5(4):208-214.

- [77] .Farid Vakili-Tahami, Ali Ziaei-Asl. "Numerical and experimental investigation of T-shape fillet welding of AISI 304 stainless steel plates". *Materials & Design*, 2013,47:615-623.
- [78] .Sysweld reference manual and material data, ESI group; 2005.
- [79] .W.F. Brown, H. Mindlin, C.Y. Ho, "Aerospace Structural Metals Handbook", *Purdue University*, West Lafayette, IN, USA, 1993.
- [80] .Y.C. Kim, A. Fuji, T.H. North, "Residual stress and plastic strain in AISI 304L stainless steel/titanium friction welds", *Mater. Sci. Technol.* 1995, 11:383–388.
- [81] .Zhu, X.K., Chao, Y.J., "Numerical simulation of transient temperature and residual stresses in friction stir welding of 304L stainless steel", *Journal of Materials Processing Technology*, 2004,146:263–272.
- [82] .I.F.Z. Fanous, M.Y.A. Younan and A.S. Wifi. 3-D Finite Element Modeling of Welding Process using Element Birth and Element Movement Techniques. *ASME Journal of Pressure Vessel Technology*, 2003,125(2):144–150.
- [83] .P.J. Withers and H.K.D.H. Bhadeshia. Residual Stress Part 2: Nature and Origins. *Journal of Materials Science & Technology*, 2001,17(4): 366-375.
- [84] .C.C. Silva and J.P. Farias. Non-uniformity of Residual Stress Profiles in Butt Welded Pipes in Manual Arc Welding. *Journal of Materials Processing Technology*, 2008,199(6):452–455.

- [85] .Afzaal M. Malik, Ejaz M. Qureshi, Naeem Ullah Dar, Iqbal Khan, Analysis of circumferentially arc welded thin-walled cylinders to investigate the residual stress fields, *Thin-Walled Structures*, 2008,46(12):1391-1401.
- [86] .Goldak, J., A. Chakravarti and M. Bibby. A New Finite Element Model for Welding Heat Sources. *Metallurgical Transactions B*, 1984, 15(B):299-305.
- [87] .Goldak, J., Zhou, J., Breiguine, V., and Montoya, F., Thermal Stress Analysis of Welds: From melting Point to Room Temperature, *Trans. JWRI*, 1996, 25(2):1851-1889.
- [88] .Evans G. M. and Bailey N., "Metallurgy of Basic Weld Metal", *Abington Publishing*, 1997.
- [89] .Radaj. D., Heat Effects of Welding—Temperature Field, Residual Stress, Distortion, *Springer-Verlag*, Berlin, 1992.
- [90] . Xuejun Zheng, Jiangyu Li, Yichun Zhou, X-ray diffraction measurement of residual stress in PZT thin films prepared by pulsed laser deposition, *Acta Materialia*,2004, 52 (11): 3313-3322.
- [91] .James, M. R., An Examination of Experimental Techniques in X-ray Residual Stress Analysis, Ph.D. Thesis , *Northwestern University*, Evanston, IL, 1977.